THE DOUBLE SCROLL FAMILY PART I AND PART II

by

Leon O. Chua, Motomasa Komuro and Takashi Matsumoto

Note: 6/11/86

Student brought in
changes: pp 26-32,
& new Fig 18 —
no Fig captions
were changed, also
Fig #'s.
      Before re-ordering,
check w/ chua

per the student —
I was told not to
change this master
copy now.

(a xerox copy
of today's changes
may be found
with the original
manuscript

THE DOUBLE SCROLL FAMILY PART I AND PART II

by

Leon O. Chua, Motomasa Komuro and Takashi Matsumoto

ELECTRONICS RESEARCH LABORATORY

College of Engineering
University of California, Berkeley
94720

THE DOUBLE SCROLL FAMILY
PART I: RIGOROUS PROOF OF CHAOS[†]

Leon O. Chua, Motomasa Komuro and Takashi Matsumoto[‡]

Department of Electrical Engineering and Computer Sciences
and the Electronics Research Laboratory
University of California, Berkeley, CA 94720

ABSTRACT

This paper represents Part I of a 2-part paper which provides a rigorous mathematical proof that the double scroll is indeed *chaotic*. Our approach is to derive a *linearly equivalent* class of piecewise-linear differential equations which includes the double scroll as a special case. Necessary and sufficient condition for two piecewise-linear vector fields to be linearly equivalent is that their respective eigenvalues be a scaled version of each other. In the special case where they are identical, we have exact equivalence in the sense of *linear conjugacy*.

Explicit *normal form* equation in the context of global bifurcation is derived and parametrized by their eigenvalues. Analytical expressions for various *Poincare maps* are then derived and used to characterize the *birth* and the *death* of the double scroll, as well as to derive an approximate one-dimensional map in analytic form which is useful for further bifurcation analysis. In particular, the analytical expressions characterizing various *half-return maps* associated with the Poincare map are used in a crucial way to prove the existence of a Shilnikov-type homoclinic orbit, thereby establishing rigorously the chaotic nature of the double scroll. These analytical expressions are also fundamental in our in-depth analysis of the *birth* (onset of the double scroll) and *death* (extinction of chaos) of the double scroll.

The unifying theme throughout this paper is to analyze the double scroll system as an *unfolding* of a large family of piecewise-linear vector fields in $\mathbb{R}^3$. Using this approach, we were able to prove that the *chaotic dynamics* of the double scroll is quite common and robust. In fact, it is exhibited by a large family (in fact, infinitely many *linearly-equivalent circuits*) of vector fields whose associated piecewise-linear differential equations bear no resemblance to each other. It is therefore remarkable that the normalized eigenvalues, which is a *local* concept, completely determines the system's *global* qualitative behavior.

1. INTRODUCTION

The *double scroll* is a strange attractor recently observed from a *physical* electronic circuit made of 4 *linear* circuit elements (1 resistor, 1 inductor, and 2 capacitors) and a 2-terminal *nonlinear resistor* characterized by a 5-segment $v-i$ curve [1-3]. The nonlinear resistor can/realized in the laboratory by several equivalent electronic circuits using 2 op amps [2], 1 op amp and 2 diodes [3], or 2 transistors and 2 diodes [4]. Since its recent discovery, this rather simple electronic circuit has been observed, both *experimentally* [5-6] and by computer *simulation* [6], to exhibit a surprisingly rich variety of bifurcation phenomena [6] and routes to chaos [7-9]. Although the *chaotic* nature of the double scroll appears to be very convincing from both experimental analysis and computer simulations, there remains legitimate objections from some critics who demand no less than a rigorous mathematical proof. Our main objective in this paper is to supply such a proof.

Proving a circuit is chaotic is a non-trivial task. Indeed, only 3 nonlinear circuits have so far been proved rigorously to be chaotic: the first two circuits [10-11] are described by a *one-dimensional discrete map* while the third circuit [12] is described by a *2nd-order non-autonomous differential equation*. The double scroll system to be studied in this paper is described by a *3rd-order autonomous differential equation*. In particular, we will choose the dimensionless form given by (2.4) of [3] which we rewrite in the equivalent form

$$\boxed{\begin{aligned} \dot{x} &= \alpha(y-h(x)) \\ \dot{y} &= x-y+z \\ \dot{z} &= -\beta y \end{aligned}}$$

(1.1)

where

$$h(x) \triangleq x+f(x) = m_1 x + \frac{1}{2}(m_0-m_1)[\,|x+1| - |x-1|\,]$$

(1.2)

is the canonical piecewise-linear equation [13] describing an odd-symmetric 3-segment piecewise-linear curve[†] having a *breakpoint* at $x = -1$ and $x = 1$ and a *slope* equal to $m_0 \triangleq a+1 < 0$ at the inner segment and $m_1 \triangleq b+1 > 0$ at the outer segments, respectively; namely,

---

[†]We include only 3 segments of the 5-segment piecewise-linear $v-i$ curve because the 2 outermost segments do not play any role in the formation of the double scroll.

$$h(x) = m_1 x + (m_0 - m_1) \ , \ x \geq 1$$

$$= m_0 x \qquad\qquad , \ |x| \leq 1 \qquad\qquad\qquad (1.3)$$

$$= m_1 x - (m_0 - m_1) \ , \ x \leq -1$$

Note that (1.1) is slightly simpler than (2.4) in [3] because $h(x)$ includes both $f(x)$ and x. The double scroll system is therefore described by 4 parameters $\{\alpha, \beta, m_0, m_1\}$, with the double scroll attractor occurring in a neighborhood of $\{9, 14 \frac{2}{7}, -\frac{1}{7}, \frac{2}{7}\}$.

Since the techniques and concepts to be used in proving that the double scroll is chaotic are quite novel and general, we will develop our theory for a much larger class of piecewise-linear differential equations of which (1.1) is a special case. Mathematically, our approach is to consider the vector field associated with the double scroll system as an *unfolding* of a family of 3-dimensional continuous piecewise-linear vector fields characterized by 6 parameters, instead of 4 in the double scroll system. However, unlike the literatures on unfoldings which consider only *differentiable* functions [14], our results are novel in the sense that our functions are required to be only continuous, not differentiable.[t]

Because of the nature of piecewise-linear analysis, a substantial amount of symbols and notations are necessary to avoid ambiguity and clutter. They are summarized in *Section 2* for ease of reference.

The family of piecewise-linear vector fields whose *unfolding* gives the double scroll system is defined and characterized in *Section 3*. The main results in this section are summarized in *theorems* 1, 2, and 3. In particular, we have derived the *necessary* and *sufficient* conditions for any two vector fields in this family to be *linearly conjugate*, which is a *strong form* of equivalence from the circuit theoretic point of view and an important mathematical property in the theory of *structural stability* of vector fields [9]. It is remarkable that while it is often impossible to establish any *topological conjugacy* between *nonlinear* vector fields, we were able to prove that the necessary and sufficient conditions for linear conjugacy (which is a special case of topological conjugacy) between 2 piecewise-linear vector fields in our family is that their *eigenvalues* in corresponding regions be identical.

This important result, which is stated in two equivalent forms (theorems 1 and 2) allows us to derive the *explicit* form of *all* members of our family of piecewise-linear vector fields which are equivalent (i.e., linearly conjugate) to each other in terms of their *eigenvalues* alone. This major result, which is formulated in the form of a *canonical piecewise-linear*

---

[t]Consequently, a more precise title for this paper is: "unfoldings of piecewise-linear vector fields in $\mathbb{R}^3$.

equation [13] parametrized by their eigenvalues, will henceforth be called the *normal form equation for the double scroll.*[†] Again, this result is remarkable because finding normal forms of parametrized nonlinear vector fields is extremely difficult if not impossible.

Our results from *Section 3* provide the necessary foundation in *Section 4* for deriving the *exact* (i.e., analytical) expressions describing various *Poincare maps* of an important class of vector fields which are unfoldings of our normal form equation. These results are then used in a crucial way in *Section 5* to prove that *homoclinic orbits* of the Shilnikov type [9] exist in the double scroll, thereby providing a rigorous proof that the double scroll is indeed chaotic[‡]

The analytical formula for Poincaré maps in Section 4 allows us to derive the *exact* coordinates of the return map of any trajectory of the double scroll system. These coordinates are used in *Section 6* to derive the analytical expression describing the image of several strategic loci (to be defined in *Section 6*) which allows us to explain the *birth* (i.e., onset) and the *death* (i.e., extinction) of the double scroll attractor. Unlike the preceding 5 sections, however, where complete mathematical rigor is achieved, some reasonable numerical calculations are used in this section to calculate two curves—called the *birth* and the *death loci* — which bound the region in the $\alpha-\beta$ parameter space where the double scroll exists.

Finally, in *Section 7,* we derive the analytic expression of an "approximate" *one-dimensional map* which can be used for further bifurcation analysis of the double scroll.

2. PIECEWISE-LINEAR GEOMETRY AND ITS JORDAN FORM

Unless otherwise stated, vectors and matrices are denoted by lower and upper case boldface letters, respectively. Vectors in $\mathbb{R}^3$ are denoted by $\underset{\sim}{x} = (x,y,z)^T$. Real and imaginary part of a complex eigen value will be denoted by σ and ω respectively. Real eigenvalues will be denoted by γ. Vector fields will be denoted by $\xi : \mathbb{R}^3 \to \mathbb{R}^3$. Hence $\xi(\underset{\sim}{x})$ denotes the vector field evaluated at $\underset{\sim}{x}$ and is therefore itself a vector in $\mathbb{R}^3$ emanating always from the origin $\underset{\sim}{0}$, unless otherwise stated.

We will now extract the essential properties of the vector field associated with the double scroll system (1.1) to define the following family of vector fields $\mathscr{L}$.

Definition 2.1. Piecewise-linear vector field family $\mathscr{L}$

[†]The term "normal form" is used here in the same context as that used in global bifurcation theory of vector fields [9], and *not* in the circuit-theoretic sense of a state equation.

[‡]The reader is referred to an interesting related work by Mees and Chapman [15] where they used optimization techniques to locate a *heteroclinic* orbit in the double scroll system.

We define $\mathcal{L}$ to be a family of *continuous vector fields* $\xi : \mathbb{R}^3 \to \mathbb{R}^3$ satisfying the following properties:

(P.1) ξ is symmetric with respect to the origin, i.e.,[†] $\xi(-x,-y,-z) = -\xi(x,y,z)$.

(P.2)   There are two planes U_1 and U_{-1} which are symmetric with respect to the origin (i.e., $(x,y,z) \in U_1$ iff $(-x,-y,-z) \in U_{-1}$) and they partition $\mathbb{R}^3$ into three closed regions D_1, D_0, and D_{-1}, as shown in Fig. 1. Here, the reference frame for (x,y,z) is arbitrary.

(P.3)   In each region D_i, ($i = -1, 0, 1$), the vector field ξ is *affine*, i.e.,

$$D\xi(x,y,z) = \underset{\sim}{M}_i \quad \text{for} \quad (x,y,z) \in D_i$$

where $D\xi$ denotes the Jacobian matrix of $\underset{\sim}{\xi}(x)$ and $\underset{\sim}{M}_i$ denotes a 3 × 3 real constant matrix

(P.4) ξ has 3 equilibrium points, one at the origin 0, one in the interior of D_1 (labeled P^+) and one in the interior of D_{-1} (labeled P^-).

(P.5)   Each matrix M_i has a pair of *complex conjugate* eigenvalues (labeled $\widetilde{\sigma}_0 \pm j\widetilde{\omega}_0$ for $\underset{\sim}{M}_0$ and $\widetilde{\sigma}_1 \pm j\widetilde{\omega}_1$ for $\underset{\sim}{M}_{-1}$ and $\underset{\sim}{M}_1$, where $\widetilde{\omega}_0 > 0$ and $\widetilde{\omega}_1 > 0$) and a *real* eigenvalue (labeled $\widetilde{\gamma}_0$ for $\underset{\sim}{M}_0$ and $\widetilde{\gamma}_1$ for $\underset{\sim}{M}_{-1}$ and $\underset{\sim}{M}_1$, where $\widetilde{\gamma}_0 \neq 0$ and $\widetilde{\gamma}_1 \neq 0$).

(P.6)   The *eigenspace* associated with either the *real* or the *complex* eigenvalues[‡] at each equilibrium point is not *parallel* to U_1 or U_{-1}.

Notations associated with Fig. 1

For each vector field $\xi \in \mathcal{L}$, define[*]

$E^c(0) \triangleq$ 2-dimensional eigenspace corresponding to *complex* eigenvalue $\widetilde{\sigma}_0 \pm j\widetilde{\omega}_0$ at 0.

$E^r(0) \triangleq$ 1-dimensional eigenspace corresponding to *real* eigenvalue $\widetilde{\gamma}_0$ at 0.

$E^c(P^+) \triangleq$ 2-dimensional eigenspace corresponding to *complex* eigenvalue $\widetilde{\sigma}_1 \pm j\widetilde{\omega}_1$ at P^+.

$E^r(P^+) \triangleq$ 1-dimensional eigenspace corresponding to *real* eigenvalue $\widetilde{\gamma}_1$ at P^+.

$L_0 \triangleq U_1 \cap E^c(0)$, $L_1 \triangleq U_1 \cap E^c(P^+)$

[†]To avoid clutter, we will often use row vector (x,y,z) in place of column vector $(x,y,z)^T$.

[‡]In the case where the eigenvalue is *complex*, the eigenspace is defined to be the vector space spanned by the real and the imaginary part of the complex eigenvector.

[*]Here, superscripts "c" and "r" denote "complex" and "real", respectively.

$$L_2 \triangleq \{\underset{\sim}{x} \in U_1 : \underset{\sim}{\xi}(\underset{\sim}{x}) \mathbin{/\!/} U_1\} \tag{2.1}$$

where $\mathbin{/\!/}$ reads "is parallel to." Here, $\underset{\sim}{\xi}(\underset{\sim}{x}) \mathbin{/\!/} U_1$ means the vector $\underset{\sim}{\xi}(\underset{\sim}{x})$ lies on a plane parallel to U_1. That L_2 is a straight line in Fig. 1 follows from the following:

Straight line tangency property:

Let $\underset{\sim}{\xi}$ be a *linear vector field in* $\mathbb{R}^3$ having a pair of complex conjugate eigenvalues $\tilde{\sigma} \pm j\tilde{\omega}$ and a real eigenvalue $\tilde{\gamma}$. Let U denote any plane which is not parallel to each eigenspace and which does not pass through the origin. Then

$$L \triangleq \{\underset{\sim}{x} \in U : \underset{\sim}{\xi}(\underset{\sim}{x}) \mathbin{/\!/} U\} \tag{2.2}$$

is a straight line.

Proof. In *Appendix 1* we prove the above assumptions imply that there exists a suitable coordinate system $\underset{\sim}{x}' \triangleq (x',y',z')$ in $\mathbb{R}^3$ such that $\underset{\sim}{\xi}$ is transformed into the *real Jordan form* [16].

$$\underset{\sim}{\xi}(\underset{\sim}{x}') = \begin{bmatrix} \tilde{\sigma} & -\tilde{\omega} & 0 \\ \tilde{\omega} & \tilde{\sigma} & 0 \\ 0 & 0 & \tilde{\gamma} \end{bmatrix} \begin{bmatrix} x' \\ y' \\ z' \end{bmatrix} \tag{2.3}$$

and such that the equation for U in the new coordinate system assumes the following simplified form:

$$U = \{(x',y',z') : x' + z' = 1\} \tag{2.4}$$

For each $\underset{\sim}{x} \in L$, (2.2) implies that the vector dot product $\langle \underset{\sim}{\xi}(\underset{\sim}{x}), \underset{\sim}{h} \rangle = 0$ where $\underset{\sim}{h} \triangleq (1,0,1)^T$ is a normal vector to U in view of (2.4). Substituting $\underset{\sim}{\xi}(\underset{\sim}{x})$ from (2.3) into the above vector dot product, and solving for y', we find that L in (2.2) is a straight line defined by the equations

$$L : y' = \sigma x' + \gamma(1-x') \quad , z' = 1-x' \tag{2.5}$$

where $\sigma \triangleq \tilde{\sigma}/\tilde{\omega}$ and $\gamma \triangleq \tilde{\gamma}/\tilde{\omega}$.

∎

Remark: The above straight line L intersects the line $\{(x',y',z') : x' = 1, z' = 0\}$ at the point $(x',y',z') = (1,\sigma,0)$.

We are now ready to define the following important points in Fig. 1:

$$A \triangleq L_0 \cap L_1 \quad , \quad B \triangleq L_1 \cap L_2$$
$$C \triangleq U_1 \cap E^r(0) \quad , \quad D \triangleq U_1 \cap E^r(P^+)$$
$$E \triangleq L_0 \cap L_2 \quad , \quad F \triangleq \{\underset{\sim}{x} \in L_2 : \underset{\sim}{\xi}(x) /\!\!/ L_2\}$$

where $\underset{\sim}{\xi}(x)/\!\!/L_2$ means the vector $\underset{\sim}{\xi}(x)$ lies on U_1 and is parallel to the straight line L_2.

For simplicity, we will often suppress the superscript + and write P instead of P^+. The following strategic points play a crucial role in *Section 3:*

Definition 2.2. Fundamental points of ξ

The 4 points A, B, E, and P defined above are called the fundamental points of ξ.

Note that the *continuity* of the vector field ξ implies that

$$\xi(A) /\!\!/ E^c(P) \quad , \quad \xi(A) /\!\!/ E^c(0)$$
$$\xi(B) /\!\!/ L_1 \quad , \quad \xi(E) /\!\!/ L_0$$
$$\xi(C) /\!\!/ E^r(0) \quad , \quad \xi(D) /\!\!/ E^r(P)$$

In general, each 3×3 matrix $\underset{\sim i}{M}$ defining a vector field $\xi \in \mathcal{L}$ in region D_i requires 9 non-zero parameters. Our next objective is to eliminate as many of these parameters as possible by reducing $\underset{\sim i}{M}$ to its Jordan form and $U_{\pm 1}$ to its simplified form.

Let $\Psi_0 : D_0 \to \mathbb{R}^3$ and $\Psi_1 : D_1 \to \mathbb{R}^3$ denote the appropriate *affine* transformations which reduce $\underset{\sim 0}{M}$ and $\underset{\sim 1}{M}$ to the Jordan form in (2.3) while simultaneously transforming the equation describing $U_{\pm 1}$ to the simplified form in (2.4). It follows from (2.3) and (2.4) that in terms of the new coordinate system, we have[†]

$a)$ $\Psi_0(0) = 0$ (2.6)

$\Psi_0(U_1) = V_0 \triangleq \{(x,y,z) : x + z = 1\}$ (2.7)

$\Psi_0(U_{-1}) = V_0^- \triangleq \{(x,y,z) : x + z = -1\}$ (2.8)

[†]Strictly speaking, we should use $\underset{\sim}{x}'$ and $\underset{\sim}{x}''$ to denote vectors in the new coordinate systems, as in (2.3) and (2.4). However, we will henceforth suppress the primes and double primes to avoid clutter. Since we will be dealing mostly with the new coordinate systems in the following sections, no confusion should arise.

$$\frac{1}{\tilde{\omega}_0} D\Psi_0\left[\xi(\Psi_0^{-1}\underset{\sim}{x})\right] = \xi_0(\underset{\sim}{x}) \triangleq \begin{bmatrix} \sigma_0 & -1 & 0 \\ 1 & \sigma_0 & 0 \\ 0 & 0 & \gamma_0 \end{bmatrix} \underset{\sim}{x} \tag{2.9}$$

where $\sigma_0 \triangleq \tilde{\sigma}_0/\tilde{\omega}_0$ and $\gamma_0 \triangleq \tilde{\gamma}_0/\tilde{\omega}_0$.

b) $\Psi_1(P) = 0$ $\tag{2.10}$

$$\Psi_1(U_1) = V_1 \triangleq \{(x,y,z): x + z = 1\} \tag{2.11}$$

$$\frac{1}{\tilde{\omega}_1} D\Psi_1(\xi(\Psi_1^{-1}(\underset{\sim}{x})) = \xi_1(\underset{\sim}{x}) \triangleq \begin{bmatrix} \sigma_1 & -1 & 0 \\ 1 & \sigma_1 & 0 \\ 0 & 0 & \gamma_1 \end{bmatrix} \underset{\sim}{x} \tag{2.12}$$

where $\sigma_1 \triangleq \tilde{\sigma}_1/\tilde{\omega}_1$ and $\gamma_1 \triangleq \tilde{\gamma}_1/\tilde{\omega}_1$. We will henceforth call (2.9) and (2.12) the *normalized Jordan form* of $\underset{\sim}{M}_0$ and $\underset{\sim}{M}_1$, respectively.

Definition 2.3. D_0-unit and D_1-unit of ξ

We define the set $\{\xi_0, V_0, \Psi_0\}$ as the D_0- *unit* of ξ and the set of $\{\xi_1, V_1, \Psi_1\}$ as the D_1- *unit of ξ*.

Geometrically, the D_0-unit of ξ is simply the middle region D_0 in its new reference frame (x',y',z') which we labeled simply as (x,y,z) in Fig. 2. It is important to keep in mind, however, that these two reference frames involve different coordinate systems.

The images of the important points A, B, C, D, E, and F in Fig. 1 will be denoted by corresponding subscripts in an obvious way:[†]

$D_0: A_0 \triangleq \Psi_0(A), \ B_0 \triangleq \Psi_0(B), \ C_0 \triangleq \Psi_0(C), \ D_0 \triangleq \Psi_0(D), \ E_0 \triangleq \Psi_0(E), \ F_0 \triangleq \Psi_0(F).$

$D_1: A_1 \triangleq \Psi_1(A), \ B_1 \triangleq \Psi_1(B), \ C_1 \triangleq \Psi_1(C), \ D_1 \triangleq \Psi_1(D), \ E_1 \triangleq \Psi_1(E), \ F_1 \triangleq \Psi_1(F).$

Our next goal is to derive the coordinates of each of these points in their new reference frames. Since A, B, C, D, E, and F are located on various intersection lines in Fig. 1, their images (under any affine transformation) must lie on corresponding lines in the new reference frames. These lines are images of intersections between various eigenspaces ($E^c(0)$ or $E^r(0)$) with the plane U_1 in Fig. 1. In particular, it can be shown that

---

[†]Note that the same symbols D_0 and D_1 are used to denote a *region* in Fig. 2(a) and a *point* in Fig. 2(b). There will be no confusion, however, since its meaning will be clear from the context.

$$\Psi_0(E^c(0)) = \{(x,y,z): z = 0\} \text{ ,i.e., the x-y plane} \tag{2.13}$$

$$\Psi_0(E^r(0)) = \{(x,y,z): x = y = 0\} \text{ ,i.e., the z-axis} \tag{2.14}$$

$$\Psi_0(L_0) = \{(x,y,z): x = 1 , z = 0\} \tag{2.15}$$

$$\Psi_0(L_2) = \{(x,y,z): y = \sigma_0 x + \gamma_0(1-x) , z = 1-x\} \tag{2.16}$$

Since $C = E^r(0) \cap U_1$, it follows from (2.14) and (2.7) that $C_0 = (0,0,1)$.

Since $E = L_0 \cap L_2$, it follows from (2.15) and (2.16) that $E_0 = (1,\sigma_0,0)$.

Since $F \in L_2$ and $\xi(F)/\!/ L_2$, it follows that $F_0 \in \Psi_0(L_2)$ and $\xi_0(F_0)/\!/ \Psi_0(L_2)$. Hence the coordinate of F_0 must satisfy

$$y = \sigma_0 x + \gamma_0(1-x) , z = 1-x , \frac{\sigma_0 x - y}{1} = \frac{x + \sigma_0 y}{\sigma_0 - \gamma_0} = \frac{\gamma_0 z}{-1} . \tag{2.17}$$

Since A_0 lies on the line $\Psi_0(L_0)$, we can write $A_0 = (1,p_0,0)$ for some $p_0 \in \mathbb{R}$.

Since $B = L_1 \cap L_2$ and $\xi(B)/\!/ L_1$, the coordinate of B_0 is determined by $B_0 \in \Psi_0(L_2)$ and $\xi_0(B_0)/\!/ \overrightarrow{B_0 A_0}$ where the "arrow" denotes the vector from B_0 to A_0. Since B_0, E_0, and F_0 all lie on the line $\Psi_0(L_2)$, it follows that

$$\overrightarrow{F_0 B_0} = k_0 \overrightarrow{E_0 F_0} \tag{2.18}$$

where k_0 is a scaling constant.

Similarly, we can derive the coordinate of A_1, B_1, D_1, E_1, and F_1 in the new reference frame for the D_1-unit in Fig. 2 and obtain

$$\overrightarrow{E_1 F_1} = k_1 \overrightarrow{F_1 B_1} \tag{2.19}$$

where k_1 is a scaling constant.

For future reference, the explicit coordinate for the image of all strategic points in Fig. 1 are tabulated below:

Strategic points in D_0-unit $(\sigma_0 \triangleq \tilde{\sigma}_0 / \tilde{\omega}_0, \gamma_0 \triangleq \tilde{\gamma}_0 / \tilde{\omega}_0)$

$$A_0 = (1,p_0,0) . \tag{2.20}$$

where[†]

[†]The two expressions in (2.21) (resp. (2.27)) are equivalent to each other. The value of k_0 (resp., k_1) is specified in (2.33).

$$p_0 \triangleq \sigma_0 + \frac{k_0}{\gamma_0}(\sigma_0^2+1) \; , \; k_0 \triangleq \gamma_0(p_0-\sigma_0)/(\sigma_0^2+1) \tag{2.21}$$

$$B_0 = (\gamma_0(\gamma_0-\sigma_0-p_0)/Q_0 \, , \, \gamma_0[1-p_0(\sigma_0-\gamma_0)]/Q_0 \, , \, 1-\gamma_0(\gamma_0-\sigma_0-p_0)/Q_0) \tag{2.22}$$

where $Q_0 \triangleq (\sigma_0-\gamma_0)^2 + 1$

$$C_0 = (0,0,1) \tag{2.23}$$

$$E_0 = (1,\sigma_0,0) \tag{2.24}$$

$$F_0 = (\gamma_0(\gamma_0-2\sigma_0)/Q_0 \, , \, \gamma_0[1-\sigma_0(\sigma_0-\gamma_0)]/Q_0 \, , \, (\sigma_0^2+1)/Q_0) \tag{2.25}$$

Strategic points in D_1-unit ($\sigma_1 \triangleq \tilde{\sigma}_1/\tilde{\omega}_1 \, , \, \gamma_1 \triangleq \tilde{\gamma}_1/\tilde{\omega}_1$)

$$A_1 = (1,p_1,0) \tag{2.26}$$

where

$$p_1 \triangleq \sigma_1 + k_1(\sigma_1^2+1)/\gamma_1 \, , \, k_1 \triangleq \gamma_1(p_1-\sigma_1)/(\sigma_1^2+1) \tag{2.27}$$

$$B_1 = (1,\sigma_1,0) \tag{2.28}$$

$$D_1 = (0,0,1) \tag{2.29}$$

$$E_1 = (\gamma_1(\gamma_1-\sigma_1-p_1)/Q_1 \, , \, \gamma_1[1-p_1(\sigma_1-\gamma_1)]/Q_1 \, , \, 1-\gamma_1(\gamma_1-\sigma_1-p_1)/Q_1) \tag{2.30}$$

where

$$Q_1 \triangleq (\sigma_1-\gamma_1)^2 + 1 \tag{2.31}$$

$$F_1 = (\gamma_1(\gamma_1-2\sigma_1)/Q_1 \, , \, \gamma_1[1-\sigma_1(\sigma_1-\gamma_1)]/Q_1 \, , \, (\sigma_1^2+1)/Q_1) \tag{2.32}$$

Note that k_0 can not be calculated directly from (2.21) since it depends on p_0 which in turn depends on k_0. A similar situation applies to k_1 in (2.27). However, they can be easily calculated from the relationship

$$k_0 = 1/k_1 = k \triangleq -\tilde{\gamma}_0/\tilde{\gamma}_1 \tag{2.33}$$

which will be derived in *Section 3*. The relationship

$$k_0 k_1 = 1 \tag{2.34}$$

follows from the ratio between the lengths (denoted by $|\cdot|$) of the following vectors (see Fig. 2):

$$\frac{|\overrightarrow{F_0 B_0}|}{|\overrightarrow{E_0 F_0}|} = \frac{|\overrightarrow{F_1 B_1}|}{|\overrightarrow{E_1 F_1}|}$$

(2.35)

The above explicit expressions for the coordinates of the strategic points in the D_0-unit and the D_1-unit will play a crucial role in our derivation of Poincare maps in *Section 4*.

3. CANONICAL PIECEWISE-LINEAR NORMAL FORM

In Section 2 we have defined a very large family $\mathcal{L}$ of continuous piecewise-linear vector fields. From the circuit-theoretic point of view, $\mathcal{L}$ represents the family of all 3rd order piecewise-linear circuits whose vector fields satisfy (P1)-(P6) of Definition 1. Our objective in this section is to partition this family into "equivalence classes" so that all vector fields belonging to a given equivalence class have identical *qualitative* behaviors. We will define 2 forms of equivalence; namely, *linear equivalence* and *linear conjugacy*.

From the circuit-theoretic point of view, two circuits are said to be *linearly equivalent* iff, except possibly for a *uniform* change in the time scale, their respective solutions are qualitatively identical. If the same property holds with *the same* time scale, then the two circuits are said to be *linearly conjugate*. For example, two 1 *st* -order autonomous RC circuits [17] with time constants τ_1 and τ_2 are linearly equivalent but *not* linearly conjugate unless $\tau_1 = \tau_2$. Hence, 2 linearly conjugate but distinct vector fields essentially represent the *same* circuit but with 2 different choices of state variables which are related to each other by a linear transformation. We will now define these two concepts precisely.

Definition 3.1. Linear Equivalence

Two vector fields ξ and ξ' in $\mathbb{R}^n$ are said to be *linearly equivalent* iff there exists a *linear transformation* $G : \mathbb{R}^n \to \mathbb{R}^n$ and a real number $\nu > 0$ such that[†]

$$G \circ \xi = \nu(\xi' \circ G)$$

(3.1)

Definition 3.2. Linear Conjugacy

Two *linearly-equivalent* vector fields are said to be *linearly conjugate* of each other iff $\nu = 1$ in (3.1).

The concept of linear conjugacy is a special case of the well-known concept of *topological conjugacy* [9] where the "linear transformation " is replaced by a "homeomorphism." In general, it is extremely difficult if not impossible to prove two nonlinear vector fields are

---

[†]Here, " $\circ$ " denotes a "composition" operation. Hence (3.1) implies for each $\underset{\sim}{x} \in \mathbb{R}^n$, $G(\xi(\underset{\sim}{x})) = \nu(\xi'(G\underset{\sim}{x}))$.

topologically conjugate, let alone linearly conjugate. It is therefore remarkable that for the class of vector fields $\xi \in \mathcal{A}$, we can not only classify them into equivalence classes, but we can derive the explicit form of one vector field--called the *normal form* --in each equivalence class which is selected in accordance to a unified approach.

Recall from *Definition 2.1* that for each vector field $\xi \in \mathcal{A}$, the associated eigenvalues are denoted by $\tilde{\sigma}_0 \pm j\tilde{\omega}_0$ and $\tilde{\gamma}_0$ for $\underset{\sim}{M}_0$, and $\tilde{\sigma}_1 \pm j\tilde{\omega}_1$ and $\tilde{\gamma}_1$ for $\underset{\sim}{M}_1$. Because ξ is a *continuous* vector field by definition, these eigenvalues are constrained in some definite way so that arbitrarily specified eigenvalues of the above form may *not* correspond to a vector field in $\mathcal{A}$. Our main result in this section is to derive this constraint among the eigenvalues and to use them to completely characterize the class of all linearly conjugate vector fields.

Theorem 3.1. Linear Conjugacy Criteria

(a) For each set of eigenvalues defined by the 6 "eigenvalue parameters"

$$\{\tilde{\sigma}_0, \tilde{\omega}_0, \tilde{\gamma}_0, \tilde{\sigma}_1, \tilde{\omega}_1, \tilde{\gamma}_1\} \tag{3.2}$$

there exists a vector field $\xi \in \mathcal{A}$ having these eigenvalues <=>

$$\tilde{\omega}_0 > 0, \quad \tilde{\omega}_1 > 0, \quad \text{and } \tilde{\gamma}_0 \tilde{\gamma}_1 < 0 \tag{3.3}$$

(b) Two vector fields $\xi \in \mathcal{A}$ and $\xi' \in \mathcal{A}$ are *linearly conjugate* of each other <=> they have identical eigenvalues; i.e.,

$$\tilde{\sigma}_0 = \tilde{\sigma}_0', \quad \tilde{\omega}_0 = \tilde{\omega}_0', \quad \tilde{\gamma}_0 = \tilde{\gamma}_0'$$
$$\tilde{\sigma}_1 = \tilde{\sigma}_1', \quad \tilde{\omega}_1 = \tilde{\omega}_1', \quad \tilde{\gamma}_1 = \tilde{\gamma}_1' \tag{3.4}$$

Proof. We will first state and prove *Theorem 3.2* and then prove that it is equivalent to *Theorem 3.1*. We will then prove Theorem 3.2 since it is easier. Moreover, it is Theorem 3.2 (and not Theorem 3.1) which will be used in the following sections.

Definition 3.3. Normalized eigenvalue parameters

For each set of eigenvalues defined by the 6 eigenvalue parameters $\{\tilde{\sigma}_0, \tilde{\omega}_0, \tilde{\gamma}_0, \tilde{\sigma}_1, \tilde{\omega}_1, \tilde{\gamma}_1\}$, we define 5 *normalized eigenvalue parameters*

$$\{\sigma_0, \gamma_0, \sigma_1, \gamma_1, k\} \tag{3.5}$$

where

$$\sigma_0 \triangleq \frac{\tilde{\sigma}_0}{\tilde{\omega}_0}, \; \gamma_0 \triangleq \frac{\tilde{\gamma}_0}{\tilde{\omega}_0}, \; \sigma_1 \triangleq \frac{\tilde{\sigma}_1}{\tilde{\omega}_1}, \; \gamma_1 \triangleq \frac{\tilde{\gamma}_1}{\tilde{\omega}_1}, \; k \triangleq -\frac{\tilde{\gamma}_0}{\tilde{\gamma}_1} \tag{3.6}$$

Note that one more parameter must / be specified before the eigenvalues associated with (3.5)

can be *uniquely* recovered.

Theorem 3.2. Linear Equivalence Criteria

(a) There exists a continuous vector field $\xi \in \mathcal{L}$ having (3.5) as normalized eigenvalue parameters $\Longleftrightarrow$

$$\gamma_0\gamma_1 < 0 \quad \text{and} \quad k > 0 \tag{3.7}$$

(b) Two vector fields $\xi \in \mathcal{L}$ and $\xi' \in \mathcal{L}$ are *linearly equivalent* $\Longleftrightarrow$ they have identical normalized eigenvalue parameters. Moreover, the positive scaling constant in (3.1) is given by

$$\nu = \tilde{\omega}_0 / \tilde{\omega}_0' = \tilde{\omega}_1 / \tilde{\omega}_1' \tag{3.8}$$

Note that the eigenvalues of two distinct vector fields having *identical* normalized eigenvalue parameters are generally *not* identical because one more parameter must be specified in order to identify the eigenvalues uniquely. It follows from *Theorem 3.1* that two vector fields having identical normalized eigenvalue parameters are generally *not* linearly conjugate to each other. Indeed, (3.8) implies that the additional condition $\tilde{\omega}_0 = \tilde{\omega}_0'$ is needed for linear conjugacy.

Lemma 3.1.

Theorems 3.1 and 3.2 are equivalent.

Proof.

$\Longrightarrow$ Suppose *Theorem 3.1* holds. Then it follows from (3.3) that $\tilde{\gamma}_0\tilde{\gamma}_1 / \tilde{\omega}_0\tilde{\omega}_1 < 0$ and hence (3.7) holds. Conversely, given any $\{\sigma_0, \gamma_0, \sigma_1, \gamma_1, k\}$ satisfying (3.7), define

$$\{\tilde{\sigma}_0, \tilde{\omega}_0, \tilde{\gamma}_0, \tilde{\sigma}_1, \tilde{\omega}_1, \tilde{\gamma}_1\} \triangleq \{\sigma_0, 1, \gamma_0, -\sigma_1\gamma_0 / \gamma_1 k, -\gamma_0 / \gamma_1 k, -\gamma_0 / k\} \tag{3.9}$$

Since $\tilde{\omega}_1 \triangleq -\gamma_0 / \gamma_1 k > 0$ and $\tilde{\gamma}_0\tilde{\gamma}_1 = -\gamma_0^2 / k < 0$, (3.9) satisfies (3.3) and hence Theorem 3.1 implies there exists $\xi \in \mathcal{L}$ associated with (3.9). This proves (a) of *Theorem 3.2*.

To prove (b) of *Theorem 3.2*, suppose ξ and ξ' are linearly equivalent and hence $G \circ \xi = \dfrac{\tilde{\omega}_0}{\tilde{\omega}_0'}\xi' \circ G$ holds for some G. Then the two vector fields ξ and $(\dfrac{\tilde{\omega}_0}{\tilde{\omega}_0'})\xi'$ are linearly conjugate and must have identical eigenvalue parameters $\{\tilde{\sigma}_0, \tilde{\omega}_0, \tilde{\gamma}_0, \tilde{\sigma}_1, \tilde{\omega}_1, \tilde{\gamma}_1\}$. It follows that the eigenvalue parameters of ξ' are given by $\left\{\dfrac{\tilde{\sigma}_0\tilde{\omega}_0'}{\tilde{\omega}_0}, \tilde{\omega}_0', \dfrac{\tilde{\gamma}_0\tilde{\omega}_0'}{\tilde{\omega}_0}, \dfrac{\tilde{\sigma}_1\tilde{\omega}_0'}{\tilde{\omega}_0}, \dfrac{\tilde{\omega}_1\omega_0'}{\tilde{\omega}_0}, \dfrac{\tilde{\gamma}_1\tilde{\omega}_0'}{\tilde{\omega}_0}\right\}$. Using (3.6), we obtain the following normalized eigenvalue parameters of ξ' $\left\{\dfrac{\tilde{\sigma}_0}{\tilde{\omega}_0}, \dfrac{\tilde{\gamma}_0}{\tilde{\omega}_0}, \dfrac{\tilde{\sigma}_1}{\tilde{\omega}_1}, \dfrac{\tilde{\gamma}_1}{\tilde{\omega}_1}, -\dfrac{\tilde{\gamma}_0}{\tilde{\gamma}_1}\right\} = \{\sigma_0, \gamma_0, \sigma_1, \gamma_1, k\}$, which are identical to those of ξ.

Conversely, suppose $\left\{\dfrac{\tilde{\sigma}_0}{\tilde{\omega}_0}, \dfrac{\tilde{\gamma}_0}{\tilde{\omega}_0}, \dfrac{\tilde{\sigma}_1}{\tilde{\omega}_1}, \dfrac{\tilde{\gamma}_1}{\tilde{\omega}_1}, -\dfrac{\tilde{\gamma}_0}{\tilde{\gamma}_1}\right\} = \left\{\dfrac{\tilde{\sigma}_0'}{\tilde{\omega}_0'}, \dfrac{\tilde{\gamma}_0'}{\tilde{\omega}_0'}, \dfrac{\tilde{\sigma}_1'}{\tilde{\omega}_1'}, \dfrac{\tilde{\gamma}_1'}{\tilde{\omega}_1'}, -\dfrac{\tilde{\gamma}_0'}{\tilde{\gamma}_1'}\right\}$, then

$\left\{\tilde{\sigma}_0, \tilde{\omega}_0, \tilde{\gamma}_0, \tilde{\sigma}_1, \tilde{\omega}_1, \tilde{\gamma}_1\right\} = \left[\dfrac{\tilde{\omega}_0}{\tilde{\omega}_0'}\right] (\tilde{\sigma}_0', \tilde{\omega}_0', \tilde{\gamma}_0', \tilde{\sigma}_1', \tilde{\omega}_1', \tilde{\gamma}_1')$, and hence ξ and $\left[\dfrac{\tilde{\omega}_0}{\tilde{\omega}_0'}\right] \xi'$ are linearly conjugate to each other.

The above proves *Theorem 3.2* holds.

$\Leftarrow$ Suppose *Theorem 3.2* holds. Then given $\xi \in \mathcal{L}$, its associated $k = -\tilde{\gamma}_0/\tilde{\gamma}_1 > 0$ in view of (3.7), and hence $\tilde{\gamma}_0\tilde{\gamma}_1 < 0$. Moreover, $\tilde{\omega}_0 > 0$ and $\tilde{\omega}_1 > 0$ by definition. Hence, (3.3) holds. Conversely, given any set of eigenvalue parameters (3.2) satisfying (3.3). Its associated set of normalized eigenvalue parameters $\left\{\dfrac{\tilde{\sigma}_0}{\tilde{\omega}_0}, \dfrac{\tilde{\gamma}_0}{\tilde{\omega}_0}, \dfrac{\tilde{\sigma}_1}{\tilde{\omega}_1}, \dfrac{\tilde{\gamma}_1}{\tilde{\omega}_1}, \dfrac{-\tilde{\gamma}_0}{\tilde{\gamma}_1}\right\}$ clearly satisfies (3.7). It follows from *Theorem 3.2* that there exists a vector field $\xi' \in \mathcal{L}$ having these normalized eigenvalue parameters and $\left[\dfrac{\tilde{\omega}_0}{\tilde{\omega}_0'}\right] \xi' \in \mathcal{L}$ is linearly conjugate to ξ. Hence $\left[\dfrac{\tilde{\omega}_0}{\tilde{\omega}_0'}\right] \xi'$ and ξ have identical eigenvalue parameters; namely, $\{\tilde{\sigma}_0, \tilde{\omega}_0, \tilde{\gamma}_0, \tilde{\sigma}_1, \tilde{\omega}_1, \tilde{\gamma}_1\}$. Hence, ξ is the desired vector field.

To prove (b) of *Theorem 3.1* holds, suppose $G \circ \xi = \xi' \circ G$ holds for some G. Then, ξ and ξ' have identical normalized eigenvalue parameters $\left\{\dfrac{\tilde{\sigma}_0}{\tilde{\omega}_0}, \dfrac{\tilde{\gamma}_0}{\tilde{\omega}_0}, \dfrac{\tilde{\sigma}_1}{\tilde{\omega}_1}, \dfrac{\tilde{\gamma}_1}{\tilde{\omega}_1}, \dfrac{-\tilde{\gamma}_0}{\tilde{\gamma}_1}\right\} = \left\{\dfrac{\tilde{\sigma}_0'}{\tilde{\omega}_0'}, \dfrac{\tilde{\gamma}_0'}{\tilde{\omega}_0'}, \dfrac{\tilde{\sigma}_1'}{\tilde{\omega}_1'}, \dfrac{\tilde{\gamma}_1'}{\tilde{\omega}_1'}, \dfrac{-\tilde{\gamma}_0'}{\tilde{\gamma}_1'}\right\}$ and $\nu \triangleq \tilde{\omega}_0/\tilde{\omega}_0' = 1$. Hence, ξ and ξ' have identical eigenvalues.

Conversely, if ξ and ξ' have identical eigenvalues, then they have identical normalized eigenvalue parameters and $\nu \triangleq \tilde{\omega}_0/\tilde{\omega}_0' = 1$. It follows from *Theorem 3.2 (b)* that $G \circ \xi = \xi' \circ G$ and hence ξ and ξ' are linearly conjugate to each other.

This proves *Theorem 3.1* holds.

∎

Remark

Since two linearly-conjugate vector fields in $\mathcal{L}$ represent the same circuit (with different choice of state variables), or two equivalent circuits, the concept of *linear conjugacy* is too strong for "qualitative" analysis. Since our goal is to characterize classes of nonlinear circuits exhibiting similar qualitative behaviors, quantitative differences in circuit time constants are irrelevant: two series RC circuits with different time constants exhibit identical qualitative behaviors and belong therefore to the same class. It is not surprising therefore that the weaker concept of *linear equivalence* is all that we need to study the qualitative properties of

piecewise-linear vector fields.

Before proving *Theorem 3.2*, we need the following result:

Lemma 3.2.

Let $\xi[\underset{\sim}{\mu}]$ denote the family of all vector fields in $\mathcal{L}$ having the *same* normalized eigenvalue parameters $\underset{\sim}{\mu} \triangleq (\sigma_0, \gamma_0, \sigma_1, \gamma_1, k)$. Let $\overrightarrow{OP}$, $\overrightarrow{OA}$, $\overrightarrow{OB}$ and $\overrightarrow{OE}$ denote the 4 vectors from the origin 0 in Fig. 1 to the 4 *fundamental points* P, A, B, and E (Def. 2.2), respectively. Then the following properties hold:

(a) All polyhedrons whose vertices consist of the origin and the 4 fundamental points of vector fields belonging to the family $\xi[\underset{\sim}{\mu}]$ are *similar* in the sense that

$$\overrightarrow{OP} = l\ \overrightarrow{OA} + m\ \overrightarrow{OB} + n\ \overrightarrow{OE} \tag{3.10}$$

where $l = l(\underset{\sim}{\mu})$, $m = m(\underset{\sim}{\mu})$ and $n = n(\underset{\sim}{\mu})$ are real numbers which depend only on $\underset{\sim}{\mu}$ and hence are identical for all vector fields in $\xi[\underset{\sim}{\mu}]$.

(b) The numbers k_0, k_1, and k defined in (2.21), (2.27), and (3.6) are related by

$$k = k_0 = 1/k_1 \ . \tag{3.11}$$

(c) There exists a vector field $\xi \in \xi[\underset{\sim}{\mu}]$ <=>

$$\gamma_0 \gamma_1 < 0 \ \text{ and } \ k > 0 \tag{3.12}$$

Proof. See *Appendix 2*.

Proof of Theorem 3.2

Statement (a) is equivalent to statement (c) in *Lemma 3.2* and   is   proved in *Appendix 2. It remains to prove statement (b)*.

=> Suppose there exist a linear transformation G and a real number $\nu > 0$ such that $G \circ \xi = \nu \xi' \circ G$, then the eigenvalues of ξ and ξ' must satisfy $\tilde{\sigma}_i \pm j\tilde{\omega}_i = \nu\tilde{\sigma}'_i \pm j\nu\tilde{\omega}'_i$ and $\tilde{\gamma}_i = \nu\tilde{\gamma}'_i$, (i = 0,1). It follows from (3.6) that their respective *normalized* eigenvalue parameters are identical.

<= Let $\xi[\underset{\sim}{\mu}]$ be the family of all vector fields in $\mathcal{L}$ having the *same* $\underset{\sim}{\mu} = (\sigma_0, \gamma_0, \sigma_1, \gamma_1, k)$ as their normalized eigenvalue parameters. Let $\tilde{\sigma}_i \pm j\tilde{\omega}_i$ ($\tilde{\omega}_i > 0$) and $\tilde{\gamma}_i \neq 0$, (i = 0,1) denote the eigenvalues of $\xi \in \xi[\underset{\sim}{\mu}]$ and let $\tilde{\sigma}'_i \pm j\tilde{\omega}'_i$ ($\tilde{\omega}'_i > 0$) and $\tilde{\gamma}'_i \neq 0$ (i = 0,1) denote the eigenvalue of $\xi' \in \xi[\underset{\sim}{\mu}]$. Denote the *fundamental points*/ξ and ξ' by $\{A, B, E, P\}$ and

$\{A',B',E',P'\}$, respectively. Let the vector from the origin to these points be denoted by $\{\underset{\sim}{A},\underset{\sim}{B},\underset{\sim}{E},\underset{\sim}{P}\}$ and $\{\underset{\sim}{A'},\underset{\sim}{B'},\underset{\sim}{E'},\underset{\sim}{P'}\}$ respectively.

Hence $\underset{\sim}{A} = (A_x,A_y,A_z)$ where (A_x,A_y,A_z) denotes the coordinate of the point A.

By (P.3) of *Definition 2.1*, there exist matrices $\underset{\sim i}{M}$ and $\underset{\sim i}{M'}$ (i = 0,1) such that

$$\xi(\underset{\sim}{x}) = \begin{cases} \underset{\sim 1}{M}(\underset{\sim}{x}-\underset{\sim}{P}) & , \underset{\sim}{x} \in D_1 \\ \underset{\sim 0}{M}\underset{\sim}{x} & , \underset{\sim}{x} \in D_0 \\ \underset{\sim 1}{M}(\underset{\sim}{x}+\underset{\sim}{P}) & , \underset{\sim}{x} \in D_{-1} \end{cases} \text{ and } \xi'(\underset{\sim}{x}) = \begin{cases} \underset{\sim 1}{M'}(\underset{\sim}{x}-\underset{\sim}{P}) & , \underset{\sim}{x} \in D_1' \\ \underset{\sim 0}{M'}\underset{\sim}{x} & , \underset{\sim}{x} \in D_0' \\ \underset{\sim 1}{M'}(\underset{\sim}{x}+\underset{\sim}{P}) & , \underset{\sim}{x} \in D_{-1}' \end{cases} \qquad (3.13)$$

where D_i and D_i' (i = 0, ±1) are the affine regions of ξ and ξ', respectively. It follows from the *continuity of* ξ and ξ' that

$$\underset{\sim 0}{M}[\underset{\sim}{A},\underset{\sim}{B},\underset{\sim}{E}] = \underset{\sim 1}{M}[\underset{\sim}{A}-\underset{\sim}{P},\underset{\sim}{B}-\underset{\sim}{P},\underset{\sim}{E}-\underset{\sim}{P}] \qquad (3.14)$$

$$\underset{\sim 0}{M'}[\underset{\sim}{A'},\underset{\sim}{B'},\underset{\sim}{E'}] = \underset{\sim 1}{M'}[\underset{\sim}{A'}-\underset{\sim}{P'},\underset{\sim}{B'}-\underset{\sim}{P'},\underset{\sim}{E'}-\underset{\sim}{P'}] \qquad (3.15)$$

where $[\cdot]$ denotes a 3 × 3 matrix made up of various column vectors defined above.

Now recall that the normalized Jordan forms of $\underset{\sim 0}{M}$ in (2.9), and $\underset{\sim 1}{M}$ in (2.12) are obtained by two appropriate affine transformations Ψ_0 and Ψ_1. It follows from (2.6) and (2.10) that Ψ_0 and Ψ_1 can be expressed by

$$\Psi_0(\underset{\sim}{x}) = \underset{\sim 0}{\Phi}\underset{\sim}{x} \qquad (3.16)$$

and

$$\Psi_1(\underset{\sim}{x}) = \underset{\sim 1}{\Phi}(\underset{\sim}{x}-\underset{\sim}{P}) \qquad (3.17)$$

where $\underset{\sim 0}{\Phi}$ and $\underset{\sim 1}{\Phi}$ are 3 × 3 matrices to be determined as follow: Since Ψ_0 maps $\{A,B,E\}$ into $\{A_0,B_0,E_0\}$, we have

$$\underset{\sim 0}{\Phi}[\underset{\sim}{A},\underset{\sim}{B},\underset{\sim}{E}] = [\underset{\sim 0}{A},\underset{\sim 0}{B},\underset{\sim 0}{E}] \Rightarrow$$

$$\underset{\sim 0}{\Phi} = [\underset{\sim 0}{A},\underset{\sim 0}{B},\underset{\sim 0}{E}][\underset{\sim}{A},\underset{\sim}{B},\underset{\sim}{E}]^{-1} \qquad (3.18)$$

Similarly, since Ψ_1 maps $\{A,B,E\}$ into $\{A_1,B_1,E_1\}$, we have

$$\Phi_1[\underset{\sim}{A}-\underset{\sim}{P},\underset{\sim}{B}-\underset{\sim}{P},\underset{\sim}{E}-\underset{\sim}{P}] = [\underset{\sim 1}{A},\underset{\sim 1}{B},\underset{\sim 1}{E}] \Rightarrow$$

$$\Phi_{\sim 1} = [A_{\sim 1}, B_{\sim 1}, E_{\sim 1}] \, [A_{\sim}-P_{\sim}, B_{\sim}-P_{\sim}, E_{\sim}-P_{\sim}]^{-1} \tag{3.19}$$

It follows from (2.9) and (2.12) that

$$\frac{1}{\widetilde{\omega}_i}(\Phi_{\sim i} \, M_{\sim i} \, \Phi_{\sim i}^{-1}) = J_{\sim i} \quad , \quad (i = 0,1) \tag{3.20}$$

where

$$J_{\sim i} \triangleq \begin{bmatrix} \sigma_i & -1 & 0 \\ 1 & \sigma_i & 0 \\ 0 & 0 & \gamma_i \end{bmatrix} \tag{3.21}$$

Now, by hypothesis, ξ and ξ' have identical *normalized* eigenvalue parameters. Hence their respective normalized Jordan forms $J_{\sim 0}$ and $J_{\sim 0}'$ of $M_{\sim 0}$ and $M_{\sim 0}'$ are identical. Substituting (3.18) into (3.20), we obtain

$$
\begin{aligned}
J_{\sim 0} &= \frac{1}{\widetilde{\omega}_0}[A_{\sim 0}, B_{\sim 0}, E_{\sim 0}] \, [A_{\sim}, B_{\sim}, E_{\sim}]^{-1} M_{\sim 0}[A_{\sim}, B_{\sim}, E_{\sim}][A_{\sim 0}, B_{\sim 0}, E_{\sim 0}]^{-1} \\
&= \frac{1}{\widetilde{\omega}_0'}[A_{\sim 0}, B_{\sim 0}, E_{\sim 0}][A_{\sim}', B_{\sim}', E_{\sim}']^{-1} M_{\sim 0}'[A_{\sim}', B_{\sim}', E_{\sim}'][A_{\sim 0}, B_{\sim 0}, E_{\sim 0}]^{-1} = J_{\sim 0}'
\end{aligned}
\tag{3.22}
$$

Let us define next a linear transformation $G : \mathbb{R}^3 \to \mathbb{R}^3$ and a real number $\nu > 0$ as follow:

$$G_{\sim} \triangleq [A_{\sim}', B_{\sim}', E_{\sim}'][A_{\sim}, B_{\sim}, E_{\sim}]^{-1} \quad , \quad \nu \triangleq \widetilde{\omega}_0 / \widetilde{\omega}_0' \tag{3.23}$$

Premultiplying both sides of (3.22) by $\widetilde{\omega}_0[A_{\sim}', B_{\sim}', E_{\sim}'] \, [A_{\sim 0}, B_{\sim 0}, E_{\sim 0}]^{-1}$ and postmultiplying both sides by $[A_{\sim 0}, B_{\sim 0}, E_{\sim 0}] \, [A_{\sim}', B_{\sim}', E_{\sim}']^{-1}$, we obtain

$$[A_{\sim}', B_{\sim}', E_{\sim}'][A_{\sim}, B_{\sim}, E_{\sim}]^{-1} M_{\sim 0}[A_{\sim}, B_{\sim}, E_{\sim}][A_{\sim}', B_{\sim}', E_{\sim}']^{-1} = \left(\frac{\widetilde{\omega}_0}{\widetilde{\omega}_0'}\right) M_{\sim 0}' \tag{3.24}$$

Substituting (3.23) into (3.24) we obtain

$$\nu M_{\sim 0}' = G_{\sim} M_{\sim 0} G_{\sim}^{-1} \tag{3.25}$$

Equation (3.23) implies

$$\nu \xi'(x_{\sim})|_{D_0} = G_{\sim}(\xi(G_{\sim}^{-1} x_{\sim})|_{D_0}), \quad x_{\sim} \in D_0' \tag{3.26}$$

Now rewrite (3.10) from *Lemma 3.2* in the following vector form:

$$\underset{\sim}{P} = [\underset{\sim}{A},\underset{\sim}{B},\underset{\sim}{E}][l,m,n]^T \ , \ \underset{\sim}{P'} = [\underset{\sim}{A'},\underset{\sim}{B'},\underset{\sim}{E'}][l,m,n]^T \qquad (3.27)$$

But

$$\underset{\sim}{G}\underset{\sim}{P} = \underset{\sim}{G}[\underset{\sim}{A},\underset{\sim}{B},\underset{\sim}{E}][l,m,n]^T = [\underset{\sim}{A'}\underset{\sim}{B'}\underset{\sim}{E'}][l,m,n]^T = P' \qquad (3.28) \ -$$

Now solving (3.15) for $\underset{\sim}{M'_1}$ and (3.14) for $\underset{\sim}{M_1}$ and using (3.25) and (3.23) repeatedly, we obtain

$$
\begin{aligned}
\nu \underset{\sim}{M'_1} &= \nu \underset{\sim}{M'_0}[\underset{\sim}{A'},\underset{\sim}{B'},\underset{\sim}{E'}][\underset{\sim}{A'}-\underset{\sim}{P'},\underset{\sim}{B'}-\underset{\sim}{P'},\underset{\sim}{E'}-\underset{\sim}{P'}]^{-1} \\[4pt]
&= \underset{\sim}{G}\underset{\sim}{M_0}\underset{\sim}{G}^{-1}[\underset{\sim}{A'},\underset{\sim}{B'},\underset{\sim}{E'}][\underset{\sim}{G}(\underset{\sim}{A}-\underset{\sim}{P}),\underset{\sim}{G}(\underset{\sim}{B}-\underset{\sim}{P}),\underset{\sim}{G}(\underset{\sim}{E}-\underset{\sim}{P})]^{-1} \\[4pt]
&= \underset{\sim}{G}\underset{\sim}{M_0}[\underset{\sim}{A},\underset{\sim}{B},\underset{\sim}{E}][\underset{\sim}{A}-\underset{\sim}{P},\underset{\sim}{B}-\underset{\sim}{P},\underset{\sim}{E}-\underset{\sim}{P}]^{-1}\underset{\sim}{G}^{-1} \\[4pt]
&= \underset{\sim}{G}\underset{\sim}{M_1}\underset{\sim}{G}^{-1}
\end{aligned}
\qquad (3.29)
$$

Now for any $\underset{\sim}{x} \in D'_{\pm 1}$, (3.13) implies

$$
\begin{aligned}
\nu \, \underset{\sim}{\xi'}(\underset{\sim}{x})\Big|_{D'_{\pm 1}} &= \nu \underset{\sim}{M'_1}(\underset{\sim}{x} \mp \underset{\sim}{P'}) \\[4pt]
&= \underset{\sim}{G}\underset{\sim}{M_1}\underset{\sim}{G}^{-1}(\underset{\sim}{x} \mp \underset{\sim}{P'}) \quad (\text{ in view of } (3.29)) \\[4pt]
&= \underset{\sim}{G}\underset{\sim}{M_1}(\underset{\sim}{G}^{-1}\underset{\sim}{x} \mp \underset{\sim}{P}) \quad (\text{in view of } (3.28)) \\[4pt]
&= \underset{\sim}{G}\underset{\sim}{\xi}(\underset{\sim}{G}^{-1}\underset{\sim}{x})\Big|_{D'_{\pm 1}} \quad (\text{in view of } (3.13))
\end{aligned}
\qquad (3.30)
$$

Equations (3.26) and (3.30) together imply

$$\nu \underset{\sim}{\xi'}(\underset{\sim}{x}) = \underset{\sim}{G}\underset{\sim}{\xi}(\underset{\sim}{G}^{-1}\underset{\sim}{x}) \qquad (3.31)$$

for all $\underset{\sim}{x} \in D'_0 \cup D'_{\pm 1}$. Hence (3.1) holds and ξ and ξ' are linearly equivalent. This completes our proof of *Theorem 3.2.*

$\blacksquare$

Our main result *(Theorem 3.1)* allows us to partition all vector fields in $\mathcal{L}$ into *linearly conjugate equivalence classes*, each one parametrized by the eigenvalues $\tilde{\sigma}_0 \pm j\tilde{\omega}_0$, $\tilde{\gamma}_0$, $\tilde{\sigma}_1 \pm j\tilde{\omega}_1$ and $\tilde{\gamma}_1$. Since all vector fields in $\mathcal{L}$ having the same eigenvalues have identical *qualitative* behaviors, it suffices to investigate only one member in each class. Our next theorem provides a *canonical piecewise-linear* equation involving 12 parameters each of which is expressed *explicitly* in terms of only 6 eigenvalue parameters; namely, $\{\tilde{\sigma}_0, \tilde{\omega}_0, \tilde{\gamma}_0, \tilde{\sigma}_1, \tilde{\omega}_1, \tilde{\gamma}_1\}$. Since these are the *minimum* number of parameters needed to uniquely identify a vector

field $\xi \in \mathcal{L}$, and since there exists a one-to-one correspondence between each linearly-conjugate equivalence class of vector fields in $\mathcal{L}$ and each equation in (3.32) of Theorem 3.3 below with a fixed set of numerical parameters, we will henceforth call (3.32) the *normal form equation* for the vector fields in $\mathcal{L}$. Although this term has already been used in circuit theory to mean "state equations," we have adopted this terminology here at the risk of some ambiguity in order to be consistent with the terminology used by Poincare, Arnold, etc. [9].

Theorem 3.3. Normal Form Equation for $\mathcal{L}$

Every *linearly conjugate* equivalence class of vector fields in $\mathcal{L}$ defined by $\{\tilde{\sigma}_0, \tilde{\omega}_0, \tilde{\gamma}_0, \tilde{\sigma}_1, \tilde{\omega}_1, \tilde{\gamma}_1\}$ satisfying (3.3) can be described analytically by the following canonical piecewise-linear equation

$$
\begin{bmatrix} \dot{x} \\ \dot{y} \\ \dot{z} \end{bmatrix} = \begin{bmatrix} a_{11} & a_{12} & a_{13} \\ a_{21} & a_{22} & a_{23} \\ a_{31} & a_{32} & a_{33} \end{bmatrix} \begin{bmatrix} x \\ y \\ z \end{bmatrix} + (|z-1| - |z+1|) \begin{bmatrix} b_1 \\ b_2 \\ b_3 \end{bmatrix}
\tag{3.32}
$$

The 12 parameters in (3.32) are expressed explicitly in terms of $\{\tilde{\sigma}_0, \tilde{\omega}_0, \tilde{\gamma}_0, \tilde{\sigma}_1, \tilde{\omega}_1, \tilde{\gamma}_1\}$ as follow:

$$
a_{11} = \tilde{\gamma}_1 - \frac{(\tilde{\sigma}_1^2 + \tilde{\omega}_1^2)\{(\tilde{\sigma}_0 - \tilde{\gamma}_1)^2 + \tilde{\omega}_0^2\}}{(\tilde{\sigma}_1^2 + \tilde{\omega}_1^2)\tilde{\gamma}_1 - (\tilde{\sigma}_0^2 + \tilde{\omega}_0^2)\tilde{\gamma}_0}
\tag{3.33}
$$

$$
a_{12} = \frac{(\tilde{\sigma}_1^2 + \tilde{\omega}_1^2)\tilde{\gamma}_1\{(\tilde{\sigma}_1 - \tilde{\gamma}_0)^2 + \tilde{\omega}_1^2\}}{\tilde{\gamma}_0\{(\tilde{\sigma}_1^2 + \tilde{\omega}_1^2)\tilde{\gamma}_1 - (\tilde{\sigma}_0^2 + \tilde{\omega}_0^2)\tilde{\gamma}_0\}}
\tag{3.34}
$$

$$
a_{13} = \frac{(\tilde{\sigma}_1^2 + \tilde{\omega}_1^2)\tilde{\gamma}_1}{(\tilde{\sigma}_0^2 + \tilde{\omega}_0^2)\tilde{\gamma}_0} \left\{ \frac{(\tilde{\sigma}_1^2 + \tilde{\omega}_1^2)\tilde{\gamma}_1(2(\tilde{\sigma}_1 - \tilde{\sigma}_0) + \tilde{\gamma}_1 - \tilde{\gamma}_0)}{(\tilde{\sigma}_1^2 + \tilde{\omega}_1^2)\tilde{\gamma}_1 - (\tilde{\sigma}_0^2 + \tilde{\omega}_0^2)\tilde{\gamma}_0} - \tilde{\gamma}_1 \right\}
\tag{3.35}
$$

$$
a_{21} = - \frac{(\tilde{\sigma}_0^2 + \tilde{\omega}_0^2)\tilde{\gamma}_0\{(\tilde{\sigma}_0 - \tilde{\gamma}_1)^2 + \tilde{\omega}_0^2\}}{\tilde{\gamma}_1\{(\tilde{\sigma}_1^2 + \tilde{\omega}_1^2)\tilde{\gamma}_1 - (\tilde{\sigma}_0^2 + \tilde{\omega}_0^2)\tilde{\gamma}_0\}}
\tag{3.36}
$$

$$
a_{22} = \tilde{\gamma}_0 + \frac{(\tilde{\sigma}_0^2 + \tilde{\omega}_0^2)\{(\tilde{\sigma}_1 - \tilde{\gamma}_0)^2 + \tilde{\omega}_1^2\}}{(\tilde{\sigma}_1^2 + \tilde{\omega}_1^2)\tilde{\gamma}_1 - (\tilde{\sigma}_0^2 + \tilde{\omega}_0^2)\tilde{\gamma}_0}
\tag{3.37}
$$

$$
a_{23} = \frac{(\tilde{\sigma}_1^2 + \tilde{\omega}_1^2)\tilde{\gamma}_1}{(\tilde{\sigma}_0^2 + \tilde{\omega}_0^2)\tilde{\gamma}_0} \left\{ \frac{(\tilde{\sigma}_0^2 + \tilde{\omega}_0^2)\tilde{\gamma}_0(2(\tilde{\sigma}_1 - \tilde{\sigma}_0) + \tilde{\gamma}_1 - \tilde{\gamma}_0)}{(\tilde{\sigma}_1^2 + \tilde{\omega}_1^2)\tilde{\gamma}_1 - (\tilde{\sigma}_0^2 + \tilde{\omega}_0^2)\tilde{\gamma}_0} - \tilde{\gamma}_0 \right\}
\tag{3.38}
$$

$$
a_{31} = a_{21}
\tag{3.39}
$$

$$a_{32} = \frac{(\tilde{\sigma}_0^2 + \tilde{\omega}_0^2)\{(\tilde{\sigma}_1 - \tilde{\gamma}_0)^2 + \tilde{\omega}_1^2\}}{(\tilde{\sigma}_1^2 + \tilde{\omega}_1^2)\tilde{\gamma}_1 - (\tilde{\sigma}_0^2 + \tilde{\omega}_0^2)\tilde{\gamma}_0} \tag{3.40}$$

$$a_{33} = \frac{(\tilde{\sigma}_1^2 + \tilde{\omega}_1^2)\tilde{\gamma}_1(2(\tilde{\sigma}_1 - \tilde{\sigma}_0) + \tilde{\gamma}_1 - \tilde{\gamma}_0)}{(\tilde{\sigma}_1^2 + \tilde{\omega}_1^2)\tilde{\gamma}_1 - (\tilde{\sigma}_0^2 + \tilde{\omega}_0^2)\tilde{\gamma}_0} \tag{3.41}$$

$$b_1 = \frac{(\tilde{\sigma}_1^2 + \tilde{\omega}_1^2)\tilde{\gamma}_1 - (\tilde{\sigma}_0^2 + \tilde{\omega}_0^2)\tilde{\gamma}_0}{2(\tilde{\sigma}_1^2 + \tilde{\omega}_1^2)\tilde{\gamma}_1} \, a_{13} \tag{3.42}$$

$$b_2 = \frac{(\tilde{\sigma}_1^2 + \tilde{\omega}_1^2)\tilde{\gamma}_1 - (\tilde{\sigma}_0^2 + \tilde{\omega}_0^2)\tilde{\gamma}_0}{2(\tilde{\sigma}_1^2 + \tilde{\omega}_1^2)\tilde{\gamma}_1} \, a_{23} \tag{3.43}$$

$$b_3 = \frac{(\tilde{\sigma}_1^2 + \tilde{\omega}_1^2)\tilde{\gamma}_1 - (\tilde{\sigma}_0^2 + \tilde{\omega}_0^2)\tilde{\gamma}_0}{2(\tilde{\sigma}_1^2 + \tilde{\omega}_1^2)\tilde{\gamma}_1} \, a_{33} \tag{3.44}$$

Proof. See *Appendix 3*.

Remark. The equation (3.32) is equivalent to the following equation

$$\xi(x,y,z) = \begin{cases} \underset{\sim 1}{M}(x,y,z-s)^T , & z \geq 1 \\ \underset{\sim 0}{M}(x,y,z)^T , & |z| \leq 1 \\ \underset{\sim 1}{M}(x,y,z+s)^T , & z \leq -1 \end{cases} \tag{3.45}$$

where

$$\underset{\sim 0}{M} = \begin{bmatrix} a_{11} & a_{12} & (1-s)a_{13} \\ a_{21} & a_{22} & (1-s)a_{23} \\ a_{31} & a_{32} & (1-s)a_{33} \end{bmatrix} , \quad \underset{\sim 1}{M} = \begin{bmatrix} a_{11} & a_{12} & a_{13} \\ a_{21} & a_{22} & a_{23} \\ a_{31} & a_{32} & a_{33} \end{bmatrix} \tag{3.46}$$

$$s = 1 - \frac{(\tilde{\sigma}_0^2 + \tilde{\omega}_0^2)\tilde{\gamma}_0}{(\tilde{\sigma}_1^2 + \tilde{\omega}_1^2)\tilde{\gamma}_1} \tag{3.47}$$

and a_{ij} $(1 \leq i, j \leq 3)$ are defined by (3.33)-(3.41).

4. POINCARÉ AND HALF-RETURN MAPS

Definition 3.1 implies that in so far as the *qualitative* behaviors are concerned, we only need to study one member of each *linearly equivalent* family of vector fields $\xi \in \mathcal{L}$. *Theorem 3.2* implies that we can, without loss of generality, choose the *simplest* vector field $\xi \in \mathcal{L}$ having a given set of normalized eigenvalue parameters $\{\sigma_0, \gamma_0, \sigma_1, \gamma_1, k\}$ as defined in (3.6), where $\gamma_0 \gamma_1 < 0$ and $k > 0$.

Note that a piecewise-linear vector field with an *arbitrary* $\{\sigma_0, \gamma_0, \sigma_1, \gamma_1, k\}$ may be *discontinuous* at the boundary planes U_1 and U_{-1} and hence is *not* a member of $\mathcal{L}$ even though it satisfies (P.1)-(P.6) of *Definition 2.1*. *Theorem 3.2* therefore provides the foundation for this section by stipulating the additional necessary and sufficient condition (3.7) for such vector fields to be continuous.[†] Stated in words, this eigenvalue condition asserts that the *real* eigenvalue associated with the equilibrium point P^+ (resp. P^-) must be opposite in *sign* to that at 0. Hence, trajectories along the real eigenvector at P^+ (resp., P^-) and those at 0 must have opposite stability properties.

Since our main motivation in this paper is to characterize the *double scroll* in [3] where $\gamma_0 > 0$, we will henceforth restrict our analysis to the following subset $\mathcal{L}_0 \subset \mathcal{L}$ of vector fields, henceforth called the *double scroll family* $\xi(\sigma_0, \gamma_0, \sigma_1, \gamma_1, k)$

$$\mathcal{L}_0 \triangleq \{\xi(\sigma_0, \gamma_0, \sigma_1, \gamma_1, k) \,|\, \sigma_0 < 0, \gamma_0 > 0, \sigma_1 > 0, \gamma_1 < 0, k > 0\} \tag{4.1}$$

where $\{\sigma_0, \gamma_0, \sigma_1, \gamma_1, k\}$ are the *normalized eigenvalue parameters*. *Stated in words, the eigenvalue pattern* of any member of the double scroll family at the equilibrium point P^+ (resp. P^-) must be a mirror image (except for scales) of that at the origin 0.[‡]

Remark: It follows from Theorem 3.3 that to study the global dynamics of the double scroll family, it suffices to study the *canonical piecewise-linear equation* (3.32).

The *eigenspaces* (defined by the *real* and *imaginary* parts of the complex eigenvectors) of a typical vector field $\xi \in \mathcal{L}_0$ are shown in Fig. 2(a) along with two typical trajectories. Since all trajectories occur in odd-symmetric pairs (property (P.1)), Fig. 2(a) shows only half of the salient features. Note that the qualitative behavior of Figs. 9 and 11 in [3] are identical to that of Fig. 2(a).

The *upper* trajectory Γ_1 in Fig. 2(a) originates from some point on U_1, moves downward,

---

[†]This eigenvalue condition (3.7) is *not* necessary for continuity of the vector field if we allow the piecewise-linear system to have only *one* equilibrium point instead of three, as stipulated in (P.4).

[‡]Since the eigenvalue pattern of the feedback system in [18] satisfies this property, it too is a *special case* of the double scroll family of vector fields to be investigated in this paper.

turns around (before reaching U_{-1}) and returns to U_1 after a finite amount of time. It continues to move upward before turning around and returns once more to U_1.[†] This typical trajectory defines a return map, called a *Poincaré map* from some subset $S \subset U_1$ into S.[‡] We can decompose this Poincaré map into two components: a "half-return map" which maps the initial point on U_1 to the first-return point on U_1, and a "second-half return map" which maps the first-return point to the second-return point on U_1.

The *lower* trajectory Γ_2 in Fig. 2(a) also originates from U_1, moves downward, penetrates U_{-1}, and after some finite amount of time, turns around, and returns to U_{-1} a *second* time. By the odd-symmetry of the vector field, however, we can identify each return point $\underset{\sim}{x}$ in U_{-1} by its reflected image $-\underset{\sim}{x}$ in U_1. Similarly, the portion of Γ_2 below U_{-1} can be identified with a corresponding version of Γ_1 above U_1. Through this identification scheme, both typical types of trajectories Γ_1 and Γ_2 actually define the same Poincaré map, which in turn is simply the composition of *two half-return maps*.

Unfortunately, the half return maps in Fig. 2(a) cannot in general be calculated by an *explicit* formula or algorithm because the coordinates of the return points can only be found by solving a pair of transcendental equations. Since these half return maps will be used in a crucial way in *section 5* to prove the double scroll is indeed chaotic in a rigorous mathematical sense, we must find a new coordinate system so that these half return maps can be easily calculated and its errors can be rigorously estimated. That such a coordinate system always exists for any $\xi \in \mathscr{A}_0$ constitutes one of the key contribution of this paper. Our approach for deriving this new coordinate system is to work with the greatly simplified but equivalent Jordan forms of the regions D_0 and D_1 in Fig. 2(a), namely, the D_0-unit and the D_1-unit in Fig. 2(b) described earlier (Definition 2.3).

4.1. Half-Return Map π_0

Consider first the D_0-unit at the bottom of Fig. 2(b) representing the image of D_0 in Fig. 2(a) under the affine transformation Ψ_0 (recall (2.6)-(2.9)). The 3 *fundamental points* A, B, and E in D_0 map into A_0, B_0, and E_0, respectively. Since L_2 maps into the straight line L_{2_0} passing through B_0 and E_0, it follows from (2.1) and the qualitative nature of trajectories in

---

[†]This typical trajectory can never penetrate the upper oblique plane because this plane is an eigenspace and is therefore an invariant set.

[‡]In the following we will choose S to be the "infinite" wedge $A_\infty BE_\infty \subset U_1$ in Fig. 2(a) representing the area bounded by the 2 straight lines BA_∞ and BE_∞, where A_∞ and E_∞ denote that these 2 lines both originate from B and extend to ∞.

D_0 that the vector field $\underset{\sim}{\xi}_0(\underset{\sim}{x})$ has a downward [†] component for all $\underset{\sim}{x}$ to the **right** of L_{2_0}, and an upward component to the **left**. Hence, any trajectory originating **inside** the **triangular region**

$$\Delta A_0 B_0 E_0 \triangleq \{\underset{\sim}{x} \in V_0 \mid \underset{\sim}{x} \text{ is bounded within triangle } A_0 B_0 E_0\} \tag{4.2}$$

must move down initially. But because the z-axis in the D_0-unit is the image of an unstable eigenvector, this trajectory must move toward V_0 as depicted by the upper trajectory in the D_0-unit. This trajectory defines the map

$$\pi_0^+ : \Delta A_0 B_0 C_0 \to V_0 \tag{4.3}$$

. via the obvious image

$$\pi_0^+(\underset{\sim}{x}) = \varphi_0^T(\underset{\sim}{x}) \tag{4.4a}$$

where $\varphi_0^T(\underset{\sim}{x})$ denotes the **flow** (in the D_0-unit) from $\underset{\sim}{x}$ to the **first** return point where the trajectory first intersects V_0 at some time $T > 0$, where

$$T = T(\underset{\sim}{x}) \triangleq inf\{t > 0 \mid \varphi_0^t(\underset{\sim}{x}) \in V_0\} \tag{4.4b}$$

Consider next a **typical** trajectory originating from a point in the **infinite wedge** (angular region)

$$\angle A_0 B_0 E_0 \triangleq \{\underset{\sim}{x} \in V_0 \mid \underset{\sim}{x} \text{ lies within the wedge-like extension of } \Delta A_0 B_0 E_0\} \tag{4.5}$$

to the **right** of $A_0 E_0$ in the D_0-unit as depicted in Fig. 2(b). This trajectory must move downward (because it originates to the right of L_{2_0}) and eventually intersects V_0^-. This trajectory corresponds to the portion of Γ_2 within D_0 in Fig. 2(a) and defines the map[‡]

$$\pi_0^- : \angle A_0 B_0 E_0 \backslash \Delta A_0 B_0 E_0 \to V_0^- \tag{4.6}$$

via the obvious image

$$\pi_0^-(\underset{\sim}{x}) = \varphi_0^T(\underset{\sim}{x}) \tag{4.7a}$$

where

$$T = T(\underset{\sim}{x}) \triangleq inf\{t > 0 \mid \varphi_0^t(\underset{\sim}{x}) \in V_0^-\} \tag{4.7b}$$

[†] Throughout this section, "downward component" or "moving down" (resp., "upward component" or "moving up") means the vector field enters the boundary plane V_0 from above (resp., leaves V_0 from below).

[‡] The symbol \ denotes set difference operator throughout this paper.

is the time this trajectory first penetrates V_0^-. By identifying this return point in V_0^- with its reflected *odd-symmetric*[†] image in V_0, we can define the following *half-return map*

$$\pi_0 : \angle\, A_0 B_0 E_0 \rightarrow V_0 \tag{4.8}$$

by

$$\pi_0(\underset{\sim}{x}) = \begin{cases} \pi_0^+(\underset{\sim}{x}) & , \quad \underset{\sim}{x} \in \Delta A_0 B_0 E_0 \\ -\pi_0^-(\underset{\sim}{x}) & , \quad \underset{\sim}{x} \in \angle A_0 B_0 E_0 \setminus \Delta A_0 B_0 E_0 \end{cases} \tag{4.9}$$

In order to derive an algorithm for calculating $\pi_0^+(\underset{\sim}{x})$ and $\pi_0^-(\underset{\sim}{x})$, let us magnify the *triangular region* $\Delta A_0 B_0 E_0$ on V_0 and the *angular region* $\angle A_0 B_0 E_0$ on V_0 as shown in Fig. 3(a). Since the z-coordinate of each point (x,y,z) on V_0 is simply $z = 1-x$, it suffices to specify each point on V_0 by its (x,y) coordinate. Our next crucial step is to define a "local" coordinate system (u,v) on V_0 so that each point $\underset{\sim 0}{x} = (x,y)^T$ is uniquely specified in terms of (u,v) such that $\pi_0^+(\underset{\sim}{x})$ and $\pi_0^-(\underset{\sim}{x})$ can be expressed in terms of u and v.

We will define our local (u,v) coordinates[‡] as a *weighted sum* of the 4 corner points A_0, B_0, E_0, and F_0 whose (x,y) coordinates have already been found in (2.20), (2.22), (2.24) and (2.25) in terms of the normalized eigenvalue parameters, namely,

$$\underset{\sim 0}{x}(u,v) = u[vA_0 + (1-v)E_0] + (1-u)[vB_0 + (1-v)F_0] \tag{4.10}$$

where $0 \le u < \infty$ and $0 \le v \le 1$. Here, we have abused our notation by denoting the (x,y) coordinates of the 4 corner points by A_0, B_0, E_0 and F_0, respectively. Note that $\underset{\sim 0}{x}(1,1) = A_0$, $\underset{\sim 0}{x}(1,0) = E_0$, $\underset{\sim 0}{x}(0,1) = B_0$ and $\underset{\sim 0}{x}(0,0) = F_0$. Note also that all points along the line segments $\overline{E_0 A_0}$ and $\overline{F_0 B_0}$ have a u-coordinate equal to 1 and 0, respectively. Similarly, all points along the line segments $\overline{B_0 A_0}$ and $\overline{F_0 E_0}$ have a v-coordinate equal to 1 and 0, respectively. A typical point H with a (u_0, v_0) coordinate can be identified as the intersection between the $u = u_0$ coordinate line and the $v = v_0$ coordinate line. All points inside the triangular region $\Delta A_0 B_0 E_0$ have $0 < u < 1$, and all points inside the angular region $\angle A_0 B_0 E_0$ outside of the $\Delta A_0 B_0 E_0$ have $1 < u < \infty$. Hence, in terms of the (u,v) coordinate systems

---

[†]Throughout this paper, odd-symmetry in $\mathbb{R}^3$ means symmetry with respect to the origin. Hence,2 points (x,y,z) and (x',y',z') are *odd symmetric* iff $(x',y',z') = (-x,-y,-z)$.

[‡]The reason for choosing this unconventional coordinate system will be obvious in Section 4.6.

(4.2) and (4.5) assume the following equivalent form:

$$\Delta A_0 B_0 E_0 = \{ \underset{\sim}{x}_0(u,v) \,|\, (u,v) \in [0,1] \times [0,1] \} \tag{4.11}$$

$$\angle A_0 B_0 E_0 = \{ \underset{\sim}{x}_0(u,v) \,|\, (u,v) \in [0,\infty) \times [0,1] \} \tag{4.12}$$

Theorem 4.1: Calculating the π_0^+ return map

Given $\underset{\sim}{x}_0 \triangleq (x_0, y_0)^T \in \Delta A_0 B_0 E_0$, the return map $\pi_0^+(\underset{\sim}{x}_0)$ is given by

$$\pi_0^+ \left[\underset{\sim}{x}_0(u,v) \right] = e^{\sigma_0 t} \begin{bmatrix} \cos t & -\sin t \\ \sin t & \cos t \end{bmatrix} \underset{\sim}{x}_0(u,v) \tag{4.13}$$

where (u,v) is the local coordinate of $(x_0, y_0) = \left[x_0(u,v), y_0(u,v) \right]$, where $0 \le u \le 1$, $0 \le v \le 1$, and t is the "first-return time" calculated explicitly as follow:

(a) Use the second local coordinate "v" to calculate the *inverse return-time function*[†] defined by

$$u^+(v,t) \triangleq \frac{\langle \varphi_0^t(B_{0v}), \underset{\sim}{h} \rangle - 1}{\langle \varphi_0^t(B_{0v} - A_{0v}), \underset{\sim}{h} \rangle} \tag{4.14}$$

where

$\varphi_0^t(\underset{\sim}{x})$ denotes the location of the trajectory *in* $\mathbb{R}^3$ *which originates from* $\underset{\sim}{x}$.

$A_{0v} \triangleq \underset{\sim}{x}_0(1,v)$ denotes the location *in* $\mathbb{R}^3$ of a point along the line segment $\overline{E_0 A_0}$ "v" units from E_0.

$B_{0v} \triangleq \underset{\sim}{x}_0(0,v)$ denotes the location *in* $\mathbb{R}^3$ of a point along the line segment $\overline{F_0 B_0}$ "v" units from F_0.

$\underset{\sim}{h} \triangleq (1,0,1)^T$ denotes the *normal* vector from the origin to V_0. and $\langle , \rangle$ denotes the usual vector dot product in $\mathbb{R}^3$.

(b) Use the first local coordinate "u" $(0 \le u \le 1)$ to calculate

$$t =: \inf\{ t \ge 0 \,|\, u^+(v,t) = u \} \tag{4.15}$$

[†]Given any "return time t_0, $0 \le t_0 < \infty$, and any coordinate line $v = v_0$, (4.14) implies that there exists a unique $u = u_0 \triangleq u^+(v_0, t_0)$ such that the trajectory $\varphi_0^{t_0}(\underset{\sim}{x}(u_0, v_0))$ starting from $\underset{\sim}{x}_0(u_0, v_0)$ at $t = 0$ would hit V_0 at $t = t_0$.

Proof. The dynamics in the D_0-unit is (2.9) whose flow $\varphi_0^t(\underset{\sim}{x}_0)$ from a point $\underset{\sim}{x}_0 = (x_0, y_0, z_0)^T$ is given by

$$\varphi_0^t(\underset{\sim}{x}_0) = \begin{bmatrix} e^{\sigma_0 t}\cos t & -e^{\sigma_0 t}\sin t & 0 \\ e^{\sigma_0 t}\sin t & e^{\sigma_0 t}\cos t & 0 \\ 0 & 0 & e^{\gamma_0 t} \end{bmatrix} \begin{bmatrix} x_0 \\ y_0 \\ z_0 \end{bmatrix} \tag{4.16}$$

Since $A_{0v} \to \varphi_0^t(A_{0v})$, $B_{0v} \to \varphi_0^t(B_{0v})$ and since for *fixed* t, $\varphi_0^t(\underset{\sim}{x}_0)$ in (4.16) is a *linear* transformation, the straight line segment $\overline{A_{0v}B_{0v}}$ joining A_{0v} and B_{0v} in Fig. 3(a) maps into a *straight* line segment $\overline{\varphi_0^t(A_{0v})\varphi_0^t(B_{0v})}$ joining $\varphi_0^t(A_{0v})$ and $\varphi_0^t(B_{0v})$. Now if we let $\underset{\sim}{\hat{x}}_0 \triangleq \varphi_0^t(\underset{\sim}{x}_0)$, then $\underset{\sim}{\hat{x}}_0$ must divide the *length* of the *vector* $\overrightarrow{\varphi_0^t(A_{0v})\varphi_0^t(B_{0v})}$ into the same *proportion* as $\underset{\sim}{x}_0$ (i.e., point H in Fig. 3(a)) divides the vector $\overrightarrow{A_{0v}B_{0v}}$ into lengths u and 1-u respectively. In particular[†]

$$u = \frac{u}{u+(1-u)} = \frac{|\overrightarrow{\underset{\sim}{\hat{x}}_0\varphi_0^t(B_{0v})}|}{|\overrightarrow{\varphi_0^t(A_{0v})\varphi_0^t(B_{0v})}|}$$

$$= \frac{\langle \overrightarrow{\underset{\sim}{\hat{x}}_0\varphi_0^t(B_{0v})}, \underset{\sim}{h}\rangle}{\langle \overrightarrow{\varphi_0^t(A_{0v})\varphi_0^t(B_{0v})}, \underset{\sim}{h}\rangle} \tag{4.17}$$

$$= \frac{\langle \varphi_0^t(B_{0v}), \underset{\sim}{h}\rangle - \langle \underset{\sim}{\hat{x}}_0, \underset{\sim}{h}\rangle}{\langle \varphi_0^t(B_{0v}-A_{0v}), \underset{\sim}{h}\rangle} \tag{4.18}$$

where (4.18) is simply the ratio between the *projections* along the normal vector $\underset{\sim}{h}$ of the vectors in the numerator and the denominator in (4.17), respectively. But

$$\langle \underset{\sim}{\hat{x}}_0, \underset{\sim}{h}\rangle = \langle (\hat{x}_0, \hat{y}_0, \hat{z}_0), (1,0,1)\rangle = \hat{x}_0 + \hat{z}_0 = 1 \tag{4.19}$$

since $\hat{\underset{\sim}{x}}_0$ lies on V_0. Substituting $\langle \underset{\sim}{\hat{x}}_0, \underset{\sim}{h}\rangle = 1$ into (4.18) we obtain (4.14), where we have written $u^+(v,t)$ in place of u to emphasize that the right hand side of (4.14) is a well-defined *continuous single-valued* function of $v \in [0,1]$ and $t \in (0,\infty)$. The superscript "+" denotes its association with π_0^+ to distinguish it from $u^-(v,t)$ in *Theorem 4.2* which is associated with π_v. ∎

[†] *A vector from point x to point y in* $\mathbb{R}^3$ *is denoted throughout this paper by* $\overrightarrow{xy}$. *The length of* $\overrightarrow{xy}$ *is denoted by* $|\overrightarrow{xy}|$.

Remarks

1. Since any initial point $\underset{\sim}{x}_0(1,v)$ lies on the stable eigenspace $\Psi_0\big[E^c(0)\big]$, $\varphi_0^t\big[\underset{\sim}{x}_0(1,v)\big]$ may not return to V_0 but instead converges to the origin 0 as $t \to \infty$. In this case, however, it is logical and convenient to define $\pi_0^+\big[\underset{\sim}{x}_0(1,v)\big] \triangleq C_0 = \Psi_0(C)$ since we have earlier identified C_0 and 0 as the same point. It follows from this definition that $u^+(v,t) \to 1$ as $t \to \infty$.

2. It can be shown that the vector field $\xi_0(E_0)$ is directed from E_0 to A_0, $\xi_0(B_0)$ is directed from A_0 to B_0, and $\xi_0(F_0)$ is directed from F_0 to B_0, as shown in Fig. 3(a). It follows from the continuity of $\underset{\sim}{\xi}(\underset{\sim}{x})$ that the vectors along the line segment $\overline{B_0F_0}$ are as depicted in Fig. 3(a).

Since the vector field $\underset{\sim}{\xi}(\underset{\sim}{x})$ has a *downward component for all $\underset{\sim}{x}$ to the right* of the line segment $\overline{E_0F_0}$ in Fig. 3(a), and since $\underset{\sim}{\xi}(\underset{\sim}{x})$ is directed to the right for all $\underset{\sim}{x} \in \overline{E_0F_0}$, it follows that all trajectories starting on $\overline{E_0F_0}$ or slightly to the right of $\overline{E_0F_0}$ will first move downward towards the right before returning to V_0. Hence $\pi_0^+(\underset{\sim}{x})$ is *continuous* even along the points on $\overline{E_0F_0}$.

In contrast, the vector field $\underset{\sim}{\xi}(\underset{\sim}{x})$ has an *upward* component for all $\underset{\sim}{x}$ to the *left* of the line segment $\overline{F_0B_0}$ in Fig. 3(a). Moreover, since $\underset{\sim}{\xi}(\underset{\sim}{x})$ is directed to the left for all $\underset{\sim}{x} \in \overline{F_0B_0}$, it follows that the trajectories starting from points along $\overline{F_0B_0}$ will first move *upward* before returning to V_0 whereas trajectories starting from points arbitrarily close to $\overline{F_0B_0}$ (but on the right hand side) will first move downward and return to V_0 after a relatively much shorter time. Consequently, $\pi_0^+(\underset{\sim}{x})$ is *discontinuous* along $\overline{F_0B_0}$. For convenience, we will define

$$\pi_0^+(\underset{\sim}{x}) = \underset{\sim}{x} \text{ for all } \underset{\sim}{x} \in \overline{F_0B_0} \tag{4.20}$$

In other words, we *define* each point $\underset{\sim}{x} \in \overline{F_0B_0}$ as a fixed point of $\pi_0^+(\underset{\sim}{x})$ and hence its first return time is equal to zero; namely,

$$u^+(v,t) \triangleq 0 \quad \text{at} \quad t = 0 \tag{4.21}$$

3. Between $t = 0$ and $t = \infty$, $u^+(v,t)$ is a <u>continuous</u> but not necessarily monotonic function of t. The continuity follows from (4.13).

4. Remarks 1-3 imply that a typical *inverse return-time function* $u^+(v,t)$ has the form shown in Fig. 3(b): it starts from the origin and approaches $u = 1$ asymptotically while making some (possibly none) oscillations in between. It follows from (4.15) that the set

$I^+(v)$ of "first-return times" t as u changes from 0 to 1 is in general not a connected set. For the example in Fig. 3(b), we have $I^+(v) = [0,t_1] \cup (t_2,\infty)$.

5. The example in Fig. 3(b) demonstrates that in general the return time t is a *discontinuous* function of u and hence of the initial point $x_{\sim 0}$. This shows that it is in general impossible to express the return time t as a continuous function of $x_{\sim 0}$. Consequently, our algorithm for calculating t in *Theorem 4.1* is the best result obtainable.

Following the same notation and proof as *Theorem 4.2*, we obtain:

Theorem 4.2: Calculating the π_0^- return map

Given $x_{\sim 0} \triangleq (x_0,y_0)^T \in \angle A_0 B_0 E_0 \setminus \Delta A_0 B_0 E_0$, the return map $\pi_0^-(x_{\sim 0})$ is given by (4.13), where (u,v) is the local coordinates of (x_0,y_0), $1 < u < \infty$, $0 \le v \le 1$, and t is the first return time calculated explicitly as follow:

(a) Use the second local coordinate "v" to calculate the *inverse return-time function*

$$u^-(v,t) \triangleq \frac{\langle \varphi_0^t(B_{0v}), h_{\sim} \rangle + 1}{\langle \varphi_0^t(B_{0v} - A_{0v}), h_{\sim} \rangle} \tag{4.22}$$

(b) Use the first local coordinate "u" ($1 < u < \infty$) to calculate

$$t = \inf\{t \ge 0 \mid u^-(v,t) = u\} \tag{4.23}$$

It follows from *Theorems 4.1 and 4.2* that the *half-return map* π_0 defined in (4.9) can be *explicitly* calculated, i.e., without solving any system of nonlinear equations. Here, we assume that the inverse return time functions $u^+(v,t)$ in (4.14) and $u^-(v,t)$ in (4.22) have been plotted and hence the first return times t in (4.15) and (4.23) are simply read off these curves. This operation is of course equivalent to finding the *inverse* of a function of *one* variable — a simple reliable task compared to that of solving a system of transcendental equations.

For the rigorous proof and analysis in the following sections, it is <u>never</u> necessary to calculate the first-return time t. Instead, the image under π_0 of various constant-v lines, which is given <u>explicitly</u> via (4.10), (4.13), (4.14) and (4.22), is used directly.

Example 4.1: π_0 with monotone inverse return-time function

Consider the vector field ξ with $(\sigma_0, \gamma_0, \sigma_1, \gamma_1, k) = (-0.3, 1.5, 0.2, -2.0, 0.75)$. The images of the line segments $\overline{B_0 A_0}$ and $\overline{F_0 E_0}$ in the V_0-plane under the half return map $\pi_0 = \pi_0^+$ are shown in Fig. 4(a) as two "spirals" from B_0 to C_0, and from F_0 to C_0, respectively. We will henceforth denote such curves by $[\widehat{B_0 C_0}]$ and $[\widehat{F_0 C_0}]$, where $[\cdot]$ denotes both end points are

included.

The images of the line segment $\overline{A_0A_{0\infty}}$ and $\overline{E_0E_{0\infty}}$ (where $A_{0\infty}$ and $E_{0\infty}$ denote the extension of the respective straight lines to $+\infty$) in the V_0-plane under the half return map $\pi_0 = -\pi_0^-$ are also shown in Fig. 4(a) by the "spirals" $[\overparen{C_0A'_{0\infty}})$ and $[\overparen{C_0E'_{0\infty}})$ where $A'_{0\infty}$ and $E'_{0\infty}$ denote respectively the extension of the respective curves to $+\infty$.

The graphs of the inverse return-time functions $u \doteq u^+(1,t)$ along $\overline{B_0A_0}$ and $u = u^-(1,t)$ along $\overline{A_0A_{0\infty}}$ are shown in Figs. 4(b). A magnification of these curves in Fig. 4(c) shows that both functions are *monotone* functions.

Example 4.2: π_0 with non-monotone inverse return-time function

Consider the vector field ξ with $(\sigma_0,\gamma_0,\sigma_1,\gamma_1,k) = (-0.2,0.75,0.2,-1.0,0.75)$. The image in the V_0-plane under the half return map $\pi_0 = \pi_0^+$ of the line segment $\overline{B_0A_0}$ is shown by the spiral $[\overparen{B_0C_0}]$ in Fig. 5(a). Its corresponding inverse return-time function $u^+(1,t)$ as shown in Fig. 5(b) and magnified in Fig. 5(c) is a monotone function as in *Example 4.1*.

However, the image in the V_0-plane under the half return map $\pi_0 = -\pi_0^-$ of the line segment $\overline{A_0A_{0\infty}}$ consist of the union of two *disconnected* curves $(\overparen{b'C_0}]$ and $[\overparen{bA'_{0\infty}})$. This phenomenon can be explained by looking at the associated inverse return-time function $u^-(1,t)$ in Fig. 5(b) whose magnification in Fig. 5(c) shows a *non-monotonic* curve with a local minimum at t_1, and a local *maximum at* t_2. The image of the line segment $\overline{x_0(u_1,1)x_0(u_2,1)}$ under $\pi_0 = -\pi_0^-$ is the spiral $[\overparen{ab}]$ in Fig. 5(a).

If we plot the *second* and the *third* return maps of $\overline{x_0(u_1,1)x_0(u_2,1)}$, we would obtain the curves $(\overparen{ba'}]$ during the time interval $t_1 < t \leq t_2$ and $(\overparen{a'b'})$ during the time interval $t_2 < t < t_3$, where $t_3 = inf\{t > t_1 | u^-(1,t) = u_1\}$.

4.2. Half-return Map π_1

Consider next the D_1-unit on top of Fig. 2(b) representing the image of D_1 in Fig. 2(a) under the affine transformation Ψ_1 (recall (2.10)-(2.12)). The 3 *fundamental points* A, B, and E in D_1 map into A_1, B_1, and E_1, respectively. Here we abuse our notation by using the same symbol D_1 to denote the top region in Fig. 2(a) and a point on the z-axis in the D_1 unit in Fig. 2(b). We will inherit the same notations in the preceding section with the exception that all subscript "0" corresponding to D_0-unit should be changed to "1" for the D_1-unit. Hence, we define again a *local coordinate system* (u,v) such that the line segments $\overline{E_1F_1}$ and $\overline{A_1B_1}$ in V_1 in Fig. 2 correspond to the $v = 0$ and $v = 1$ coordinate line, respectively. Likewise, the line segments $\overline{F_1B_1}$ and $\overline{E_1A_1}$ correspond to the $u = 0$ and $u = 1$ coordinate line,

respectively. Any point $\underset{\sim 1}{x}$ inside the wedge (angular region) bounded by $\overline{B_1A_{1\infty}}$ and $\overline{B_1E_{1\infty}}$ is uniquely identified by:

$$\underset{\sim 1}{x}(u,v) = u[vA_1 + (1-v)E_1] + (1-u)[vB_1 + (1-v)F_1],$$

$$\text{for } 0 \leq u < \infty, \text{ and } 0 \leq v \leq 1 \tag{4.24}$$

Under this local coordinate system, we can define the *triangular region* $\Delta A_1B_1E_1$ and the *angular region* $\angle A_1B_1E_1$ as follow:

$$\Delta A_1B_1E_1 \triangleq \{\underset{\sim 1}{x}(u,v)|(u,v) \in [0,1] \times [0,1]\} \tag{4.25}$$

$$\angle A_1B_1E_1 \triangleq \{\underset{\sim 1}{x}(u,v)|(u,v) \in [0,\infty) \times [0,1]\} \tag{4.26}$$

Finally we define the second *half return map*

$$\pi_1(\underset{\sim}{x}): \angle A_1B_1E_1 \rightarrow V_1 \tag{4.27a}$$

via the obvious *inverse* image

$$\pi_1(x) = \varphi_1^{-T}(\underset{\sim}{x}) \tag{4.27b}$$

where $\varphi_1^{-T}(\underset{\sim}{x})$ denotes the *flow* (in the D_1-unit) from $\underset{\sim}{x}$ to the *first* return point where the trajectory first intersects V_1 at some "reverse" time $-T < 0$, where

$$T = T(\underset{\sim}{x}) \triangleq inf\{t > 0|\varphi_1^{-t}(\underset{\sim}{x}) \in V_1\} \tag{4.27c}$$

Our next theorem shows that π_1 can be calculated by an explicit algorithm similar to that of π_0.

Theorem 4.3: Calculating the π_1 return map

Given $\underset{\sim 1}{x} \triangleq (x_1,y_1)^T \in \angle A_1B_1E_1$, the half-return map $\pi_1(\underset{\sim 0}{x})$ is given by

$$\pi_1\left[\underset{\sim 1}{x}(u,v)\right] = e^{-\sigma_1 t}\begin{bmatrix} \cos t & \sin t \\ -\sin t & \cos t \end{bmatrix}\underset{\sim 1}{x}(u,v) \tag{4.28}$$

where (u,v) is the local coordinates of $(x_1,y_1) = \left[x_1(u,v),y_1(u,v)\right]$, where $0 \leq u < \infty$, $0 \leq v \leq 1$, and t is the "first-return time calculated explicitly as follow:

(a) Use the first local coordinate "u" to calculate the *inverse return-time function*

$$v(u,t) \triangleq \frac{\langle \varphi_1^{-t}(E_{1u}), \underset{\sim}{h} \rangle - 1}{\langle \varphi_1^{-t}(E_{1u} - A_{1u}), \underset{\sim}{h} \rangle} \qquad (4.29)$$

where $E_{1u} \triangleq \underset{\sim}{x}_1(u,0)$ denotes the location *in* $\mathbb{R}^3$ of a point along the line segment $\overline{F_1 E_1}$ "u" units from F_1, and $A_{1u} \triangleq \underset{\sim}{x}_1(u,1)$ denotes the location in $\mathbb{R}^3$ of a point along the line segment $\overline{B_1 A_1}$ "u" units from B_1.

(b) Use the second local coordinate "v" ($0 \leq v \leq 1$) to calculate

$$t = inf\{t \geq 0 | v(u,t) = v\} \qquad (4.30)$$

Proof. Follows *mutatis mutandis* the proof for *Theorem 4.1*.

■

Example 4.3: π_1 with non-monotonic inverse return-time function

Consider the vector field ξ with $(\sigma_0, \gamma_0, \sigma_1, \gamma_1, k) = (-0.4, 0.3, 0.2, -1.0, 0.3)$. Since $\pi_1(\underset{\sim}{x})$ is defined to be the *reverse* flow, the vector field $\xi_1(\underset{\sim}{x})$ on V_1 becomes - $\xi_1(\underset{\sim}{x})$ in following the image of $\underset{\sim}{x}$ under $\pi_1(\underset{\sim}{x})$. Hence the direction of $\xi(\underset{\sim}{x})$ along the line $L_{2_0} = \Psi_0(L_2)$ in Fig. 3(a) must be *reversed* in the corresponding line $L_{2_1} = \Psi_1(L_2)$ in Fig. 6. Hence, $\pi_1(\underset{\sim}{x})$ is *discontinuous* along the line segment $\overline{E_1 F_1}$ in Fig. 6 whereas it is continuous along the line segment $\overline{F_1 B_1}$. This is the opposite of $\pi_0(\underset{\sim}{x})$ which is discontinuous along $\overline{F_0 B_0}$ but continuous along $\overline{E_0 F_0}$. Note that $\overline{E_1 F_1}$ corresponds to our $v = 0$ coordinate line.

The image of $\overline{F_1 B_1}$ under π_1 is the spiral $[\overparen{F_1 W_1 D_1}]$ in Fig. 6. In *Appendix 4* we shall prove that this spiral is *tangent* to the line $\overline{E_1 B_1}$ at F_1. The image of the line segment $E_1 A_1$ is shown in Fig. 6 as part of a large spiral $[\overparen{E_1 A_1'}]$. The continuation of this spiral to the right of A_1' is the image of the extension of $\overline{E_1 A_1}$ beyond A_1.

The inverse return-time function $v = v(0,t)$ in Fig. 7(a) and its magnification in Fig. 7(b) shows that it is a monotonic increasing function of t. However, the inverse return-time function $v = v(1,t)$ in Fig. 7(g) and its magnification in Fig. 7(h) shows that it is *not* monotonic and has a value larger than 1 for $t_3 < t < t_4$ where $t_3 \triangleq inf\{t > 0 | v(1,t) = 1\}$ is the time it takes A_1 to go to A_1'. The time interval (t_3, t_4) therefore corresponds to the time where the extension of the outer spiral $[\overparen{E_1 A_1'}]$ lies to the right of the line segment $\overline{B_1 A_1}$ (i.e., the $v = 1$ coordinate line).

Recall that $\overline{F_1 B_1}$ and $\overline{E_1 A_1}$ correspond to our $u = 0$ and $u = 1$ coordinate lines, respectively. There exist $0 < u_1 < u_2 < 1$ such that the corresponding coordinate lines $\overline{a_1 e_1}$

$(u = u_1,$ line) and $\overline{a_2e_2}$ $(u = u_2$ line) are mapped under π_1 into the following two curves:

(a) $\pi_1(\overline{a_1e_1})$ is a spiral $[\overset{\frown}{e_1F_1W_2D_1}]$ which is tangent to $\overline{E_1B_1}$ at F_1.

(b) $\pi_1(\overline{a_2e_2})$ is a curve $[\overset{\frown}{e_2B_1}]$ which is tangent to $\overline{A_1A_1}$ at B_1.

The graph of the inverse return-time functions $v = v(u_1,t)$ is shown in Fig. 7(c) and its magnification in Fig. 7(d) shows that it is monotonic with an inflection point $\left[\dfrac{dv}{dt} = 0 \text{ and } \dfrac{d^2v}{dt^2} = 0\right]$ at some time t_1. The graph of the inverse function $v = v(u_2,t)$ is shown in Fig. 7(e) and its magnification in Fig. 7(f) shows that it is non-monotonic with a maximum value $v = 1$ at $t = t_2$, where t_2 is the time it takes to go from a_2 to B_1.

Now let f_1 be the inverse image of F_1 in Fig. 6, i.e., $\pi_1(f_1) = F_1$. Similarly, let the inverse image of $\overline{F_1B_1}$ be denoted by $[f_1a_2]$, namely, the curve $\overset{\frown}{f_1a_2}$ in Fig. 6. Since the region bounded by the closed curve $e_1e_2a_2f_1e_1$ is found to map into the region bounded by the closed curve $\overset{\frown}{e_1F_1B_1e_2e_1}$ whereas the neighboring region bounded by the closed curve $\overset{\frown}{f_1a_1a_2f_1}$ is mapped into the region bounded by the closed curve $\overset{\frown}{F_1W_1D_1W_2F_1}$ in Fig. 6, it follows that $\pi_1(\underset{\sim}{x})$ is *discontinuous* along the curve $\overset{\frown}{f_1a_2}$, in addition to already being discontinuous along $\overline{E_1F_1}$.[†]

Let us summarize the behaviors of π_1 in Fig. 6 as follow:

(1) $\pi_1(\Delta A_1B_1E_1) =$ a fan-like closed region $\square A_1'B_1E_1$

   (shown shaded) in Fig. 6.

$$(4.31)$$

(2) $\pi_1(\overline{B_1a_2}) = D_1$ $$(4.32)$$

Here $\pi_1(\overline{B_1a_2})$ actually maps into the origin in the unstable eigenspace $\Psi_1\left[E^c(P)\right]$ which becomes a stable equilibrium under the reverse flow φ_1^{-t}. It is logical and convenient to identify the origin with $D_1 = \Psi_1(P^+)$ in V_1.

(3) Since π_1 is discontinuous along $\overline{E_1F_1}$, we will define (as in π_0):

   $$\pi_1(\underset{\sim}{x}) \overset{\Delta}{=} \underset{\sim}{x} \text{ for all } \underset{\sim}{x} \in \overline{E_1F_1} \tag{4.33}$$

In particular,

[†] These additional discontinuity points occur when we choose our parameters close to those which gave us the double scroll. They may not occur inside $\Delta A_1B_1E_1$ for other choices of parameters.

$$\pi_1(f_1) = \pi_1(F_1) = F_1 \tag{4.34}$$

With this definition, π_1 becomes continuous at $\overline{E_1F_1}$.

(4) π_1 is *one-to-one* at all points inside the triangular region $\Delta A_1B_1E_1$ and its boundary except the points along the line segment $[\overline{B_1a_2})$ and the isolated point f_1, i.e., on $\Delta A_1B_1E_1 \setminus ([\overline{B_1a_2}) \cup \{f_1\})$.

(5) π_1^{-1} is *well defined* at all points in the fan-like region $\square A_1'B_1E_1$ except for the two isolated points F_1 and D_1.

(6) The spiral $(\overarc{F_1W_1D_1})$ is the set of *discontinuous* points of π^{-1}. The function π^{-1} is discontinuous at these points because $\pi_1^{-1}(x) \to \overarc{f_1a_2}$ from the right as $x \to W_1$ from the right, whereas $\pi_1^{-1}(x) \to \overline{F_1B_1}$ from the right as $x \to W_1$ from the left. This follows because the return map π_1^{-1} corresponds to a flow in *forward* time, and hence has exactly the same discontinuity property *as* that of π_0 along the corresponding segment $\overline{F_0B_0}$.

Using the above properties, we can now define the *inverse half return map* π_1^{-1} as follow:

$$\pi_1^{-1}: \ \square A_{1\infty}'B_1E_{1\infty} \to \angle A_1B_1E_1 \tag{4.35}$$

where $\ \square A_{1\infty}'B_1E_{1\infty} \triangleq \{(x,y,z) \in V_1 | y \geq \sigma_1 x + \gamma_1(1-x), x \leq 1\}$ $\tag{4.36}$

is the region above the line $B_1E_{1\infty}$ and to the left of $A_1A_{1\infty}'$ in Fig. 6.

$$\pi_1^{-1}(D_1) \triangleq B_1 \tag{4.37}$$

$$\pi_1^{-1}(F_1) \triangleq f_1 \tag{4.38}$$

Note that π_1^{-1} is *discontinuous* along $[\overarc{F_1W_1D_1}]$.

4.3. Connection Map Φ

Since the D_0-unit and the D_1-unit in Fig. 2 have different reference frames, let us "match" the two units by defining the *affine connection map*

$$\Phi \triangleq (\Psi_1|_{U_1}) \circ (\Psi_0|_{U_1})^{-1} \tag{4.39}$$

where $\Psi_1|_{U_1}$ and $\Psi_0|_{U_1}$ denote the restriction of Ψ_1 and Ψ_0 on U_1. Again, since $z_i = 1 - x_i$, it suffices to find the explicit formula relating $(x_0,y_0) \in D_0$ to $(x_1,y_1) \in D_1$. Since $A_0 = (1,p_0,0) \to A_1 = (1,p_1,0)$,

$$\begin{bmatrix} x_1 \\ y_1 \end{bmatrix} = \Phi \begin{bmatrix} x_0 \\ y_0 \end{bmatrix} = \underset{\sim}{L} \begin{bmatrix} x_0-1 \\ y_0-p_0 \end{bmatrix} + \begin{bmatrix} 1 \\ p_1 \end{bmatrix} \tag{4.40}$$

Hence

$$\begin{bmatrix} (x_1-1) \\ (y_1-p_1) \end{bmatrix} = \underset{\sim}{L} \begin{bmatrix} (x_0-1) \\ (y_0-p_0) \end{bmatrix} \text{ for any } (x_0,y_0) \in D_0 \tag{4.41}$$

Now since $B_0 \triangleq (B_{0x},B_{0y}) \rightarrow B_1 \triangleq (B_{1x},B_{1y})$ and $E_0 \triangleq (E_{0x},E_{0y}) \rightarrow E_1 \triangleq (E_{1x},E_{1y})$, it follows from the action of $\underset{\sim}{L}$ in (4.41) that

$$\begin{bmatrix} B_{1x}-A_{1x} \\ B_{1y}-A_{1y} \end{bmatrix} = \underset{\sim}{L} \begin{bmatrix} B_{0x}-A_{0x} \\ B_{0y}-A_{0y} \end{bmatrix}, \begin{bmatrix} E_{1x}-A_{1x} \\ E_{1y}-A_{1y} \end{bmatrix} = \underset{\sim}{L} \begin{bmatrix} E_{0x}-A_{0x} \\ E_{0y}-A_{0y} \end{bmatrix} \tag{4.42}$$

It follows from (4.42) that

$$\underset{\sim}{L} = \begin{bmatrix} B_{1x}-A_{1x} & E_{1x}-A_{1x} \\ B_{1y}-A_{1y} & E_{1y}-A_{1y} \end{bmatrix} \begin{bmatrix} B_{0x}-A_{0x} & E_{0x}-A_{0x} \\ B_{0y}-A_{0y} & E_{0y}-A_{0y} \end{bmatrix}^{-1} \tag{4.43}$$

Substituting (2.20), (2.22), (2.24), (2.26), (2.28), and (2.30) for the respective components of A_i, B_i, E_i into (4.42), we obtain the followinng formula for $\underset{\sim}{L}$:

$$\underset{\sim}{L} = \frac{(\sigma_1^2+1)k_1}{(\sigma_0^2+1)(k_0+1)Q_1\gamma_1}$$

$$\cdot \begin{bmatrix} -\gamma_1(k_0+1)[Q_0 + \gamma_0(\sigma_0-\gamma_0)(k_1+1)] & \gamma_0\gamma_1(k_0+1)(k_1+1) \\ \\ \begin{array}{l} -\gamma_0(k_1+1)(\sigma_0-\gamma_0)[\sigma_1(\sigma_1-\gamma_1)+1] \\ - \gamma_1(k_0+1)(\sigma_1-\gamma_1)[\sigma_0(\sigma_0-\gamma_0)+1] \end{array} & \gamma_0(k_1+1)[Q_1 + \gamma_1(\sigma_1-\gamma_1)(k_0+1)] \end{bmatrix}$$

where $Q_i \triangleq (\sigma_i-\gamma_i)^2 + 1$, $k_0 \triangleq k$, and $k_1 \triangleq 1/k$. \hfill (4.44)

Note that L is expressed directly in terms of the normalized eigenvalue parameters $\{\sigma_0,\gamma_0,\sigma_1,\gamma_1,k\}$.

4.4. Poincare Map π

We will now use the *half-return maps* π_0 and π_1 and the *connection map* Φ to define a *Poincare map*

$$\pi : V_1' \rightarrow V_1' \tag{4.45a}$$

where

$$V_1' \triangleq \{(x,y) \in V_1 | x \leq 1\} \qquad \text{(4.45b)}$$

via the formula

$$
\boxed{
\begin{aligned}
\pi(\underset{\sim}{x}) &= \pi_1^{-1}\Phi\pi_0\Phi^{-1}(\underset{\sim}{x}) \ , \ \text{if } \underset{\sim}{x} \in \angle A_1 B_1 E_1 \\
&= \Phi\pi_0\Phi^{-1}\pi_1^{-1}(\underset{\sim}{x}) \ , \ \text{if } \underset{\sim}{x} \in V_1' \setminus \angle A_1 B_1 E_1
\end{aligned}
}
\qquad \text{(4.46)}
$$

Note that $\pi(\angle A_1 B_1 E_1) \subset \angle A_1 B_1 E_1$ and π_1^{-1} is well defined for all $\underset{\sim}{x} \in V_1' \setminus \angle A_1 B_1 E_1$ in view of (4.36). Here V_1' denotes the V_1-plane to the left of x = 1.

4.5. V_1-Portrait of V_0

In our study of the global dynamics of the double scroll family in the following sections, we will often need to look at the image via Φ of the half-return map of several line segments defined as follow:

$$\overset{\frown}{B_1 C_1} \triangleq \Phi\pi_0\Phi^{-1}(\overline{A_1 B_1}) = \Phi\pi_0(\overline{A_0 B_0}) \qquad \text{(4.47)}$$

$$\overset{\frown}{F_1 C_1} \triangleq \Phi\pi_0\Phi^{-1}(\overline{F_1 E_1}) = \Phi\pi_0(\overline{F_0 E_0}) \qquad \text{(4.48)}$$

$$\overset{\frown}{C_1 A_{1\infty}'} \triangleq \Phi\pi_0\Phi^{-1}(\overline{A_1 A_{1\infty}}) = \Phi\pi_0(\overline{A_0 A_{0\infty}}) \qquad \text{(4.49)}$$

$$\overset{\frown}{C_1 E_{1\infty}'} \triangleq \Phi\pi_0\Phi^{-1}(\overline{E_1 E_{1\infty}}) = \Phi\pi_0(\overline{E_0 E_{0\infty}}) \qquad \text{(4.50)}$$

$$\overset{\frown}{E_1 A_1'} \triangleq \pi_1(\overline{E_1 A_1}) \qquad \text{(4.51)}$$

The images $\overset{\frown}{B_1 C_1}$, $\overset{\frown}{F_1 C_1}$, $\overset{\frown}{C_1 A_{1\infty}'}$, $\overset{\frown}{C_1 E_{1\infty}'}$ and $\overset{\frown}{E_1 A_1'}$ for a typical set of normalized eigenvalue parameters $\{\sigma_0, \gamma_0, \sigma_1, \gamma_1, k\}$ for a vector field $\xi \in \mathcal{L}_0$ are shown in Fig. 8. We will henceforth refer to this picture as the V_1-portrait of V_0. Note that $C_1 \triangleq \Phi(C_0) = \Psi_1(C)$.

Stated in words, the V_1-portrait of V_0 consists of 4 distinct sets of points:

Set 1. Two boundary lines $\overline{B_1 A_{1\infty}}$ and $\overline{B_1 E_{1\infty}}$ representing the V_1-coordinates of points along the boundary lines $\overline{B_0 A_{0\infty}}$ and $\overline{B_0 E_{0\infty}}$ of the *infinite* wedge $\angle A_0 B_0 E_0$.

Set 2. The boundary line $\overline{E_1 A_1}$ of the triangular region $\Delta A_1 B_1 E_1$.

Set 3. 4 spirals representing the *image* of points in *Set 1* under the π_0-map (in D_0-unit) but translated into the coordinates on V_1.

Set 4. A partial spiral representing the image of the points in *Set 2* under the π_1-map.

In Section 5, we will consider the important case when *Set 4* includes the point C_1, i.e., $C_1 \in \widehat{E_1 A_1'}$.

4.6. Spiral Image Property

The various spirals in Figs. 4(a), 5(a), 6, and 8 were calculated by computers for various specific sets of parameters. In general, the image under π_0^+, π_0^-, or π_1 of any bounded straight-line segment along a $u = u_0$ or $v = v_0$ coordinate line is always a spiral. To prove this important property, it is convenient to rewrite (4.13) and (4.28) in a more compact form by identifying a point $\underset{\sim}{x} = (x_i, y_i)$ in the V_i-plane (i = 0,1) by a *complex number (phasor)* $\underset{\sim}{X} = (x_i + jy_i)$.[†] For example, (4.28) can be rewritten into the equivalent form

$$\pi_1 \Big[X_1(u,v) \Big] = X_1(u,v) e^{-(\sigma_1 + j1)t} \tag{4.52}$$

where $X_1(u,v) \triangleq x_{1a}(u,v) + jx_{1b}(u,v)$ and $\underset{\sim 1}{x}(u,v) \triangleq [x_{1a}(u,v), x_{1b}(u,v)]^T$.

Now for $t \in (0,\infty)$, $X_1 \Big[u_0, v(u_0, t) \Big]$ represents one point along the $u = u_0$ coordinate line. If $v(u_0, t)$ increases monotonically from $v = 0$ to $v = 1$ as in Fig. 7(a) when $u_0 = 0$, then $X_1(u,v)$ moves monotonically from $v = 0$ to $v = 1$ as t increases from 0 to ∞. If $v(u_0, t)$ is not monotonic but is bounded between v_a and v_b as in Fig. 7(h), $X_1 \Big[u_0, v(u_0, t) \Big]$ will move back and forth along portions of the $u = u_0$ coordinate line while moving from v_a to v_b. In either case, since $x_{1a}^2(u,v) + x_{1b}^2(u,v) < \infty$, $\pi_1 \Big[u_0, v(u_0, t) \Big] \to 0$ as $t \to \infty$. The loci of points under π_1 along $u = u_0$ is therefore a shrinking spiral whose amplitude is modulated in accordance with $\underset{\sim 1}{x} \Big[u_0, v(u_0, t) \Big]$. If $\underset{\sim 1}{x} \Big[u_0, v(u_0, t) \Big]$ varies only slightly for all $t \in (0,\infty)$, as in the cases shown in Figs. 6 and 8, the shrinking spiral would look almost like a "logarithmic spiral." The same interpretations apply to π_0^+ and π_0^-.

In view of the odd symmetry of the vector field ξ, spiral images under π_0^+, π_0^-, and π_1 always occur in odd-symmetric pairs. This proves formally that the cross section along the U_1 and U_{-1} boundary planes of the double scroll attractor consists of 2 tightly wound odd-symmetric spirals, thereby justifying our choice of the name "double scroll."

Since the image of π_0^+, π_0^- and π_1 of an *arbitrary* curve or line segment in U_1 is in general a curve with no special properties, it is indeed remarkable that the images along the $u = u_0$ and $v = v_0$ coordinate lines are always spirals. It is precisely this observation that prompted us to choose this unconventional local coordinate system .

[†]We use capital letters to denote phasors.

APPENDIX

Appendix 1. Derivation of Real Jordan Form

Choose vectors $\underset{\sim a}{e}$, $\underset{\sim b}{e}$ and $\underset{\sim c}{e}$ in $\mathbb{R}^3$ such that

(1) $\underset{\sim a}{e}$ is the real part of the complex eigenvector corresponding to $\tilde{\sigma} \pm j\tilde{\omega}$,

(2) $\underset{\sim b}{e}$ is the negative imaginary part of the complex eigenvector corresponding to $\tilde{\sigma} \pm j\tilde{\omega}$,

(3) $\underset{\sim c}{e}$ is the eigenvector corresponding to $\tilde{\gamma}$.

If we choose $\underset{\sim}{Q} \triangleq [\underset{\sim a}{e}, \underset{\sim b}{e}, \underset{\sim c}{e}]$, then $\underset{\sim}{J} = \underset{\sim}{Q}^{-1}\underset{\sim}{M}\underset{\sim}{Q}$ transforms an arbitrary 3×3 matrix with eigenvalues $\tilde{\sigma} \pm j\tilde{\omega}$ and $\tilde{\gamma}$ into its *real* Jordan form (see Theorem 3, p. 68 of [16]): Hence, under this new coordinate system $\underset{\sim}{x}'' = \underset{\sim}{Q}^{-1}\underset{\sim}{x}$, $\tilde{\xi}$ assumes the following real Jordan form:

$$\tilde{\xi}(\underset{\sim}{x}'') = \begin{bmatrix} \tilde{\sigma} & -\tilde{\omega} & 0 \\ \tilde{\omega} & \tilde{\sigma} & 0 \\ 0 & 0 & \tilde{\gamma} \end{bmatrix} \begin{bmatrix} x'' \\ y'' \\ z'' \end{bmatrix} \tag{A1.1}$$

where $\underset{\sim}{x}'' = (x'', y'', z'')$. Moreover U is represented by

$$lx'' + my'' + nz'' = d \tag{A1.2}$$

where $l^2 + m^2 \neq 0$, $n \neq 0$ and $d \neq 0$, because U is not parallel to either / eigenspace and does not pass through the origin.

In the new $\underset{\sim}{x}''$ coordinate system, the 3 vectors $\underset{\sim a}{e}$, $\underset{\sim b}{e}$ and $\underset{\sim c}{e}$ are transformed into 3 orthonormal axes, / the eigenspace spanned by $\underset{\sim a}{e}$ and $\underset{\sim b}{e}$ is transformed into the $x'' - y''$ plane, and the real eigenvector $\underset{\sim c}{e}$ is transformed into the z''-axis.

The U-plane is of course transformed into another plane U'' not passing through the origin and is not parallel to the $x'' - y''$ plane. Our next goal is to rotate U'' so that it makes a $45°$-degree angle with the $x'' - y''$ plane, and intersecting it at $x'' = 1$.[†] This can be achieved by choosing yet another coordinate system $\underset{\sim}{x}' = (x', y', z')$ such that the 3 orthonormal vectors $\underset{\sim a}{e}' \triangleq [1,0,0]$, $\underset{\sim b}{e}' \triangleq [0,1,0]$, and $\underset{\sim c}{e}' \triangleq [0,0,1]$ in the $\underset{\sim}{x}'$-coordinate system are transformed from $\underset{\sim 1}{e}$, $\underset{\sim 2}{e}$, and $\underset{\sim 3}{e}$ with the geometrical property which achieves the above transformation; namely, (i) make $\underset{\sim 2}{e}$ parallel to U'', (ii) make $\underset{\sim 1}{e}$ perpendicular to $\underset{\sim 2}{e}$, and such that the tip of

---

[†]The choice of $45°$ and $x'' = 1$ is strictly for convenience.

$e_{\sim 1}$ lies on U'', (iii) make $e_{\sim 1}$ and $e_{\sim 2}$ lie on the $x'' - y''$ plane, (iv) make $|e_{\sim 2}| = |e_{\sim 1}|$, (v) make $e_{\sim 3} = [0,0,d_3]$ where d_3 is chosen so that the tip of $e_{\sim 3}$ lies on U''. The above requirements defined $e_{\sim 1}$, $e_{\sim 2}$, and $e_{\sim 3}$ uniquely as follow:

$$e_{\sim 1} \triangleq \left[d/(l^2+m^2)\right][l,m,0] , \tag{A1.3}$$

$$e_{\sim 2} \triangleq \left[d/(l^2+m^2)\right][-m,l,0] , \tag{A1.4}$$

$$e_{\sim 3} \triangleq (d/n)[0,0,1] \tag{A1.5}$$

Note that the new coordinate system $x'_{\sim}$ is related to $x''_{\sim}$ by $x'_{\sim} = Q_{\sim 1}^{-1} x''_{\sim}$, where $Q_{\sim 1} \triangleq [e_{\sim 1}, e_{\sim 2}, e_{\sim 3}]$. In the $x'_{\sim}$-coordinate system, the expression of ξ and U will assume the form given in (2.3) and (2.4). To see this, define

$$Q_{\sim 1} \triangleq [e_{\sim 1}, e_{\sim 2}, e_{\sim 3}] = \begin{bmatrix} dl/(l^2+m^2) & -dm/(l^2+m^2) & 0 \\ dm/(l^2+m^2) & dl/(l^2+m^2) & 0 \\ 0 & 0 & d/n \end{bmatrix}, \tag{A1.6}$$

$$\begin{bmatrix} x' \\ y' \\ z' \end{bmatrix} \triangleq Q_{\sim 1}^{-1} \begin{bmatrix} x'' \\ y'' \\ z'' \end{bmatrix} = \begin{bmatrix} l/d(l^2+m^2) & m/d(l^2+m^2) & 0 \\ -m/d(l^2+m^2) & l/d(l^2+m^2) & 0 \\ 0 & 0 & n/d \end{bmatrix} \begin{bmatrix} x'' \\ y'' \\ z'' \end{bmatrix} \tag{A1.7}$$

Then we have[†]

$$\xi(x'_{\sim}) = Q_{\sim 1}^{-1} \begin{bmatrix} \tilde{\sigma} & -\tilde{\omega} & 0 \\ \tilde{\omega} & \tilde{\sigma} & 0 \\ 0 & 0 & \tilde{\gamma} \end{bmatrix} Q_1 \begin{bmatrix} x' \\ y' \\ z' \end{bmatrix} = \begin{bmatrix} \tilde{\sigma} & -\tilde{\omega} & 0 \\ \tilde{\omega} & \tilde{\sigma} & 0 \\ 0 & 0 & \tilde{\gamma} \end{bmatrix} \begin{bmatrix} x' \\ y' \\ z' \end{bmatrix} \tag{A1.8}$$

and

$$U : (l,m,n) \begin{bmatrix} x'' \\ y'' \\ z'' \end{bmatrix} = d \tag{A1.9}$$

[†]Note that $Q_{\sim 1}^{-1} J Q_{\sim 1} = J$ because by choosing $|e_{\sim 1}| = |e_{\sim 2}|$, and $e_{\sim 1} \perp e_{\sim 2}$, the first two rows of $Q_{\sim 1}$ are a product of a scalar and a planar rotation, and since the first two rows of J define a planar rotation.

<=>

$$(l,m,n) \, \underset{\sim}{Q}_1 \begin{bmatrix} x' \\ y' \\ z' \end{bmatrix} = d \qquad\qquad (A1.10)$$

<=>

$$(d,0,d) \begin{bmatrix} x' \\ y' \\ z' \end{bmatrix} = d \qquad\qquad (A1.11)$$

<=>

$$x' + z' = 1 \ . \qquad\qquad (A1.12)$$

Appendix 2. Proof of Lemma 3.2

To prove Lemma 3.2, we need the following lemma.

Lemma A2.1. $\overrightarrow{OA}$, $\overrightarrow{OB}$, and $\overrightarrow{OE}$ are linearly independent.

Proof. Case (i): $E \neq B$. Assume that $\overrightarrow{OA}$ can be written as a linear combination of $\overrightarrow{OB}$ and $\overrightarrow{OE}$. Then, since $B,E \in L_2$, we have $A \in L_2$, and so $A_0 \in \Psi_0(L_2)$. Since $A_0 = (1,p_0,0)$, from the equation of $\Psi_0(L_2)$ in (2.16), it follows that $p_0 = \sigma_0$. Therefore $A_0 = E_0$. Similarly, from $A_1 \in \Psi_1(L_2)$, we have $p_1 = \sigma_1$ and hence $A_1 = B_1$. Therefore we obtain $E = A = B$, a contradiction.

Case (ii): $E = B$. Choose a point K on U_1 defined by $\overrightarrow{OK} = \overrightarrow{OE} + \xi(E)$. Since $E \in L_0$ and $\xi(E) /\!/ L_0$, we have $K \in L_0$. Since $E_0 = (1,\sigma_0,0)$ and $B_1 = (1,\sigma_1,0)$, from the expression of ξ_i ($i = 0,1$) in (2.9) and (2.12), it follows that

$$K_0 \triangleq \Psi_0(K) = \Psi_0(E) + \Psi_0\left[\xi(E)\right]$$

$$= E_0 + \widetilde{\omega}_0 \xi_0(E_0) = \left[1,\sigma_0+\widetilde{\omega}_0(\sigma_0^2+1),0\right]$$

Hence,

$$\xi_0(K_0) = \left[-\widetilde{\omega}_0(\sigma_0^2+1),(\sigma_0^2+1)(1+\sigma_0\widetilde{\omega}_0),0\right] \ .$$

Since $B = E$,

$$K_1 \triangleq \Psi_1(K) = \Psi_1\Big[B + \xi(B)\Big]$$

$$= B_1 + \widetilde{\omega}_1 \xi_1(B) = \Big[1, \sigma_1 + \widetilde{\omega}_1(\sigma_1^2 + 1), 0\Big] \ .$$

Hence,

$$\xi_1(K_1) = \Big[-\widetilde{\omega}_1(\sigma_1^2 + 1), (\sigma_1^2 + 1)(1 + \sigma_1 \widetilde{\omega}_1), 0\Big] \ .$$

Defining the normal vector $\underset{\sim}{h} \triangleq (1, 0, 1)$ of V_i ($i = 0, 1$), we obtain

$$\langle \underset{\sim}{h}, \xi_0(K_0) \rangle = -\widetilde{\omega}_0(\sigma_0^2 + 1) < 0 \tag{A2.1}$$

$$\langle \underset{\sim}{h}, \xi_1(K_1) \rangle = -\widetilde{\omega}_1(\sigma_1^2 + 1) < 0 \tag{A2.2}$$

Now (A2.1) implies that the vector $\xi_0(K_0)$ at the point $K_0 \in \Psi_0(U_1)$ must point towards the origin of the eigenspace $\Psi_0\Big[E^c(0)\Big]$ in the D_0-unit in Fig. 2(b), i.e., below V_0. This implies that $\xi(K)$ at $K \in U_1$ must point toward the interior of the D_0-region, i.e., downwards. However, (A2.2) implies that the vector $\xi_1(K_1)$ at the point $K_1 \in \Psi_1(U_1)$ must point towards the origin of the eigenspace $\Psi_1\Big[E^c(P)\Big]$ in the D_1-unit in Fig. 2(b), i.e., below V_1. This implies that $\xi(K)$ at $K \in U_1$ must point towards the interior of the D_1-region, i.e., upwards. This is a contradiction and Lemma A2.1 is proved.

∎

We are now ready to prove *Lemma 3.2*. Given $\underset{\sim}{\mu} = (\sigma_0, \gamma_0, \sigma_1, \gamma_1, k)$, choose any $\xi \in \xi[\underset{\sim}{\mu}]$. Denote the eignevalue parameters of ξ by $(\widetilde{\sigma}_0, \widetilde{\omega}_0, \widetilde{\gamma}_0, \widetilde{\sigma}_1, \widetilde{\omega}_1, \widetilde{\gamma}_1)$. Let the vector from the origin to the fundamental points $\{A, B, E, P\}$ be denoted by $\{\underset{\sim}{A}, \underset{\sim}{B}, \underset{\sim}{E}, \underset{\sim}{P}\}$ respectively. By *Lemma A2.1*, the matrices $[\underset{\sim}{A}, \underset{\sim}{B}, \underset{\sim}{E}]$ and $[\underset{\sim}{A} - \underset{\sim}{P}, \underset{\sim}{B} - \underset{\sim}{P}, \underset{\sim}{E} - \underset{\sim}{P}]$ are invertible. Since the affine maps Ψ_i carry $\{A, B, E\}$ into $\{A_i, B_i, E_i\}$, $i = 0, 1$, respectively, Φ_i can be written as follows;

$$\Psi_0(\underset{\sim}{x}) = \underset{\sim}{\Phi}_0 \underset{\sim}{x} \quad , \underset{\sim}{\Phi}_0 = [\underset{\sim}{A}_0, \underset{\sim}{B}_0, \underset{\sim}{E}_0][\underset{\sim}{A}, \underset{\sim}{B}, \underset{\sim}{E}]^{-1} , \quad (\underset{\sim}{x} \in D_0) \tag{A2.3}$$

$$\Psi_1(\underset{\sim}{x}) = \underset{\sim}{\Phi}_1(\underset{\sim}{x} - \underset{\sim}{P}) , \underset{\sim}{\Phi}_1 = [\underset{\sim}{A}_1, \underset{\sim}{B}_1, \underset{\sim}{E}_1][\underset{\sim}{A} - \underset{\sim}{P}, \underset{\sim}{B} - \underset{\sim}{P}, \underset{\sim}{E} - \underset{\sim}{P}]^{-1} , \quad (\underset{\sim}{x} \in D_1) \tag{A2.4}$$

By (2.9) and (2.12), since for $i = 0, 1$,

$$\frac{1}{\widetilde{\omega}_i} D\Psi_i\Big[\xi\Big[\Psi_i^{-1}(\underset{\sim}{x})\Big]\Big] = \underset{\sim}{J}_i \underset{\sim}{x} \tag{A2.5}$$

where

$$
\underset{\sim i}{J} \triangleq \begin{bmatrix} \sigma_i & -1 & 0 \\ 1 & \sigma_i & 0 \\ 0 & 0 & \gamma_i \end{bmatrix} ,
$$

we obtain

$$
\xi|_{D_0}(\underset{\sim}{x}) = \widetilde{\omega}_0 \underset{\sim 0}{\Phi^{-1}} \underset{\sim 0}{J} \underset{\sim 0}{\Phi} \underset{\sim}{x} \tag{A2.6}
$$

$$
\xi|_{D_1}(\underset{\sim}{x}) = \widetilde{\omega}_1 \underset{\sim 1}{\Phi^{-1}} \underset{\sim 1}{J} \underset{\sim 1}{\Phi} (\underset{\sim}{x} - \underset{\sim}{P}) \tag{A2.7}
$$

The *continuity* of ξ is equivalent to the condition

$$
\xi|_{D_0}(\underset{\sim}{x}) = \xi|_{D_1}(\underset{\sim}{x}) \tag{A2.8}
$$

for all $\underset{\sim}{x} \in U_1 = D_0 \cap D_1$. Since each $\underset{\sim}{x} \in U_1$ is a linear combination of $\underset{\sim}{A}$, $\underset{\sim}{B}$, and $\underset{\sim}{E}$ in view of *Lemma A2.1*, the continuity of ξ is equivalent to the condition that (A2.8) holds for $\underset{\sim}{x} = $ A, B, and E. Substituting $\underset{\sim}{x} = \underset{\sim}{A}$, $\underset{\sim}{B}$, $\underset{\sim}{E}$ in (A2.6)-(A2.8), we obtain

$$
\underset{\sim 0}{\Phi^{-1}} \underset{\sim 0}{J} \underset{\sim 0}{\Phi} [\underset{\sim}{A}, \underset{\sim}{B}, \underset{\sim}{E}] = \lambda \underset{\sim 1}{\Phi^{-1}} \underset{\sim 1}{J} \underset{\sim 1}{\Phi} [\underset{\sim}{A} - \underset{\sim}{P}, \underset{\sim}{B} - \underset{\sim}{P}, \underset{\sim}{E} - \underset{\sim}{P}] \tag{A2.9}
$$

where $\lambda \triangleq \widetilde{\omega}_1 / \widetilde{\omega}_0$. Defining

$$
\underset{\sim 0}{W} \triangleq [\underset{\sim 0}{A}, \underset{\sim 0}{B}, \underset{\sim 0}{E}]^{-1} \underset{\sim 0}{J} [\underset{\sim 0}{A}, \underset{\sim 0}{B}, \underset{\sim 0}{E}] \tag{A2.10}
$$

and

$$
\underset{\sim 1}{W} \triangleq [\underset{\sim 1}{A}, \underset{\sim 1}{B}, \underset{\sim 1}{E}]^{-1} \underset{\sim 1}{J} [\underset{\sim 1}{A}, \underset{\sim 1}{B}, \underset{\sim 1}{E}] . \tag{A2.11}
$$

and using (A2.3)-(A2.2), we can rewrite (A2.9) as $[\underset{\sim}{A}, \underset{\sim}{B}, \underset{\sim}{E}] \underset{\sim 0}{W} = \lambda [\underset{\sim}{A} - \underset{\sim}{P}, \underset{\sim}{B} - \underset{\sim}{P}, \underset{\sim}{E} - \underset{\sim}{P}] \underset{\sim 1}{W}$, and hence

$$
[\underset{\sim}{A}, \underset{\sim}{B}, \underset{\sim}{E}](\lambda \underset{\sim 1}{W} - \underset{\sim 0}{W}) = \lambda [\underset{\sim}{P}, \underset{\sim}{P}, \underset{\sim}{P}] \underset{\sim 1}{W} . \tag{A2.12}
$$

Substituting the coordinate of A_i, B_i, and E_i (i = 0,1) in (2.20)-(2.24) and (2.26)-(2.31) into (A2.10)-(A2.11), we obtain after some algebraic simplification the following:

$$
\underset{\sim 0}{W} = \frac{1}{\sigma_0 - p_0} \begin{bmatrix} (\sigma_0 - p_0)^2 - (p_0^2 + 1) & -\gamma_0(\sigma_0 - p_0) & -(\sigma_0^2 + 1) \\ 0 & \gamma_0(\sigma_0 - p_0) & 0 \\ p_0^2 + 1 & 0 & \sigma_0^2 + 1 \end{bmatrix} \tag{A2.13}
$$

$$\underset{\sim}{W}_1 = \frac{1}{\sigma_1-p_1} \begin{vmatrix} (\sigma_1-p_1)^2-(p_1^2+1) & -(\sigma_1^2+1) & -\gamma_1(\sigma_1-p_1) \\ p_1^2+1 & \sigma_1^2+1 & 0 \\ 0 & 0 & \gamma_1(\sigma_1-p_1) \end{vmatrix} \qquad \text{(A2.14)}$$

where $p_i = \sigma_i + (\sigma_i^2 + 1)k_i / \gamma_i$ (i = 0,1). Note that $\underset{\sim}{W}_i$ is determined by only σ_i, γ_i and k_i

(i = 0,1). Defining $c_i \triangleq \alpha_i - p_i$ (i = 0,1), we obtain (1,1,1) $\underset{\sim}{W}_i = (c_i,0,0)$. Since $[\underset{\sim}{P},\underset{\sim}{P},\underset{\sim}{P}] = \underset{\sim}{P}(1,1,1)$, by (A2.12),

$$[\underset{\sim}{A},\underset{\sim}{B},\underset{\sim}{E}](\lambda \underset{\sim}{W}_1 - \underset{\sim}{W}_0) = \lambda \underset{\sim}{P}(1,1,1)\underset{\sim}{W}_1 = \lambda \underset{\sim}{P}(c_1,0,0) = \lambda c_1[\underset{\sim}{P},0,0] \ . \qquad \text{(A2.15)}$$

The column vectors in (A2.15) can be written as follow:

$$\underset{\sim}{P} = \frac{1}{\lambda c_1}[\underset{\sim}{A},\underset{\sim}{B},\underset{\sim}{E}](\lambda \underset{\sim}{W}_1 - \underset{\sim}{W}_0)(1,0,0)^T \qquad \text{(A2.16)}$$

$$\underset{\sim}{0} = (\lambda \underset{\sim}{W}_1 - \underset{\sim}{W}_0)(0,1,0)^T \qquad \text{(A2.17)}$$

$$\underset{\sim}{0} = (\lambda \underset{\sim}{W}_1 - \underset{\sim}{W}_0)(0,0,1)^T \qquad \text{(A2.18)}$$

It follows from (A2.13), (A2.14), (A2.17), and (A2.18) that

$$\lambda = \gamma_0 \frac{\sigma_1-p_1}{\sigma_1^2+1} = \frac{\sigma_0^2+1}{\gamma_1(\sigma_0-p_0)} \qquad \text{(A2.19)}$$

Since $k_0 \triangleq \gamma_0(p_0-\sigma_0)/(\sigma_0^2+1)$ in (2.21), (A2.19) implies

$$\lambda = -\frac{\gamma_0}{\gamma_1 k_0} \qquad \text{(A2.20)}$$

Since $\lambda = \tilde{\omega}_1/\tilde{\omega}_0$, and since $k_0 = 1/k_1$ as stated in (2.34), we obtain

$$\frac{1}{k_1} = k_0 = -\frac{\gamma_0 \tilde{\omega}_0}{\gamma_1 \tilde{\omega}_1} = -\frac{\tilde{\gamma}_0}{\tilde{\gamma}_1} = k \ . \qquad \text{(A2.21)}$$

This proves statement (b) of *Lemma 3.2.*

To prove statement (a), define

$$(l,m,n)^T = \frac{1}{\lambda c_1}(\lambda \underset{\sim}{W}_1 - \underset{\sim}{W}_0)(1,0,0)^T \qquad \text{(A2.22)}$$

This is determined by σ_0, γ_0, σ_1, γ_1, and k in view of (A2.13), (A2.14), (A2.20), and (A2.21). It follows from (A2.16) that

$$\underset{\sim}{P} = [\underset{\sim}{A}, \underset{\sim}{B}, \underset{\sim}{E}](l,m,n)^T = l\underset{\sim}{A} + m\underset{\sim}{B} + n\underset{\sim}{E} \tag{A2.23}$$

Hence (3.10) holds.

To prove statement (c) of *Lemma 3.2*, note that (2.21) and (2.27) imply

$$c_i \triangleq \sigma_i - p_i = -\frac{k_i(\sigma_i^2+1)}{\gamma_i} \quad (i = 0,1) \tag{A2.24}$$

Using (A2.13), (A2.14), (A2.20), and (A2.24), we obtain

$$s \triangleq l + m + n = \frac{1}{\lambda c_1}(1,1,1)(\gamma \underset{\sim}{W}_1 - \underset{\sim}{W}_0)(1,0,0,)^T$$

$$= 1 - \frac{c_0}{\lambda c_1} = 1 + k^3\gamma_1^2(\sigma_0^2+1)/\gamma_0^2(\sigma_1^2+1) \tag{A2.25}$$

Since by (P.4) in *Definition 2.1*, $P = P^+$ must be *located in the* interior of D_1, it follows from (A2.23) that $s = l + m + n > 1$, that is

$$s - 1 = k^3\gamma_1^2(\sigma_0^2+1)/\gamma_0^2(\sigma_1^2+1) > 0 \tag{A2.26}$$

Therefore $k > 0$ holds. Since $-\gamma_0/\gamma_1 k = \lambda = \tilde{\omega}_1/\tilde{\omega}_0 > 0$, we have $\gamma_0\gamma_1 < 0$. This proves that $\xi \in \xi[\underset{\sim}{\mu}] \Rightarrow \gamma_0\gamma_1 < 0$ and $k > 0$.

To prove the converse, let $\underset{\sim}{\mu} = (\sigma_0,\gamma_0,\sigma_1,\gamma_1,k)$ be given such that $\gamma_0\gamma_1 < 0$ and $k > 0$. Using (A2.21), define λ, c_i, $\underset{\sim}{W}_0$, $\underset{\sim}{W}_1$, (l,m,n) and s by (A2.20), (A2.24), (A2.13), (A2.14), (A2.22), and (A2.25) respectively. Define 4 vectors as follows:

$$\underset{\sim}{A} = (1,1,1) \; , \; \underset{\sim}{B} = (1,-(l+n)/m,1) \tag{A2.23}$$

$$\underset{\sim}{E} = (-(l+m)/n,1,1) \; , \; \underset{\sim}{P} = (0,0,s) \; .$$

Using (A2.23), we obtain

$$[\underset{\sim}{A}, \underset{\sim}{B}, \underset{\sim}{E}]\underset{\sim}{W}_0 = \lambda[\underset{\sim}{A} - \underset{\sim}{P}, \underset{\sim}{B} - \underset{\sim}{P}, \underset{\sim}{E} - \underset{\sim}{P}]\underset{\sim}{W}_1 \tag{A2.24}$$

This guarantees that the vector field ξ defined by

$$\xi(\underset{\sim}{x}) \triangleq \lambda[\underset{\sim}{A} - \underset{\sim}{P}, \underset{\sim}{B} - \underset{\sim}{P}, \underset{\sim}{E} - \underset{\sim}{P}]\underset{\sim}{W}_1[\underset{\sim}{A} - \underset{\sim}{P}, \underset{\sim}{B} - \underset{\sim}{P}, \underset{\sim}{E} - \underset{\sim}{P}]^{-1}(\underset{\sim}{x}-\underset{\sim}{P}) \; , \; z \geq 1$$

$$\triangleq [\underset{\sim}{A}, \underset{\sim}{B}, \underset{\sim}{E}]\underset{\sim}{W}_0[\underset{\sim}{A}, \underset{\sim}{B}, \underset{\sim}{E}]^{-1}\underset{\sim}{x} \qquad\qquad , \; |z| \leq 1 \tag{A2.25}$$

$$\triangleq \lambda[\underset{\sim}{A} - \underset{\sim}{P}, \underset{\sim}{B} - \underset{\sim}{P}, \underset{\sim}{E} - \underset{\sim}{P}]\underset{\sim}{W}_1[\underset{\sim}{A} - \underset{\sim}{P}, \underset{\sim}{B} - \underset{\sim}{P}, \underset{\sim}{E} - \underset{\sim}{P}]^{-1}(\underset{\sim}{x}+\underset{\sim}{P}) \; , \; z \leq -1$$

for $\underset{\sim}{x} = (x,y,z)^T$, is *continuous*. Moreover we can verify that the piecewise-linear vector field ξ as defined in (A2.25) satisfies (P.1)-(P.6) in *Definition 2.1*. Therefore $\xi \in \mathcal{L}$. This proves statement (c).

Appendix 3. Proof of Theorem 3.3

Let $\{\tilde{\sigma}_0,\tilde{\omega}_0,\tilde{\gamma}_0,\tilde{\sigma}_1,\tilde{\omega}_1,\tilde{\gamma}_1\}$ be given such that $\tilde{\omega}_0 > 0$, $\tilde{\omega}_1 > 0$, and $\tilde{\gamma}_0\tilde{\gamma}_1 < 0$. Put $\underset{\sim}{\mu} = (\sigma_0,\gamma_0,\sigma_1,\gamma_1,k) \triangleq (\tilde{\sigma}_0/\tilde{\omega}_0,\tilde{\gamma}_0/\tilde{\omega}_0,\tilde{\sigma}_1/\tilde{\omega}_1,\tilde{\gamma}_1/\tilde{\omega}_1,-\tilde{\gamma}_0/\tilde{\gamma}_1)$. As shown in (A2.22), $l = l(\underset{\sim}{\mu})$, $m = m(\underset{\sim}{\mu})$ and $n = n(\underset{\sim}{\mu})$ are given by

$$(l,m,n) = \frac{1}{\lambda c_1}(\lambda \underset{\sim}{W}_1 - \underset{\sim}{W}_0)(1,0,0)^T . \tag{A3.1}$$

Using $c_1 = \sigma_1 - p_1 = -k_0(\sigma_0^2 + 1)/\gamma_0$ (by (A2.24)), $\lambda = -\gamma_0/\gamma_1 k_0$ (by (A2.20)) and $k_0 = k$ (by (A2.21)), and substituting (A2.13) and (A2.14) for $\underset{\sim}{W}_i$, we obtain after simplification:

$$l = -k\gamma_0\gamma_1\{2(\sigma_0\gamma_1 k + \sigma_1\gamma_0) + \gamma_0\gamma_1(k+1)\}/\{\gamma_0^2(\sigma_1^2+1)\} \tag{A3.2}$$

$$m = \{(\gamma_1 k + \sigma_1)^2 + 1\}/(\sigma_1^2 + 1) \tag{A3.3}$$

$$n = k^3\gamma_1^2\{(\gamma_0 k + \sigma_0)^2 + 1\}/\{\gamma_0^2(\sigma_1^2+1)\} \tag{A3.4}$$

$$s = l + m + n = 1 + k^3\gamma_1^2(\sigma_0^2+1)/\{\gamma_0^2(\sigma_1^2+1)\} \tag{A3.5}$$

Defining $\Delta_i = (\tilde{\sigma}_i^2 + \tilde{\omega}_i^2)\tilde{\gamma}_i$ and $T_i = 2\tilde{\sigma}_i + \tilde{\gamma}_i$ (i = 0,1), we can rewrite (A3.2)-(A3.5) as follow:

$$l = \tilde{\gamma}_0\tilde{\gamma}_1(T_1 - T_0)/\Delta_1 \tag{A3.6}$$

$$m = -\{\tilde{\gamma}_0\tilde{\gamma}_1[T_1 - (\tilde{\gamma}_0 + \tilde{\gamma}_1)] - \Delta_1\}/\Delta_1 \tag{A3.7}$$

$$n = \{\tilde{\gamma}_0\tilde{\gamma}_1[T_0 - (\tilde{\gamma}_0 + \tilde{\gamma}_1)] - \Delta_0\}/\Delta_1 \tag{A3.8}$$

$$s = 1 - \Delta_0/\Delta_1 \tag{A3.9}$$

The vector field ξ defined by (A2.25) has eigenvalues $\sigma_0 \pm j 1$, γ_0 (in D_0-region) and $(\tilde{\omega}_1/\tilde{\omega}_0)$ $(\sigma_1 \pm j 1)$, $(\tilde{\omega}_1/\tilde{\omega}_0)\gamma_1$ (in D_1-region), because matrix $\underset{\sim i}{W}$ is similar to $\underset{\sim i}{J}$ (i = 0,1) in (A2.5) and $\lambda = \tilde{\omega}_1/\tilde{\omega}_0$. Hence, the piecewise-linear vector field

$$\xi(\underset{\sim}{x}) \triangleq \widetilde{\omega}_1[\underset{\sim}{A} - \underset{\sim}{P}, \underset{\sim}{B} - \underset{\sim}{P}, \underset{\sim}{E} - \underset{\sim}{P}]\underset{\sim}{W}_1[\underset{\sim}{A} - \underset{\sim}{P}, \underset{\sim}{B} - \underset{\sim}{P}, \underset{\sim}{E} - \underset{\sim}{P}]^{-1}(\underset{\sim}{x} - \underset{\sim}{P}) \quad , z \geq 1$$

$$\triangleq \widetilde{\omega}_0[\underset{\sim}{A}, \underset{\sim}{B}, \underset{\sim}{E}]\underset{\sim}{W}_0[\underset{\sim}{A}, \underset{\sim}{B}, \underset{\sim}{E}]^{-1}\underset{\sim}{x} \quad\quad\quad , |z| \leq 1 \quad\quad\quad \textbf{(A3.10)}$$

$$\triangleq \widetilde{\omega}_1[\underset{\sim}{A} - \underset{\sim}{P}, \underset{\sim}{B} - \underset{\sim}{P}, \underset{\sim}{E} - \underset{\sim}{P}]\underset{\sim}{W}_1[\underset{\sim}{A} - \underset{\sim}{P}, \underset{\sim}{B} - \underset{\sim}{P}, \underset{\sim}{E} - \underset{\sim}{P}]^{-1}(\underset{\sim}{x} + \underset{\sim}{P}) \quad , z \leq -1$$

where $\underset{\sim}{x} = (x, y, z)^T$ must have eigenvalues $\widetilde{\sigma}_i \pm j\widetilde{\omega}_i$ and $\widetilde{\gamma}_i$ in the D_i-region (i = 0,1). Substituting (A3.6)-(A3.9) into (A2.23), (A2.13)-(A2.14) into (A3.10), and expressing $\underset{\sim}{A}$, $\underset{\sim}{B}$, $\underset{\sim}{E}$, and $\underset{\sim}{P}$ in terms of $\widetilde{\sigma}_i$, $\widetilde{\omega}_i$, and $\widetilde{\gamma}_i$ (i = 0,1), we can recast $\xi(\underset{\sim}{x})$ in (A3.10) in terms of only the 6 eigenvalue parameters. Finally, we can verify, after some involved algebraic manipulations, that (3.32) is equivalent to (A3.10).

∎

THE DOUBLE SCROLL FAMILY
PART II: RIGOROUS ANALYSIS OF BIFURCATION PHENOMENA

Leon O. Chua, Motomasa Komuro and Takashi Matsumoto[‡]

Department of Electrical Engineering and Computer Sciences
and the Electronics Research Laboratory
University of California, Berkeley, CA 94720

ABSTRACT

This paper represents Part II of a 2-part paper which provides a rigorous mathematical proof that the double scroll is indeed *chaotic*. Our approach is to derive a *linearly equivalent* class of piecewise-linear differential equations which includes the double scroll as a special case. Necessary and sufficient condition for two piecewise-linear vector fields to be linearly equivalent is that their respective eigenvalues be a scaled version of each other. In the special case where they are identical, we have exact equivalence in the sense of *linear conjugacy*.

Explicit *normal form* equation in the context of global bifurcation is derived and parametrized by their eigenvalues. Analytical expressions for various *Poincare maps* are then derived and used to characterize the *birth* and the *death* of the double scroll, as well as to derive an approximate one-dimensional map in analytic form which is useful for further bifurcation analysis. In particular, the analytical expressions characterizing various *half-return maps* associated with the Poincare map are used in a crucial way to prove the existence of a Shilnikov-type homoclinic orbit, thereby establishing rigorously the chaotic nature of the double scroll. These analytical expressions are also fundamental in our in-depth analysis of the *birth* (onset of the double scroll) and *death* (extinction of chaos) of the double scroll.

The unifying theme throughout this paper is to analyze the double scroll system as an *unfolding* of a large family of piecewise-linear vector fields in $\mathbb{R}^3$. Using this approach, we were able to prove that the *chaotic dynamics* of the double scroll is quite common and robust. In fact, it is exhibited by a large family (in fact, infinitely many *linearly-equivalent circuits*) of vector fields whose associated piecewise-linear differential equations bear no resemblance to each other. It is therefore remarkable that the normalized eigenvalues, which is a *local* concept, completely determines the system's *global* qualitative behavior.

5. PROOF OF CHAOS IN THE DOUBLE SCROLL

An equilibrium point Q of a vector field ξ is said to have a *homoclinic point* if there exists a trajectory which tends to Q as $t \to +\infty$ and as $t \to -\infty$. Such a trajectory is called a *homoclinic orbit* through Q. The significance of homoclinic orbits is given by the following important result:

Shilnikov's Theorem [9,15,19][†]

Let ξ be a continuous piecewise-linear vector field associated with a 3rd order autonomous system $\dot{x} = f(x)$, $x \in \mathbb{R}^3$. Assume the origin is an equilibrium point with a pair of complex eigenvalues $\sigma \pm j\omega$ ($\sigma < 0$, $\omega \neq 0$) and a real eigenvalue $\gamma > 0$ satisfying $|\sigma| < \gamma$. If in addition, ξ has a *homoclinic orbit* through the origin, then ξ can be infinitesimally perturbed into a nearby vector field ξ' with a countable set of *horseshoes*.

Since *horseshoes* give rise to extremely complicated behaviors typically observed in chaotic systems [9], one of the few *rigorous* methods to prove a system is chaotic is to apply Shilnikov's theorem. In this section, we will prove the double scroll family (4.1) is chaotic by showing Shilnikov's theorem is satisfied. In particular, we will prove that there exist parameters such that the trajectory along the *unstable* real eigenvector $E^r(0)$ from the origin will enter the *stable* eigenspace $E^c(0)$ in Fig. 2(a) and hence return to the origin. By symmetry, the trajectory along the other unstable real eigenvector would behave in the same way. These 2 special trajectories are shown in Fig. 9(b) and are therefore both homoclinic orbits.

Theorem 5.1: Homoclinic orbits in the double scroll family

Let ξ be any vector field in the *double scroll family*

$$\mathcal{L}_0 \triangleq \{\xi(\sigma_0,\gamma_0,\sigma_1,\gamma_1,k)\,|\,\sigma_0 < 0,\gamma_0 > 0,\sigma_1 > 0,\gamma_1 < 0,k > 0\} \tag{5.1}$$

Assume ξ satisfies the following conditions:

(i) Let $C_1 \triangleq \Psi_1(C)$ map under π_1^{-1} into a point on the line segment $\overline{A_1E_1}$ in the D_1-unit (see the V_1-portrait/V_0 in Fig. 9(a).[‡]

(ii) In the D_0-unit (Fig. 2(b)), no trajectory starting from points on the line segment $\overline{A_0E_0}$ in the eigenspace $z = 0$ intersects the boundary line $x = -1$.

[†]The original Shilnikov theorem requires $f(\cdot)$ to be an analytic function. The piecewise linear version we invoke in this paper is used in [15,19].

[‡]Recall C is the intersection of the unstable real eigenvector at the origin with the upper boundary U_1 in Fig. 2(a) and π_1 is the half-return map defined in Section 4.2. Condition (i) means that $\widehat{E_1A_1} = \pi_1(\overline{E_1A_1})$ must pass through the point C_1.

Then ξ has a *homoclinic orbit* through the origin.

If, in addition,

(iii) $|\sigma_0| < \gamma_0$ (5.2)

Then ξ is *chaotic* in the sense of Shilnikov's theorem.

Proof.

Theorem 3.2 guarantees that the vector field $\xi \in \mathcal{L}_0$ is continuous and the half-return map π_1 is well defined.

Consider the trajectory Γ_0 through the origin and moving upward along the *unstable real eigenvector* $E^r(0)$ in Fig. 2(a) until it hits U_1 at point C. Since $C_1 = \Psi_1(C)$ and $C_1' \triangleq \pi_1^{-1}(C_1) \in \overline{A_1 E_1} = \Psi_1(\overline{AE})$ (see Fig. 9(a)) in view of condition (i), it follows that the trajectory Γ_C through C must land at a point C_2 on segment $\overline{AE}$ in Fig. 2(a). But $\overline{AE}$ lies on the *stable eigenspace* $E^c(0)$ at the origin, and since condition (ii) guarantees that the trajectory Γ_{C_2} through C_2 will not intersect the lower boundary U_{-1}, it follows that Γ_{C_2} must remain on the eigenspace $E^c(0)$ and converge to the origin as $t \to \infty$. Since $\Gamma \triangleq \Gamma_0 \cup \Gamma_C \cup \Gamma_{C_2}$ tends to the origin as $t \to +\infty$ and $t \to -\infty$, it is a *homoclinic* orbit.

If in addition $|\sigma_0| < \gamma_0$, then the hypotheses of Shilnikov's theorem are satisfied and hence ξ is chaotic .

       ■

Theorem 5.2: Chaos in the double scroll

The double scroll system (1.1)-(1.3) is *chaotic* in the sense of Shilnikov's theorem for some parameters m_0, m_1, α and β. In particular, if $m_0 = -1/7$, $m_1 = 2/7$ and $\alpha = 7$, then there exists some β in the range $6.5 \leq \beta \leq 10.5$ such that the hypotheses of Shilnikov's theorem are satisfied.

Before we can prove Theorem 5.2, we will need 4 *lemmas* to be stated and proved below. To avoid repetition, we make the following assumption:

Standing Assumption:

The parameters for all lemmas are:

$$m_0 = -1/7 , \quad m_1 = 2/7 , \quad \alpha = 7 , \quad \beta \in J \triangleq [6.5, 10.5] \tag{5.3}$$

Also, we will use the abbreviated notation

$$\lambda \uparrow \text{ in } a \leq \lambda \leq b \quad (\text{resp.}, \lambda \downarrow \text{ in } b \geq \lambda \geq a) \tag{5.4}$$

$a \leq \min(\lambda) \leq \max(\lambda) \leq b$ as β increases monotonically in the range J.

Lemma 5.1

As β increases monotonically from $\beta_1 = 6.5$ to $\beta_2 = 10.5$, the following parameters also vary monotonically as indicated:[†]

(i) $\tilde{\sigma}_0 \uparrow$ in $-1.066296 \leq \tilde{\sigma}_0 \leq -0.906832$

$\tilde{\omega}_0 \uparrow$ in $1.382371 \leq \tilde{\omega}_0 \leq 2.228686$ $\qquad$ (5.5)

$\tilde{\gamma}_0 \downarrow$ in $2.132590 \geq \tilde{\gamma}_0 \geq 1.813664$

(ii) $\tilde{\sigma}_1 \downarrow$ in $0.295297 \geq \tilde{\sigma}_1 \geq 0.138551$

$\tilde{\omega}_1 \uparrow$ in $1.879726 \leq \tilde{\omega}_1 \leq 2.527628$ $\qquad$ (5.6)

$\tilde{\gamma}_1 \uparrow$ in $-3.590593 \leq \tilde{\gamma}_1 \leq -3.277103$

(iii) $\sigma_0 \uparrow$ in $-0.771352 \leq \sigma_0 \leq -0.406890$

$\sigma_1 \downarrow$ in $0.157096 \geq \sigma_1 \geq 0.054814$

$\gamma_0 \downarrow$ in $1.542794 \geq \gamma_0 \geq 0.813782$ $\qquad$ (5.7)

$\gamma_1 \uparrow$ in $-1.910168 \leq \gamma_1 \leq -1.296513$

(iv) $k_0/\gamma_0 \uparrow$ in $0.384997 \leq k_0/\gamma_0 \leq 0.680079$

$k_1/\gamma_1 \downarrow$ in $-0.881427 \geq k_1/\gamma_1 \geq -1.393659$ $\qquad$ (5.8)

Moreover, the above bounds can be calculated to *any desired* accuracy.

Proof. It follows from (1.1)-(1.3) that the real eigenvalue $\tilde{\gamma}_i$ corresponding to $m = m_i$ ($i = 0,1$) is a real root of the characteristic polynomial equation

$$x^3 + (\alpha m + 1)x^2 + (\alpha m - \alpha + \beta)\, x + \alpha \beta m = 0 \qquad (5.9)$$

Solving (5.9) for β we obtain

$$\beta = \beta(x) \triangleq \alpha - x(x+1) - \frac{\alpha^2 m}{x + \alpha m} \qquad (5.10)$$

It follows from (5.10) that if $\alpha > 0$ and $\alpha m > 1$, then $\beta : (-\infty, -\alpha m) \to \mathbb{R}$ is an increasing bijection (i.e., one-to-one and onto), and if $\alpha > 0$ and $\alpha m < 0$, then $\beta : (\alpha m, \infty) \to \mathbb{R}$ is a

---

[†]Recall the following definitions: for $i = 0$ or 1, $\sigma_i \triangleq \tilde{\sigma}_i / \tilde{\omega}_i$, $\gamma_i \triangleq \tilde{\gamma}_i / \tilde{\omega}_i$, $k_0 \triangleq 1/k_1 \triangleq k \triangleq -\tilde{\gamma}_0/\tilde{\gamma}_1$, $Q_i \triangleq (\sigma_i - \gamma_i)^2 + 1$, $p_i \triangleq \sigma_i + (\sigma_i^2 + 1)(k_i / \gamma_i)$.

decreasing bijection. Hence, for $\alpha = 7$ and $m_0 = -1/7$ (resp., $m_1 = 2/7$), $\tilde{\gamma}_0$ (resp., $\tilde{\gamma}_1$) decreases (resp., increases) and satisfies

$$1.813664 \leq \min(\tilde{\gamma}_0) \leq \max(\tilde{\gamma}_0) \leq 2.132590$$

$$(resp.,-3.590593 \leq \min(\tilde{\gamma}_1) \leq \max(\tilde{\gamma}_1) \leq -3.277103) \tag{5.11}$$

as β increases from 6.5 to 10.5.

Now the solutions of (5.9) are related to its coefficients as follow:

$$2\tilde{\sigma}_i + \tilde{\gamma}_i = -(\alpha m_i + 1) \ , \ \tilde{\sigma}_i^2 + \tilde{\omega}_i^2 + 2\tilde{\sigma}_i\tilde{\gamma}_i = \alpha(m_i - 1) + \beta$$

$$\tilde{\gamma}_i(\tilde{\sigma}_i^2 + \tilde{\omega}_i^2) = -\alpha\beta m_i \tag{5.12}$$

Solving for $\tilde{\sigma}_i$ and $\tilde{\omega}_i^2$ from (5.12), we obtain for i = 0, 1:

$$\tilde{\sigma}_i = -\frac{1}{2}(\alpha m_i + 1 + \tilde{\gamma}_i) \ , \ \tilde{\omega}_i^2 = -\frac{1}{4}(\alpha m_i - 1 - \tilde{\gamma}_i)^2 - \frac{\alpha^2 m_i}{\tilde{\gamma}_i + \alpha m_i} \tag{5.13}$$

Combining (5.11) and (5.13), we obtain properties (i) and (ii).

Property (iii) follows directly from properties (i) and (ii) and the assumptions $\sigma_0 < 0$, $\gamma_0 > 0$, and $\tilde{\omega}_0 > 0$.

Property (iv) follows from properties (i) and (ii) and the relationships

$$\frac{k_0}{\gamma_0} = -\left[\frac{\tilde{\gamma}_0}{\tilde{\gamma}_1}\right] \Big/ \left[\frac{\tilde{\gamma}_0}{\tilde{\omega}_0}\right] = -\frac{\tilde{\omega}_0}{\tilde{\gamma}_1} \ , \ \frac{k_1}{\gamma_1} = -\left[\frac{\tilde{\gamma}_1}{\tilde{\gamma}_0}\right] \Big/ \left[\frac{\tilde{\gamma}_1}{\tilde{\omega}_1}\right] = -\frac{\tilde{\omega}_1}{\tilde{\gamma}_0} \tag{5.14}$$

Finally, note that the bounds in properties (i)-(iv) can be calculated to be exact to any number of digits because (5.10) and (5.13) are rational expressions.

■

Our next goal is to examine the loci of points obtained by applying the half-return map π_1 to the segment $\overline{E_1 A_1}$ (i.e., $u = 1$, $0 \leq v \leq 1$) on V_1: they are obtained by substituting $u = 1$ and $v = v(1,t)$ for $t \in I(1)$ into (4.28), where $I(1)$ denotes the set of "first-return times" for $v \in [0,1]$:

$$\underset{\sim}{x}(t) = \pi_1\left[\underset{\sim}{x}\Big[1,v(1,t)\Big]\right] = e^{-\sigma_1 t}\begin{bmatrix} \cos t & \sin t \\ -\sin t & \cos t \end{bmatrix} \underset{\sim}{x}\Big[1,v(1,t)\Big] \tag{5.15}$$

for $t \in I(1)$. Using the phasor notation (4.52), (5.15) assumes the following compact form

$$\underset{\sim}{X}(t) = \underset{\sim}{X}\Big[1,v(1,t)\Big]e^{-(\sigma_1 + j1)t} \ , \ t \in I(1) \tag{5.16}$$

Similarly, it follows from (4.13) that the loci of points obtained by applying the half-return map π_0^+ to the segment $\overline{B_0A_0}$ (i.e., $v = 1$, $0 \leq u \leq 1$) on V_0 assumes the following compact form

$$\underset{\sim}{X}(t) = \underset{\sim 0}{X}\left[u^+(1,t),1\right]e^{(\sigma_0+j1)t} \quad, \quad t \in I^+(1) \tag{5.17}$$

where $\underset{\sim 0}{X}$ is the phasor associated with $\underset{\sim 0}{x}$ and $I^+(1)$ is the set of "first-return times" for $u \in [0,1]$. We have already identified the set of points in (5.16) and (5.17) as portions of a shrinking spiral whose amplitude is modulated in time. Our next lemma shows that these two spirals are sandwiched between two logarithmic spirals.

Lemma 5.2[†]

(i)   For each $\beta \in J$, and any time $t \in I(1)$, the magnitude of $\underset{\sim}{x}(t)$ of the spiral (5.16) in V_1 is bounded by two exponentials:

$$|A_1|e^{-\sigma_1 t} \geq |\underset{\sim}{x}(t)| \geq |E_1|e^{-\sigma_1 t} \tag{5.18}$$

(ii) For each $\beta \in J$, and any time $t \in I^+(1)$, the magnitude of $\underset{\sim}{x}(t)$ of the spiral (5.17) in V_0 is bounded by two exponentials:

$$|A_0|e^{\sigma_0 t} \geq |\underset{\sim}{x}(t)| \geq |B_0|e^{\sigma_0 t} \tag{5.19}$$

(iii) For each $\beta \in J$,

$$|E_1| \leq |A_1|e^{-\sigma_1\vartheta_1} \tag{5.20}$$

where $\vartheta_1 \geq 0$ denotes the angle subtended by the two vectors $\overline{OE}_1$ and $\overline{OA}_1$ on the plane V_1.

(iv) For each $\beta \in J$,

$$|A_0| \geq |E_0|e^{\sigma_0\vartheta_0} \tag{5.21}$$

where $\vartheta_0 \geq 0$ denotes the angle subtended by the two vectors $\overline{OE}_0$ and $\overline{OA}_0$ on the plane V_0.

Proof.

[†]In Lemma 5.2, A_1, A_0, E_1, and E_0 are represented by their x-y coordinates and hence are 2-dimensional vectors.

(i) It suffices to show that

$$|A_1| \geq \left| \underset{\sim 1}{x}\left[1, v(1,t)\right] \right| \geq |E_1| \tag{5.22}$$

Since $\underset{\sim 1}{x}(1,v) = \overrightarrow{OE_1} + v\overrightarrow{E_1A_1}$, $v \in [0,1]$, it follows from plane geometry that

$$|\underset{\sim 1}{x}(1,v)|^2 = \{v|\overrightarrow{E_1A_1}| + \langle \overrightarrow{OE_1}, \overrightarrow{E_1A_1}\rangle\}^2 + \{|E_1|^2 - \langle \overrightarrow{OE_1}, \overrightarrow{E_1A_1}\rangle\}^2 \tag{5.23}$$

If we can show that

$$\langle \overrightarrow{OE_1}, \overrightarrow{E_1A_1}\rangle > 0 \tag{5.24}$$

then (5.23) would imply (5.22) because $|\underset{\sim 1}{x}(1,v)|^2$ is an increasing function of $v \in [0,1]$ and since $|A_1| = |\underset{\sim 1}{x}(1,1)|$ and $|E_1| = |\underset{\sim 1}{x}(1,0)|$.

To prove (5.24), we make use of the first two coordinates of E_1 from (2.30) and A_1 from (2.26) to write

$$\overrightarrow{OE_1} = \left[\gamma_1(\gamma_1-\sigma_1-p_1)/Q_1 \,, \, \gamma_1[1 - p_1(\sigma_1-\gamma_1)]/Q_1\right] \tag{5.25}$$

$$\overrightarrow{E_1A_1} = \left([\sigma_1(\sigma_1-\gamma_1) + 1 + \gamma_1 p_1]/Q_1 \,, \, \{p_1[\sigma_1(\sigma_1-\gamma_1) + 1] - \gamma_1\}/Q_1\right) \tag{5.26}$$

Calculating the inner product between (5.25) and (5.26), we obtain

$$\langle \overrightarrow{OE_1}, \overrightarrow{E_1A_1}\rangle = -\sigma_1\gamma_1(p_1^2+1)/Q_1 \tag{5.27}$$

Using (5.27) and Lemma 5.1 (iii) ($\sigma_1 > 0$, $\gamma_1 < 0$), we obtain the desired inequality (5.24).

(ii) This is proved by the same method as in (i).

(iii) From (5.24), we have $0 < \vartheta_1 < \frac{\pi}{2}$. Hence

$$\vartheta_1 < \tan \vartheta_1 \tag{5.28}$$

Moreover, since $0.054814 \leq \sigma_1 \leq 0.157096$ (Lemma 5.1) it is easy to verify that

$$1 - 2\sigma_1\vartheta_1 \leq e^{-2\sigma_1\vartheta_1} \tag{5.29}$$

Since (5.20) is equivalent to

$$|E_1|^2/|A_1|^2 \leq e^{-2\sigma_1\vartheta_1} \tag{5.30}$$

it follows from (5.29) that to prove (iii) of Lemma 5.2 is equivalent to proving

$$|E_1|^2/|A_1|^2 \leq 1 - 2\sigma_1 \tan \vartheta_1 \tag{5.31}$$

Now projecting A_1 and E_1 onto the $z = 0$ plane as before, we can suppress the z-

coordinate in (2.26) and (2.30) and obtain after simplification:

$$|A_1|^2 = p_1^2 + 1, \quad |E_1|^2 = \gamma_1^2(p_1^2 + 1)/Q_1 \tag{5.32}$$

Now define the *normal* vector to E_1 as follow:

$$E_1^\perp \triangleq \left[-\gamma_1(1 - p_1(\sigma_1 - \gamma_1))/Q_1, \ \gamma_1(\gamma_1 - \sigma_1 - p_1)/Q_1 \right] \tag{5.33}$$

then it follows from (2.30) that

$$|E_1| = |E_1^\perp| \quad \text{and} \quad \vec{OE_1} \perp \vec{OE_1^\perp} \tag{5.34}$$

A straightforward calculation shows

$$\tan \vartheta_1 = \langle \vec{OA_1}, \vec{OE_1^\perp} \rangle / \langle \vec{OA_1}, \vec{OE_1} \rangle = 1/(\sigma_1 - \gamma_1) \tag{5.35}$$

Substituting (5.32), (5.35), and (5.28) into (5.31) and solving for γ_1 we obtain

$$\gamma_1 \leq \sigma_1 \left[1 + \frac{2}{\sigma_1^2 - 1} \right] \tag{5.36}$$

Hence proving (iii) of Lemma 5.2 is equivalent to proving (5.36) holds over the parameter range assumed by γ_1 and σ_1 for $\beta \in J$. To verify this, note that the right hand side of (5.36) decreases over the range $0.054814 \leq \sigma_1 \leq 0.157096$ with a minimum value equal to -0.1650. Since the maximum value assumed by γ_1 is -1.296515 (lemma 5.1 (iii)), it follows that (5.36) holds for all $\beta \in J$.

■

(iv) It follows from (2.20) and (2.24) that (5.21) is equivalent to

$$(1 + p_0^2) - (1 + \sigma_0^2)e^{2\sigma_0\vartheta_0} > 0 \tag{5.37}$$

To prove this, let us define the function

$$g(t) \triangleq 1 + \tan^2(\varphi + t) - (1 + \sigma_0^2)e^{2\sigma_0 t}, \quad t \in [0, \vartheta_0] \tag{5.38}$$

and

$$\varphi \triangleq \tan^{-1}\sigma_0 \in \left(-\frac{\pi}{2}, 0\right) \tag{5.39}$$

It is easy to verify that

$$g(0) = 0 \tag{5.41}$$

$$g'(t) = 2\tan(\varphi + t)[1 + \tan^2(\varphi + t)] - 2\sigma_0(1 + \sigma_0^2)e^{2\sigma_0 t} \tag{5.42}$$

$$g'(0) = 0 \qquad\qquad (5.43)$$

$$g'(t) > 0 \quad \text{for} \quad 0 < t < \frac{\pi}{2} - \varphi \qquad\qquad (5.44)$$

where (5.44) follows from $\sigma_0 < 0$ and $-\frac{\pi}{2} < \varphi < 0$. Since $E_0 = (1,\sigma_0)$, φ is the "negative" angle between $\overrightarrow{OE}_0$ and the x-axis. Hence, $0 < \vartheta_0 < \frac{\pi}{2} - \varphi$ falls within the range of t in (5.44). Moreover, since $A_0 = (1,p_0)$ and $\varphi + \vartheta_0$ is the angle between $\overline{OA}_0$ and the x-axis, it follows that $\tan(\varphi+\vartheta_0) = p_0$. Hence, letting $t = \vartheta_0$ in (5.38) we obtain

$$g(\vartheta_0) = (1+p_0^2) - (1+\sigma_0^2)e^{2\sigma_0\vartheta_0} > 0 \quad \blacksquare \qquad\qquad (5.45)$$

Lemma 5.3

For each $\beta \in J$, the double scroll system (1.1)-(1.3) is a member of the double-scroll family (5.1) and satisfies hypotheses (ii) and (iii) of *Theorem 5.1*.

Proof.

It follows from Lemma 5.1 that for each $\beta \in J$, $\sigma_0 < 0$, $\gamma_0 > 0$, $\sigma_1 > 0$, $\gamma_1 < 0$, and $k > 0$. Hence, the vector field $\xi \in \mathcal{L}$ defined by (1.1)-(1.3) is a member of $\mathcal{L}_0 \subset \mathcal{L}$ in (5.1) for all $\beta \in J$. Moreover, the ranges assumed by σ_0 and γ_0 in Lemma 5.1 (iii) imply $|\sigma_0| < \gamma_0$ for all $\beta \in J$. Hence, we need only prove hypothesis (ii) of Theorem 5.1 holds for all $\beta \in J$.

Suppressing the z-coordinate from(2.20) and (2.21), we can write

$$A_0 = (1,p_0) \quad, \quad p_0 = \sigma_0 + \frac{k_0}{\gamma_0}(\sigma_0^2+1) \qquad\qquad (5.46)$$

where -0.771352 $\leq \sigma_0 \leq$ - 0.406890 and 0.813782 $\leq \gamma_0 \leq$ 1.542704. Since

$$p_0 \leq \max(\sigma_0) + \max\left[\frac{k_0}{\gamma_0}\right]\left[\max(\sigma_0^2) + 1\right] \approx 0.39 < 0.4 \qquad\qquad (5.47)$$

we have

$$|A_0|^2 = 1 + p_0^2 < 1.16 \quad \text{and} \quad \varphi_0 \triangleq \tan^{-1}(p_0) \in (0, \frac{\pi}{4}) \qquad\qquad (5.48)$$

where φ_0 is the angle between $\overrightarrow{OA}_0$ and the x-axis. Now, for $t \geq \frac{\pi}{2} - \varphi_0$,

$$|\underset{\sim 0}{X}(1,1)\exp[(\sigma_0+j1)t]| \;\leq\; |A_0|\,exp\left[\sigma_0\left|\frac{\pi}{2}-\varphi_0\right|\right]$$

(5.49)

$$\leq\; \sqrt{1.16}\,\exp[\frac{\pi}{4}\max(\sigma_0)] \approx 0.78 < 1$$

Since $0 < \varphi_0 < \dfrac{\pi}{4}$, it can be shown that the trajectory $\underset{\sim 0}{x}(t)$ starting from A_0 remains in the region $x > 0$ for all $0 < t < \dfrac{\pi}{2} - \varphi_0$. Consequently, $\underset{\sim 0}{x}(t)$ never reaches the line $x = -1$ for $t > 0$; namely,

$$\{\underset{\sim 0}{X}(1,1)e^{(\sigma_0+j1)t}\,|\,t>0\} \subset \{(x,y)\,|\,x>-1\}$$

(5.50)

where each phasor on the left at any time $t > 0$ is identified as a point in the x-y plane. Similarly, it can be shown that the trajectory $\underset{\sim 0}{x}(t)$ starting from E_0 never reaches the line $x = -1$ for $t > 0$; namely,

$$\{\underset{\sim 0}{X}(1,0)e^{(\sigma_0+j1)t}\,|\,t>0\} \subset \{(x,y)\,|\,x>-1\}$$

(5.51)

Since

$$\underset{\sim 0}{X}(1,v) = v\underset{\sim 0}{X}(1,1) + (1-v)\underset{\sim 0}{X}(1,0)\,,\;\; v \in [0,1]$$

(5.52)

and since at any time t, the flow of a *linear* system is a linear function of the *initial* state, it can be shown that

$$\{\underset{\sim 0}{X}(1,v)e^{(\sigma_0+j1)t}\,|\,t>0\} \subset \{(x,y)\,|\,x>-1\}$$

(5.53)

∎

Lemma 5.4.

Let $C_1 \triangleq \Psi_1(C) = (x_C, y_C)$ and $F_1 \triangleq \Psi_1(F) = (x_F, y_F)$ on the V_1-plane in Fig. 2(b). Then for every $\beta \in J$, we have

$$x_C < x_F < 1 \;\; \text{and} \;\; y_C > 0$$

(5.54)

Moreover, C_1 is a *continuous function of β for all $\beta \in J$*.

Proof. From (2.32), we identify

$$x_F = \gamma_1(\gamma_1 - 2\sigma_1)/Q_1\,,\;\; y_F = \gamma_1[1 - \sigma_1(\sigma_1 - \gamma_1)]/\,Q_1$$

(5.55)

Since $C_1 = \Phi(C_0) = \Phi(0,0)$ when projected onto the $x-y$ plane, where Φ is the *connection map* defined in (4.40) and (4.44), we can calculate the exact coordinates of x_C and y_C as

follow:

$$x_C = 1 - \frac{(\sigma_1^2+1)[(\sigma_0+\gamma_0 k_1)^2+1]}{(\sigma_0^2+1)Q_1} \tag{5.56}$$

$$y_C = \frac{\gamma_1[1-\sigma_1(\sigma_1-\gamma_1)]}{Q_1} - \frac{(\sigma_1^2+1)\gamma_0 k_1}{(\sigma_0^2+1)\gamma_1 Q_1}\{k_1\gamma_0[\sigma_1(\sigma_1-\gamma_1)+1]+2\sigma_0\gamma_1(\sigma_1-\gamma_1)\} \tag{5.57}$$

From (5.55) and (5.57) we obtain

$$x_F - x_C = \frac{\sigma_1^2+1}{Q_1(\sigma_0^2+1)}\gamma_0 k_1(\gamma_0 k_1 - 2\sigma_0) > 0 \tag{5.58}$$

because $\gamma_0 k_1 > 0$ and $\sigma_0 < 0$ for $\beta \in J$ (Lemma 5.1). Hence $x_C < x_F$. The fact that $x_F < 1$ follows from the geometry of the D_1-unit in Fig. 2(b) where $\overline{A_1 B_1}$ lies on the line $x = 1$. To prove y_C in (5.57) is positive, it suffices to show

$$(\sigma_1^2+1)k_1\gamma_0\{k_1\gamma_0[\sigma_1(\sigma_1-\gamma_1)+1]+2\sigma_0\gamma_1(\sigma_1-\gamma_1)\} > [1-\sigma_1(\sigma_1-\gamma_1)]\gamma_1^2(\sigma_0^2+1) \tag{5.59}$$

because $\gamma_1 < 0$ for $\beta \in J$. We can rewrite (5.59) as follow:

$$\frac{(\sigma_1^2+1)\sigma_0^2}{(\sigma_0^2+1)\sigma_1^2}\left\{\sigma_1(\sigma_1-\gamma_1)\left[\left(\frac{k_1\gamma_0\sigma_1}{\gamma_1\sigma_0}+1\right)^2-1\right]+\left(\frac{k_1\gamma_0\sigma_1}{\gamma_1\sigma_0}\right)^2\right\} > 1-\sigma_1(\sigma_1-\gamma_1) \tag{5.60}$$

Since for all $\beta \in J$,

$$\frac{k_1\gamma_0\sigma_1}{\gamma_1\sigma_0} = -\frac{\tilde{\sigma}_1}{\tilde{\sigma}_0} > 0 \quad \text{and} \quad \sigma_1(\sigma_1-\gamma_1) > 0 \tag{5.61}$$

we have

Left side of (5.60) - right side of (5.60)

$$= \frac{(\sigma_1^2+1)\sigma_0^2}{(\sigma_0^2+1)\sigma_1^2}\left\{\sigma_1(\sigma_1-\gamma_1)\left[\left(1-\frac{\tilde{\sigma}_1}{\tilde{\sigma}_0}\right)^2-1\right]+\left(\frac{\tilde{\sigma}_1}{\tilde{\sigma}_0}\right)^2\right\}-1+\sigma_1(\sigma_1-\gamma_1)$$

$$\geq \frac{(\sigma_1^2+1)\sigma_0^2\tilde{\sigma}_1^2}{(\sigma_0^2+1)\sigma_1^2\tilde{\sigma}_0^2}-1$$

$$= \frac{\tilde{\sigma}_1^2+\tilde{\omega}_1^2}{\tilde{\sigma}_0^2+\tilde{\omega}_0^2}-1 \quad \text{(because } \sigma_i = \tilde{\sigma}_i/\tilde{\omega}_i \;,\; i=0,1)$$

(5.62)

$$= \frac{m_1\tilde{\gamma}_0}{m_0\tilde{\gamma}_1}-1 \quad \text{(because } \tilde{\gamma}_i(\tilde{\sigma}_i^2+\tilde{\omega}_i^2) = -\alpha\beta m_i \;,\; i=0,1)$$

$$\geq \frac{-2\min(\tilde{\gamma}_0)}{\min\tilde{\gamma}_1}-1 \approx 0.0102 \quad \text{(because } m_0 = -\frac{1}{7},\; m_1=\frac{2}{7})$$

$$> 0$$

Since $\tilde{\gamma}_i$ is a *continuous* function of β in view of (5.10), it follows from (5.13) that $\tilde{\sigma}_i$, $\tilde{\omega}_i$, and k_i are also continuous function of β for i = 0,1. Since $C_1 = (x_C, y_C)$ is given in (5.56) and (5.57), C_1 is a continuous function of β.

■

5.2. Proof of Theorem 5.2

It follows from **Lemma 5.3** that it suffices for us to prove that hypothesis (i) of **Theorem 5.1** holds for some $\beta \in J$, i.e., we must prove that there exists some $\beta \in J$ such that $C_1 \in \pi_1(\overline{E_1A_1})$ as depicted in the V_1-portrait of V_0 in Fig. 9(a) when this happens.

To do this, let us draw two concentric circles S_a and S_b with center at $D_1 = (0,0)$ in the V_1-plane and a radius equal to $|A_1|$ and $|E_1|e^{-2\pi\sigma_1}$, respectively, as shown in Fig. 10. Let l be the horizontal line through D_1 (i.e., the x-axis) and l' be the vertical line through F_1. Clearly, l' is to the left of the $x=1$ line in view of **Lemma 5.4**. Let S_a intersect l and l' at points a and a', respectively. Let S_b intersect l at a point b to the left of D_1. Depending on the value of $|E_1|$ and σ_1, S_b either intersects l' at *two* points, in which case the upper point is labelled b', or otherwise, let b' be the point where f S_b intersects l to the right of D_1, as shown in Fig. 10. Let g be the upper point where S_b intersect the y-axis. Let R denote the region enclosed by the closed contour formed by either $\overset{\frown}{aa'b'g}ba$ (if b' lies on l') or $\overset{\frown}{aa'f}b'\overset{\frown}{gb}a$ (if b' lies on l). In other words, R denotes the portion of the ring (area between S_a and S_b) above the x-axis and to the left of l'. Hence, R is a *simply-connected* region.

Consider next the two logarithmic spirals

$$\underset{\sim E}{X}(t) = \underset{\sim 1}{E}\exp[-(\sigma_1 + j1)t] \ , \ t \geq 0 \tag{5.63}$$

and

$$\underset{\sim A}{X}(t) = \underset{\sim 1}{A}\exp[-(\sigma_1 + j1)t] \ , \ t \geq 0 \tag{5.64}$$

Note that $\underset{\sim A}{X}(t)$ and $\underset{\sim E}{X}(t)$ correspond to the two shrinking spirals $\overgroup{A_1 d''dd'}$ (starting from A_1 at $t=0$) and $\overgroup{E_1 cc'}$ (starting from E_1 at $t=0$), respectively, as shown in Fig. 10. Since $|\overrightarrow{D_1 E_1}| < |\overrightarrow{D_1 A_1}|$ in view of **Lemma 5.2 (i)**, d'' lies on the extension of the line $\overline{D_1 E_1}$.

Since both $|\underset{\sim E}{X}(t)|$ and $|\underset{\sim A}{X}(t)|$ shrink exponentially with the *same* rate σ_1, the time $t_{E_1 c}$ it takes $\underset{\sim E}{X}(t)$ to go from E_1 to c (where it first intersects l) is equal to the time $t_{d''d}$ it takes $\underset{\sim A}{X}(t)$ to go from d'' to d (where it first intersects l). Note that $t_{E_1 c} = t_{d''d} = \angle E_1 D_1 d$ (in radians) where $\angle E_1 D_1 d$ is the angle between $\overline{D_1 E_1}$ and $\overline{D_1 d}$. Since $\angle E_1 D_1 d < 2\pi$, it follows that d must lie to the left of c which in turn must lie to the left of b.

Depending on σ_1, the continuation of the shrinking spiral from points d and c may either intersect l' or l. Let this point of intersection be d' and c', respectively. Let $t_{dd'}$ denote the time it takes to go from d to d' and let $t_{cc'}$ denote the time it takes to go from c to c'. Since $t_{dd'} < 2\pi$ and $t_{cc'} < 2\pi$, both d' and c' must lie *outside* of S_b in Fig. 10, and c' must be below d' in view of **Lemma 5.2(iii)**. Hence, d must lie between a and c whereas d' must lie between a' and c' in Fig. 10.

Recall next the image under π_1 of the line segment

$$\overline{E_1 A_1} = \{(x(u,v), y(u,v)) | u=1, 0 \leq v \leq 1\} \tag{5.65}$$

and its extension beyond A_1 ($v > 1$) is given by[†]

$$\underset{\sim}{X}(t) = \underset{\sim 1}{X}(1, v(1,t))\exp[-(\sigma_1 + j1)t] \ , \ t \geq 0 \tag{5.66}$$

A part of this image is shown by the bold spiral $\overgroup{E_1 ee'}$ in Fig. 10 (it corresponds to a part of $\overgroup{E_1 A'_1}$ in Fig. 6 and (4.51)). Here, $e \overset{\Delta}{=} \underset{\sim}{X}(t_1)$ is the point at which $\underset{\sim}{X}(t)$ first intersects l at some time t_1 and $e' \overset{\Delta}{=} \underset{\sim}{X}(t_2)$ is the point at which $\underset{\sim}{X}(t)$ first intersects either l' or l to the right of D_1 (if it does not intersect l') at some time t_2. Since both e and e' lie to the left of

---

[†]Recall from Fig. 6 that the image under π_1 of the extension of the line segment to the right of A_1 corresponds to the extension of the outer spiral beyond A'_1 to the right and hence must lie in the region with $v > 1$.

$x=1$, its associated starting point $\underset{\sim 1}{X}(1,v(1,t))$ must lie to the left of the $v=1$ line. Hence, we must have $0 < v(1,t_i) < 1$, $i = 1, 2$, and

$$\underset{\sim 1}{X}(1,v(1,t_i)) \in \overline{A_1 E_1} \quad , \quad i=1,2 \tag{5.67}$$

It follows that e must lie between c and d, and e' must lie between c' and d' in Fig. 10 for all $\beta \in J$.

If we can show that there exists some $\beta \in J$ such that $C_1 \triangleq \Psi_1(C)$ lies on the bold spiral $\widehat{ee}'$, we will be done. Since C_1 is a function of β (assuming α, m_0, and m_1 are fixed) we will denote this function by $C_1(\beta)$. Now suppose it is possible to find a $\beta_1 \in J$ such that $C_1(\beta_1)$ is located *outside* of S_a, and a $\beta_2 \in J$ such that $C_1(\beta_2)$ is located *inside* of S_b. **Lemma 5.4** guarantees that $C_1(\beta)$ must lie in the simply-connected region

$$H \triangleq \{(x,y)\,|\,x \leq X_F \quad , \quad y \geq 0\} \tag{5.68}$$

Since $C_1(\beta)$ is a *continuous* function (**Lemma 5.4**), the set (assuming without loss of generality $\beta_1 < \beta_2$.)

$$\Gamma_c \triangleq \{C_1(\beta)\,|\,\beta_1 \leq \beta \leq \beta_2\} \subset H \tag{5.69}$$

is a plane curve (parametrized by β) starting from a point ($\beta = \beta_1$) outside S_a and ending at a point ($\beta = \beta_2$) inside S_b. Since this curve must lie within H, Γ_c must cross the $\widehat{ee}'$ spiral at some point β_0, $\beta_1 < \beta_0 < \beta_2$. Hence, hypothesis (i) of theorem 5.1 is satisfied when $\beta = \beta_0$.

It remains for us to show there exist β_1 and β_2 with the above stipulated properties. When $\beta = 10.5$, we calculate (x_C, y_C) using (5.56)-(5.57) and obtain

$$|C_1(10.5)| \approx 0.7064 < 0.8 < |E_1|e^{-2\pi\sigma_1} \approx 0.9151 \tag{5.70}$$

Similarly, when $\beta = 6.5$, we obtain

$$|C_1(6.5)| \approx 1.4155 > 1.3 > |A_1| \approx 1.2477 \tag{5.71}$$

Hence, $\beta_1 = 6.5$ and $\beta_2 = 10.5$ represent one (out of many) valid choice. ∎

Remarks:

1. By computer simulation, we have found the approximate value of $\beta_0 \approx 8.6$. The V_1-portrait of V_0 corresponding to $\beta = 10.5$, 8.6, and 6.5 are shown in Figs. 11(a), (b), and (c), respectively. It follows from Theorem 5.2 that the double scroll system (1.1)-(1.3) has a *homoclinic orbit* when $m_0 = -\dfrac{1}{7}$, $m_1 = \dfrac{2}{7}$, $\alpha = 7$, and $\beta = 8.6$.

2. Using the parameters $(\alpha, \beta, m_0, m_1) = (7, 8.6, -\dfrac{1}{7}, \dfrac{2}{7})$ we have confirmed by

computer simulation the existence of a double scroll attractor similar to those reported in [1-5].

3. Mees and Chapman [15] have also carefully analyzed the dynamics of the double scroll system (1.1)-(1.3) and confirmed the existence also of *heteroclinic* orbits.

4. Additional insights and conditions for the appearance of the double-scroll attractor are given in [20].

6. BIFURCATION ANALYSIS

By extensive and systematic computer simulations of the double scroll system (1.1)-(1.3) over a wide range of parameters $(\alpha, \beta, m_0, m_1)$ which include those cited previously in [1-6], we have observed two distinct types of chaotic attractors, in addition to various stable periodic orbits (both period-doubling types and periodic window types). The *first* type of chaotic attractor is sandwiched between the eigenspace through P^+ and the eigenspace through 0, see Fig. 2(a), and is henceforth referred to as a *Rössler* screw-type attractor[†] because it bears a strong resemblance to a screw-like structure first reported by Rössler [21]. An odd-symmetric image of this attractor has also been observed between the eigenspaces through P^- and 0, as expected. These two Rössler screw-type attractors are separated by the eigenspace through 0. The *second* type of chaotic attractor is the *double scroll* which has already been extensively reported [1-6] and which spans *all three* regions D_{-1}, D_0, and D_1 in Fig. 2(a). As we increase the value of α for fixed β, m_0 and m_1, we observed that the two disjoint Rössler screw-type attractors grow in size until eventually they collided and gave *birth* to the double scroll [6]. As we increase α further, the double scroll grows while the co-existing unstable *saddle-type periodic* orbit shrinks in size until eventually they too collided with each other and the double scroll *disappears* thereafter [6]. This evolution scenario—henceforth called the *birth and death* of the double scroll—has been found to be quite typical over wide ranges of β, m_0 and m_1.

Our objective in this section is to use the analytical tools we have developed in the previous sections to carry out a rigorous analysis of the above bifurcation phenomena. Among other things, we will give a rigorous derivation of the locations of the Rössler screw-type attractor and the double scroll attractor. This in-depth analysis in turn leads to an algorithm for actually calculating the bifurcation boundaries (see Fig. 17)—henceforth called the *birth and death boundaries* —in the $\alpha - \beta$ plane which separate the double-scroll attractors and their periodic windows from the other attractors (both chaotic and periodic).

Before getting into the formal details, examine the typical trajectories Γ_1 and Γ_2 in Fig. 2(a) again. Note that Γ_1 and Γ_2 originate from a point on U_1 to the *right*, and the *left* (*respectively*, of the boundary line L_0 passing through A and E. This line therefore bifurcates the set of all trajectories which return to D_1 from those which continue downward to D_{-1}. Recall next that all trajectories originating from U_1 to the left of L_2 (passing through E and B) must move *down* while those on the right of L_2 must move *up*. Finally, note that if $|\gamma_1|$ is

---

[†]For simplicity, we will refer to both "spiral" and "screw" attractors reported in [6] as a Rössler screw-type attractor.

large, as is the case when the Rössler screw-type attractor and the double scroll have been observed, all trajectories originating on either side of the top eigenspace $E^c(P)$ get sucked in rapidly toward $E^c(P)$ and eventually cross U_1 along an infinitesimally thin "slit" centered at the line L_1 passing through A and B.

We will shortly show that the triangle $\triangle ABE$ bounded by the 3 lines L_0, L_1 and L_2 is crucial in predicting the asymptotic behavior of the trajectories. As before, we will switch back and forth into the new reference frames corresponding to the D_1-unit and D_0-unit in Fig. 2(b) in order to take advantage of the analytical equations characterizing the Poincare map π in (4.48) and its associated half-return maps π_0 in (4.9) and π_1 in (4.27). Moreover, since it is essential to follow the dynamics originating from $\triangle A_0 B_0 E_0 \triangleq \Psi_0(\triangle ABE)$, and taking place in the D_0-unit but viewed from the reference frame in the D_1-unit, the "V_1-portrait of V_0" defined in 4.5 section (recall Fig. 8) will play a crucial role in our analysis. In particular, the dynamics taking place within the D_0-unit can be "translated" into the D_1-unit via the "pull-up map"

$$\pi_2 \triangleq \Phi \pi_0 \Phi^{-1} : \angle A_1 B_1 E_1 \to V_1 \tag{6.1}$$

6.1. Trapping Region

The V_1-portrait of V_0 corresponding to the parameters $(\alpha, \beta, m_0, m_1) = (4.0, 4.53, -1.7, 2/7)$ (which corresponds to $(\sigma_0, \gamma_0, \sigma_1, \gamma_1, k) = (-0.721, 1.075, 0.074, -1.600, 0.530))$ is shown in Fig. 12. Note that in terms of the local coordinates (u, v), $u = 1$ along $\overline{A_1 E_1}$ and $u = 1.53$ along $\overline{A_{1u} E_{1u}}$, respectively. Recalling Fig. 8, we can identify the following images under the above pull-up map π_2:

$$\overparen{B_1 C_1} = \pi_2(\overline{B_1 A_1}), \ \overparen{F_1 C_1} = \pi_2(\overline{F_1 E_1}) \tag{6.2}$$

$$\overparen{C_1 A_{1u}''} = \pi_2(\overline{A_1 A_{1u}}), \overparen{C_1 E_{1u}''} = \pi_2(\overline{E_1 E_{1u}}) \tag{6.3}$$

$$\overparen{A_{1u}'' E_{1u}''} = \pi_2(\overline{A_{1u} E_{1u}}), \overparen{F_1 W_1 D_1} = \pi_1(\overline{F_1 B_1}) \tag{6.4}$$

Recall that $C_1 = \pi_2(A_1) = \pi_2(E_1)$ and any point on $\overline{B_1 F_1}$ is defined to be a fixed point of π_2. Let S_a denote the "snake-like" area bounded by $\overparen{B_1 C_1}, \overparen{F_1 C_1}$ and $\overline{B_1 F_1}$ and let S_b denote the area bounded by $\overparen{C_1 A_{1u}''}, \overparen{C_1 E_{1u}''}$ and $\overparen{A_{1u}'' E_{1u}''}$. We will often refer to S_a and S_b as "snakes" and call

$$S_1 \triangleq S_a \cup S_b = \pi_2(\Delta A_{1u} B_1 E_{1u}) \tag{6.5}$$

as the *double-snake area*.

Let $\square A_{1u}' B_1 E_{1u}$ denote the fan-like region bounded by $\overline{A_{1u}' B_1}$, $\overline{B_1 E_{1u}}$, and

$$\widehat{E_{1u} A_{1u}'} = \pi_1(\overline{E_{1u} A_{1u}'}) \tag{6.6}$$

Note that the double-snake area S_1 is bounded *within* $\square A_{1u}' B_1 E_{1u}$. Had we chosen $\overline{E_{1u} A_{1u}}$ nearer to $\overline{E_1 A_1}$ where u is closer to 1, the corresponding fan-like region $\square A_{1u}' B_1 E_{1u}$ could actually cross the double-snake area S_1. Since a key assumption in our following analysis is that $S_1 \subset \square A_{1u}' B_1 E_{1u}$, we must choose u to be sufficiently large. However, as we will see in Section 6.3, u should *not* be chosen too large either. For the parameters associated with Fig. 12, $u = 1.53$ is a satisfactory choice.

Translating the above definitions back into U_1 in Fig. 2(a), we can interpret the corresponding snake-like area $S \triangleq \Psi_1^{-1}(S_1)$ as the set of all points $\Psi_1^{-1}(S_a)$ where returning trajectories of the type Γ_1 originating from ΔABE intersect the U_1 plane, and the set $\Psi_1^{-1}(S_b)$ representing the odd-symmetric image of the set of all points where returning trajectories of the type Γ_2 originating from $\angle ABE \backslash \Delta ABE$ intersect the U_{-1} plane. Since $\pi_1^{-1}(\square A_{1u}' B_1 E_{1u}) = \Delta A_{1u} B_1 E_{1u}$ and since $S_1 \subset \square A_{1u}' B_1 E_{1u}$, it follows that $\pi_1^{-1}(S_1) \subset \Delta A_{1u} B_1 E_{1u}$. Consequently if we restrict our *Poincare map* $\pi : V_1' \rightarrow V_1'$ to the region

$$\mathcal{J} \triangleq \Delta A_{1u} B_1 E_{1u} \tag{6.7}$$

henceforth called the *trapping region*, then $\pi(\mathcal{J}) \subset \mathcal{J}$. Hence we have isolated a small area on V_1' where the Poincare map π maps into itself.

Since the double-snake area S_1 does not intersect with the spiral $\widehat{F_1 W_1 D_1} = \pi_1(\overline{F_1 B_1})$ except F_1, it can be proved (see Appendix 5) that

(1) $\pi : \mathcal{J} \rightarrow \mathcal{J}$ is a continuous function $\tag{6.8}$

(2) $\pi(\mathcal{J})$ is a compact (i.e., bounded and closed) subset of $\mathcal{J}$ $\tag{6.9}$

It follows from (6.9) that[†]

$$\Lambda \triangleq \cap_{n \geq 0} \pi^n(\mathcal{J}) \tag{6.10}$$

[†] We denote the n th iterate of π by π^n : e.g., $\pi^0(\mathcal{J}) \triangleq \mathcal{J}$, $\pi^1(\mathcal{J}) \triangleq \pi(\mathcal{J})$; $\pi^2(\mathcal{J}) \triangleq \pi(\pi(\mathcal{J}))$, etc.

is π-invariant in the sense that

$$\pi(\Lambda) = \Lambda \tag{6.11}$$

because

$$\pi(\cap_{n \geq 0} \pi^n(\mathcal{J})) = \pi(\mathcal{J} \cap \pi^1(\mathcal{J}) \cap \pi^2(\mathcal{J}) \cap ...)$$

$$\subset \pi(\mathcal{J}) \cap \pi^1(\mathcal{J}) \cap \pi^2(\mathcal{J}) \cap \cdots \tag{6.12}$$

$$= \cap_{n \geq 1} \pi^n(\mathcal{J}) = \mathcal{J} \cap (\cap_{n \geq 1} \pi^n(\mathcal{J})) = \cap_{n \geq 0} \pi^n(\mathcal{J})$$

and because $\pi(\Lambda) \supset \Lambda$ is proved in Appendix 5.

If we define

$$\Lambda_1 \triangleq \Lambda \cup \pi_2(\Lambda) \tag{6.13a}$$

and

$$\widetilde{\Lambda} \triangleq \text{ closure of } \left\{ \cup_{t \geq 0} \varphi^t \left[\Psi_1^{-1}(\Lambda_1) \cup \left(-\Psi_1^{-1}(\Lambda_1) \right) \right] \right\} \tag{6.13b}$$

where $\varphi^t(\underset{\sim}{x})$ is the flow associated with (1.1)-(1.3), then $\widetilde{\Lambda}$ can be interpreted as the *closure*[†] of the Rössler screw-type attractors, or the double scroll, depending on the parameters. We will henceforth call $\widetilde{\Lambda}$ an *attractor* of the double scroll system (1.1)-(1.3).

Since $\pi^n(\mathcal{J}) \subset$ interior $\mathcal{J}$ for all $n \geq 2$, it follows (see Appendix 5) that there exists an open neighborhood $N(\widetilde{\Lambda})$ of $\widetilde{\Lambda}$ which satisfies

$$\widetilde{\Lambda} = \cap_{t \geq 0} \varphi^t \left[N(\widetilde{\Lambda}) \right] \tag{6.14}$$

Hence $\widetilde{\Lambda}$ possesses the properties of an attractor defined by several researchers including Hurley [22].

Observe that the region $\mathcal{J}$ in (6.7) is called a *trapping region* of Λ because $\mathcal{J}$ is a neighborhood of Λ and every trajectory originating from $\mathcal{J}$ tends to Λ under the Poincaré map π. Although there exists some attractor $\widetilde{\Lambda}$ in the literature which contains no *dense orbits*,[‡] our computer simulations strongly suggest that both the Rössler screw-type and the double scroll attractors contain at least one dense orbit.

The *macroscopic* structure of $\widetilde{\Lambda}$ associated with (1.1)-(1.3) has been carefully analyzed by computer simulations in [3]where we have discovered that each $x =$ constant cross section of $\widetilde{\Lambda}$ consists of 2 tightly-wound spirals—hence the name double scroll—for some parameter

---

[†] It is traditional to define an attractor as a *closed set*. *If we do not take the closure,* $\widetilde{\Lambda}$ would exclude the origin and hence would not be closed.

[‡] Roughly speaking, $\widetilde{\Lambda}$ has a *dense orbit* means that every trajectory originating from $\widetilde{\Lambda}$ visits a neighborhood of every point of $\widetilde{\Lambda}$. This implies that numerical errors in computer simulation are sufficient to guarantee that the entire attractor $\widetilde{\Lambda}$ will be observed by integrating from a single initial point.

values. For example, the double-snake area $S_a \cup S_b$ defined in (6.5) and shown in Fig. 12 (see also the upper snakes S_a and S_b in Fig. 14(b)) corresponds to the $x = 1$ cross section.

The *microscopic* (local) structure of $\widetilde{\Lambda}$, however, is much more complicated. Indeed, since $\widetilde{\Lambda}$ contains infinitely many *horseshoes* at least for some parameters (recall *Theorem 5.2*), we can expect that the local structure of $\widetilde{\Lambda}$ consists of a *product* between a manifold and a Cantor set similar to that described in [23].

Observe, however, that if the magnitude of the real eigenvalue $\widetilde{\gamma}_1$ at P^+ ($\widetilde{\gamma}_1 < 0$) is very large compared to the real part of the other eigenvalues, then the set Λ_1 must be tightly squeezed near the *curve*[†]

$$\Lambda_g \triangleq (\overline{A_1 B_1} \cup \overline{A_1 A_{1\infty}}) \cup (\overline{B_1 C_1} \cup \overline{C_1 A'_{1\infty}}) \tag{6.15}$$

The reason responsible for this important property is due to the strong rate of contraction of the trajectory component along the *real* eigenvector $E^r(P)$ in Fig. 2(a) on the one hand, and the fact that trajectories passing through points on Λ_1 represent the *asymptotic* behaviors, i.e., long after the trajectory component along $E^r(P)$ has shrunk to an infinitesimal value, thereby ensuring that the trajectories through Λ_1 are literally coasting on the surface of $E^c(P)$ in Fig. 2(a). This mechanism explains why the double scroll in [3] must cross the U_1 and U_{-1} plane along a very thin contour.

The above analysis shows that in so far as computer simulation is concerned, all trajectories originating from the attractor $\widetilde{\Lambda}$ can enter D_0 from D_1 only through the *infinitesimally-thin* gate centered at $\Psi_1^{-1}(\overline{A_1 B_1}) \subset L_1$, henceforth called the *upper entrance gate*, or at $\Psi_1^{-1}(\overline{A_1 A_{1\infty}}) \subset L_1$, henceforth called the *lower entrance gate*. Likewise, returning trajectories exiting from D_0 to D_1 can do so only through the *infinitesimally-thin* gate centered at $\Psi_1^{-1}(\overline{B_1 C_1})$, henceforth called the *upper exit gate*, and, (by symmetry of the vectorfield ξ) returning trajectories exiting from D_0 to D_{-1} can only do so through the *infinitesimally thin* gate - $\Psi_1^{-1}(\overline{C_1 A'_{1\infty}})$, henceforth called the *lower exit gate*.

We will often abuse our terminology by also calling $\overline{A_1 B_1}$, $\overline{A_1 A_{1\infty}}$, $\overline{B_1 C_1}$, and $\overline{C_1 A'_{1\infty}}$ as the *upper entrance gate*, *lower entrance gate*, *upper exit gate*, and *lower exit gate*, respectively. Their union Λ_g will henceforth be called $\widetilde{\Lambda}$-*gates*. These gates will play a crucial role in our following bifurcation analysis.

[†] For the parameter assumed in Fig. 12, we can replace $A_{1\infty}$ by A_{1u}.

6.2. Birth of the double scroll

Our computer simulations in [6] consistently show that as $\dot{\alpha}$ increases (for fixed β, m_0, and m_1), the 2 Rössler screw-type attractors eventually collide with each other, and that the double scroll suddenly emerges after any further infinitesimal increase in α. We will henceforth refer to this collision process as the *birth of the double scroll*. Our objective in this section is to derive the bifurcation value α which herald this event.

A qualitative picture of the structure of a Rössler screw-type attractor corresponding to the value of α at the collision point is shown in Fig. 13(a). Note that the attractor "funnels through" the *upper entrance gate* $\overline{AB}$ where its extreme left point on U_1 coincides with A in Fig. 13(a). Any further decrease in β would cause this attractor to expand with its extreme left point on U_1 appearing to the left of A, thereby causing this trajectory to move downward and eventually link up with its twin from the D_{-1} region.

Translating this picture into the V_1-plane, we obtain the V_1-portrait of V_0 in Fig. 13(b), where we have *assumed*[†] that $\widehat{E_1A_1} = \pi_1(\overline{A_1E_1})$ intersects the line $\Psi_1(L_1) = \{(x,y) \mid x = 1\}$ at A_1' as shown in Fig. 13(b). The snake area S_α bounded by $\widehat{B_1C_1}$, $\widehat{F_1C_1}$, and $\widehat{B_1F_1}$ is *tangent* to $\widehat{E_1Q_1A_1} = \pi_1(\overline{E_1A_1})$ at Q_1. Since the Rössler screw-type attractor above the eigenspace $E^c(0)$ is not connected to its twin below $E^c(0)$, only one snake S_α is shown in Fig 13(b).[‡]

The π_1^{-1} image of the upper snake S_α gives rise to another snake-like region $\widetilde{S}_\alpha \triangleq \pi_1^{-1}(S_\alpha)$ in Fig 13(b). Since $\widetilde{S}_\alpha = \pi_1^{-1}\pi_2(\Delta A_1B_1E_1) = \pi(\Delta A_1B_1E_1)$, the lower snake $\widetilde{S}_\alpha$ is the image of the triangular region $\Delta A_1B_1E_1$ under the Poincare map π. Consequently $\widetilde{S}_\alpha$ must be tangent to $\overline{E_1A_1}$ at $Q_1' = \pi_1^{-1}(Q_1)$.

It follows from the above analysis that the birth of the double scroll must occur at such a parameter value that the upper snake S_α is tangent to $\pi_1(\overline{E_1A_1})$. A computer calculated example of such a situation is shown in Fig. 13(c), which corresponds to the parameter values $(\alpha, \beta, m_0, m_1) = (8.8, 14.3, -1/7, 2/7)$.

6.3 Death of the Double Scroll

Using a "shooting method" [24], we have discovered [3] an unstable (saddle-type) *periodic* orbit actually co-*exists* with the double scroll. As we increase α while fixing β, m_0 and m_1, we observe the periodic orbit shrinks while the double scroll grows in size. At the parameter α_0 (or just below to be precise) where they collide with each other, the double scroll suddenly disappears while the unstable periodic orbit continues to exist. We refer to

---

[†]For some parameter values $\pi_1(\overline{A_1E_1})$ may clear the $x = 1$ line and spiral toward F_1 as in $\widehat{e_1F_1}$ in Fig. 6.

[‡]Recall 2 snakes S_α and S_b are present in Fig. 12 and (6.5).

this collision event as the *death of* the double scroll and our goal is to derive the parameter β when this occurs.

Figure 14(a) shows the doulbe scroll at the verge of colliding with the periodic orbit $\Gamma^{\bullet}$ (shown dotted). Let $\Gamma^{\bullet}$ intersect U_1 at point H^- in its downward swing and at point H^+ in its return upward swing. Note that H^- must lie to the *right* of the line L_1 because as $\Gamma^{\bullet}$ moves down through H^- in Fig. 14(a), it will first hit U_{-1} and turn around without hitting $E^c(P^-)$, and eventually hit U_{-1} in its upward swing at a point $\widetilde{H}^- \triangleq -H^-$ to the *left* of $\widetilde{L}_1$ (odd symmetric image of L_1). Hence, $H^- \in \angle ABE$.

Let $H_1^- \triangleq \Psi_1(H^-)$ and $H_1^+ \triangleq \Psi_1(H^+)$. Since H_1^+ and H_1^- are fixed points of π, we have

$$H_1^+ = \pi_1(H_1^-) = \pi_2(H_1^-) \tag{6.16}$$

as shown in the V_1-portrait of V_0 in Fig. 14(b). Note that a double-snake area $S_1 \triangleq S_a \cup S_b$ now appears in Fig. 14(b) because the double scroll in Fig. 14(a) intersects U_1 on both sides of the line L_0. The π_1^{-1} image of S_a and S_b is shown in Fig. 14(b) by another double-snake area $\widetilde{S}_a \triangleq \pi_1^{-1}(S_a)$ and $\widetilde{S}_b \triangleq \pi_1^{-1}(S_b)$.

Now given the coordinates of H^- as obtained by the shooting method, we can identify the corresponding local coordinates (u_0, v_0) of H_1^-, namely

$$H_1^- = \underset{\sim}{x}_1(u_0, v_0). \tag{6.17}$$

From this we can define the local coordinates of A_{1u_0} and E_{1u_0} as follows:

$$A_{1u_0} = u_0 A_1 + (1-u_0)B_1, \quad E_{1u_0} = u_0 E_1 + (1-u_0)F_1 \tag{6.18}$$

Since $\overline{E_{1u_0}A_{1u_0}}$ passes through the point H_1^-, $\pi_1(\overline{E_{1u_0}A_{1u_0}})$ passes through the point H_1^+ as shown in Fig. 14(b). In *Appendix 6*, we will show that $\overline{E_{1u_0}A_{1u_0}}$ is an excellent approximation of the *stable manifold*

$$W^s(H_1^-) = \{\underset{\sim}{x} \in \angle A_1 B_1 E_1 | \pi^n(\underset{\sim}{x}) \to H_1^- \text{ as } n \to \infty\}, \tag{6.19}$$

that is $W^s(H_1^-) \approx \overline{E_{1u_0}A_{1u_0}}$.

Now let $\widetilde{\Lambda}_{U_1}$ denote the intersection of the double scroll attractor with U_1 and define $\Lambda_1 = \Psi_1(\widetilde{\Lambda}_{U_1})$. By definition, the death of the double scroll occurs when Λ_1 intersects the points H_1^+ (and H_1^-). This condition is equivalent to the condition that Λ_1 touches the stable manifolds $W^s(H_1^+)$ because $\underset{\sim}{x} \in W^s(H_1^+) \cap \Lambda_1$ implies $H_1^+ = \lim_{n \to \infty} \pi^n(\underset{\sim}{x})$ belongs to $W^s(H_1^+) \cap \Lambda_1 \subset \Lambda_1$. Since the upper exit gate $\widehat{B_1 C_1}$ approximates a portion of Λ_1 as stated in

Section 6.1, the parameter value where $\overparen{B_1C_1}$ touches $\overparen{E_{1u_0}A'_{1u_0}} = \pi_1(\overline{A_{1u_0}E_{1u_0}}) \approx W^s(H_1^+)$ gives an excellent approximation of the value at which the double scroll disappears.

The preceding analysis shows that the V_1-portrait of V_0 corresponding to the death of the double scroll must be as shown in Fig. 14(b). Observe that the upper snake S_a must be tangent to Q_1 and, correspondingly, the lower snake $\widetilde{S}_a$ must be tangent to Q'_1.

To show that the double scroll would disappear if the parameter is further tuned so that Q'_1 crosses the stable manifold $W^s(H_1^-) \approx \overline{E_{1u_0}A_{1u_0}}$ and moves below $\overline{E_{1u_0}A_{1u_0}}$, we note that in this case[†] the iterates of Q'_1 under π would eventually leave the trapping region $\mathcal{J}$ and fail to converge to an attractor within $\mathcal{J}$.

A computer calculated V_1-portrait of V_0 corresponding to the death of the double scroll is shown in Fig. 14(c), where $(\alpha,\beta,m_0,m_1) = (10.73, 14.3,-1/7,2/7)$.

6.4. Hole-Filing and Heteroclinic Orbits

All the double scrolls given in [1-6], have a hole centered at P^+ and P^- because the parameters were such that no trajectory in $\widetilde{\Lambda}$ passes through the point D in Fig. 2(a) where the real eigenvector $E^r(P^+)$ hits U_1. It is possible, however, to choose parameters such that D lies on $\widetilde{\Lambda}$. For example, when $(\alpha,\beta,m_0,m_0) = (9.85, 14.3,-1/7,2/7)$, the corresponding V_1-portrait of V_0 is as shown in Fig. 15(a). Note that $D_1 = \Psi_1(D)$ lies on the *lower exit gate* $\overparen{C_1A'_{1\infty}} = \pi_1(\overline{A_1A_{1\infty}})$. Now, assuming[‡] that the set Λ has a *dense* orbit under the "discrete" Poincaré map $\pi: \mathcal{J} \to \mathcal{J}$ defined in (6.7), then since $\overparen{C_1A'_{1\infty}}$ converges (under π) rapidly to a point in $\Lambda_1 \triangleq \Lambda \cup \pi_2(\Lambda)$, it follows that we can make an infinitesimally-small perturbation on β so that D_1 lies on $\Lambda_1 \triangleq \Lambda \cup \pi_2(\Lambda)$. Under this condition, there exists a trajectory originating from D_0 in Fig. 2(a) which exits U_1 at exactly the point D. Such a trajectory would then follow the real eigenvector $E^r(P^+)$ and converges rapidly toward P^+. Since P^+ is an "unstable focus" when restricted to the eigenspace $E^c(P^+)$, it follows that the resulting double scroll will not have a hole and is henceforth called a *hole-filling orbit*. The double scroll in Fig. 15(b) is a case in point.

Clearly, another hold-filling orbit exists when D_1 lies on the *upper exit gate* $\overparen{C_1B_1} = \pi_1(\overline{A_1B_1})$.

[†]The *unstable* manifold $W^u(H_1^-)$ in this case must be a subset of $\widetilde{S}_b$ because $W^u(H_1^-)$ is an invariant set and the only invariant set in Fig. 14(b) other than $W^s(H_1^-)$ which contains H_1^- is $\widetilde{S}_b$. A more detail discussion of the stable and unstable manifolds of H_1^- and H_1^+ is given in *Appendix 6*.

[‡]This assumption is consistent with all computer simulations of the double scroll observed so far. Note that the *dense* orbit here differs from that associated with $\widetilde{\Lambda}$ in (6.14): the dense orbit in $\widetilde{\Lambda}$ pertains to a "continuous flow," whereas the dense orbit in Λ refers to a "discrete map."

Suppose in addition to $D_1 \in \overparen{C_1 A'_{1\infty}}$ in Fig. 15(a) the point $B'_1 \triangleq \pi_1^{-1}(B_1)$ lies on the *lower entrance gate* $\overline{A_1 A_{1\infty}}$ in Fig. 15(a).[†] This implies that $B''_1 \triangleq \pi_2(B'_1)$ lies on the *lower exit gate* $\overparen{C_1 A'_{1\infty}}$. Now assuming D_1 lies between B''_1 and C_1 on $\overparen{C_1 A'_{1\infty}}$, then the hole-filling orbit starting from P^+ would, after entering D_0 from above, continue to move downward and eventually hit U_{-1} at $D^- = -\Psi_1^{-1}(D_1)$ where the lower eigenvector $E^r(P^-)$ intersects U_{-1}. By the odd symmetry of ξ, the return orbit would be a symmetric image and hence must exit U_1 at D. Such a hole-filling orbit is called a *heteroclinic orbit*.

Since Shilnikov's theorem also applies when the "homoclinic orbit" in the hypotheses is replaced by a "heteroclinic" orbit [15,25], any rigorous demonstration of the existence of a heteroclinic orbit would also prove the existence of chaos in the double scroll system (1.1)-(1.3) in the sense of Shilnikov. Such a demonstration has been given recently in [15] where a computer calculated hole-filling heteroclinic orbit is shown.

6.5. Homoclinic Orbits [26]

We have already proved the existence of at least one *homoclinic orbit* through the equilibrium point 0 in *Section 4*. To complete our bifurcation analysis, Figure 16 shows the V_1-portrait on V_0 associated with such a homoclinic orbit, where $(\alpha,\beta,m_0,m_1) = (4.1,4.7,-1/7,2/7)$. Note that the point C_1 lies on $\overparen{E_1 A'_1}$ as required by hypothesis (i) of *Theorem 5.1*.

Homoclinic orbits through the other two equilibrium points P^+ and P^- can also occur under appropriate parameter values. In particular, they occur when one of the following two conditions is satisfied:

1.(a) $\widetilde{B}'_1 \triangleq \pi_1^{-1}(B_1)$ lies on the *upper entrance gate* $\overline{A_1 B_1}$, as shown in Fig. 15(a).

  (b) D_1 lies between $\widetilde{B}''_1 \triangleq \pi_2(\widetilde{B}'_1)$ and B_1 on the *upper exit gate* $\overparen{B_1 C_1}$.

2.(a) $\widetilde{B}'_1 \triangleq \pi^{-1}(B_1)$ lies on the *lower entrance gate* $\overline{A_1 A_{1\infty}}$.

  (b) D_1 lies on the *upper exit gate* $\overparen{B_1 C_1}$ (between B_1 and C_1).

6.6. Bifurcation Diagram

Using the conditions derived in *Sections 6.4 and 6.5* for the birth and death of the double scroll, we carry out a detailed (double-precision) computer bifurcation analysis of the $\alpha-\beta$ parameter plane (with $m_0 = -1/7$ and $m_1 = 2/7$). First, we derive the set of all (α,β) for which the eigenvalue at P^+ is pure imaginary, i.e., when $\widetilde{\sigma}_1 = 0$. It turns out that by fixing m_0

[†]Note that B'_1 corresponds to the point a_2 Fig. 6 except that for the parameter used in Fig. 6, a_2 lies on the *upper entrance gate*.

= 1/7, this set can be derived explicitly; namely

$$\beta = (1-m_1)\alpha(m_1\alpha+1) \tag{6.21}$$

Substituting $m_1 = 2/7$ into (6.21), we obtain curve ① in Fig. 17. It follows from the *Hopf bifurcation theorem* that any parameter (α,β) where P^+ and P^- are sinks (i.e., $\tilde{\sigma}_1 < 0$ and $\tilde{\gamma}_1 < 0$) lie *above* curve ① , henceforth called the *Hopf bifurcation curve*, and that for (α,β) in a small band to the right of this Hopf bifurcation curve, we can expect nearly sinusoidal oscillations.

The sets of (α,β) which give rise to the *birth* and the *death* of the double scroll are given by curve ② and curve ③ , respectively. It is natural to call curves ② and ③ the *birth boundary* and the *death boundary*, respectively.

It follows from our preceding analysis that those parameters (α,β) associated with the period-doubling and the Rössler screw-type attractor must all lie between the *Hopf bifurcation curve* ① and the *birth boundary* curve ② . All parameters associated with the double scroll must lie between this birth and the death boundary.

7. One-Dimensional-Poincaré Map.

Our analysis in *Section 6* shows that the *qualitative* behavior of the double-scroll system (1.1)-(1.3) is determined essentially by the *2-dimensional* Poincaré map π of points on an infinitesimally- *thin* "ribbon" centered along the two *entrance gates* $\overline{A_1 B_1}$ and $\overline{A_1 A_{1\infty}}$ which correspond to the semi-infinite line $L_1' \subset L_1$ in Fig. 1 to the left of point B. Since this "ribbon" is "numerically" indistinguishable from L_1' when $|\tilde{\gamma}_1|$ is relatively large compared to the other eigenvalues, it is natural therefore to define a 1-dimensional *approximation* π^* of the Poincaré map π by restricting its domain to L_1', and compare its qualitative behaviors with those of π. By brute-force computer integration of the system (1.1)-(1.3), we have constructed such a 1-D Poincaré map for many parameter values. Our "numerical" results show that inspite of the inevitable local truncation and round-off errors, this 1-D Poincaré map predicted all of the qualitative behaviors that we have so far observed by computation simulation (including *period-doubling, periodic windows*) and by rigorous analysis in the preceding sections (e.g., Rössler screw-type attractors and the double scroll).

This remarkable observation motivates a more *rigorous* analysis of this 1-D discrete map. In order to do this, it is necessary to describe this 1-D map in *analytic* form. Our main objective in this final section is to derive this 1-D map π^* and analyze its qualitative behaviors. It turns out that a much simpler analytical expression for π^* is possible if we choose the *domain* of the function π^* to be another semi-infinite line segment $\overline{P^+ N}$ and its extension beyond N to N_∞ at infinity as shown in Fig. 1. This line is constructed by connecting the point $M \triangleq \Psi_1^{-1}(1,0,0)$ and point P^+ by a straight line and extending it beyond N to ∞ and deleting the portion $\overline{P^+ M}$ in Fig. 1. In other words, we will define the 1-D Poincaré map

$$\pi^* : \overline{P^+ N_\infty} \rightarrow \overline{P^+ N_\infty} \tag{7.1}$$

In order for π^* to be well defined, we must make the following two *assumptions*:

(1) the spiral $\overparen{C\,A'_\infty}$ (i.e., Ψ_1^{-1} of the *lower exit gate* $\overparen{C_1 A'_{1\infty}}$) on U_1 of Fig. 1 does *not* intersect the line L_2 through points E, F, and B.

(2) the point D (where the real eigenvector hits U_1) on U_1 in Fig. 1 is located on the *left* of $\overparen{CA'_\infty}$.

To prove that π^* in (7.1) is well-defined under the above assumptions, it is more convenient to translate our analysis into the D_1-unit in Fig. 2(b) via the coordinate transformation Ψ_1, which we redraw in Fig. 18(a). Consider the rectangular region

$$W_1 \overset{\Delta}{=} \{(x,y,z) \in \mathbb{R}^3 \mid x \le 0, y = 0\} \tag{7.2}$$

passing through the line segments $\overline{ON}_1$ and $\overline{OD}_1$. Since $0 = \Psi_1(P^+)$, $D_1 = \Psi_1(D)$, and $N_1 = \Psi_1(N)$, it follows that W_1 corresponds to the plane W in Fig. 1 passing through the two line segments $\overline{P^+D}$ and $\overline{ND}$.

Now, in terms of the *local* coordinates (u,v), points along the line $\overline{B_1 A_{1\infty}}$ are uniquely identified by a single coordinate u since $v = 1$ on this line. In particular, any point $\underset{\sim}{x}(u)$ on this line is described by

$$\underset{\sim}{x}(u) = \underset{\sim 1}{x}(u,1),\ 0 \le u \le 1 \quad \text{if } \underset{\sim}{x}(u) \in \overline{B_1 A_1} \tag{7.3}$$

$$1 < u < \infty \quad \text{if } \underset{\sim}{x}(u) \in \overline{A_1 A_{1\infty}}$$

Since $\overline{B_1 A_{1\infty}}$ lies on the eigenspace $\Psi_1(E^c(P^+))$, all trajectories originating from $\overline{B_1 A_{1\infty}}$ (in backward time), must remain on the $x - y$ plane in Fig. 18(a) while spiraling inwards /and must eventually hit $\overline{ON_1}$ (on the negative x-axis) at some point a *distance*[†] $X(u)$ from 0 after a time interval $\pi - \vartheta$, where $\vartheta \overset{\Delta}{=} -\arg \underset{\sim}{x}(u) = -\tan^{-1}[x_y(u)/x_x(u)]$. Here, $x_x(u)$ and $x_y(u)$ denote the x and y component of $\underset{\sim}{x}(u)$, respectively. Clearly,

$$X(u) = |\underset{\sim}{x}(u)| \exp[-\sigma_1(\pi + \arg \underset{\sim}{x}(u)] \ge 0 \tag{7.4}$$

Now, *assumption 1* is equivalent to the condition the lower exit gate $\overset{\frown}{C_1 A'_{1\infty}}$ does *not* touch or intersect the line through B_1, F_1, E_1 in Fig. 18(a). It follows from our analysis of Figs. 4 and 5 that both *inverse-return functions* $u^+(1,t)$ in (4.14) and $u^-(1,t)$ in (4.22) are strictly monotone functions and hence have a unique inverse. Hence, any point $X(u) \ge 0$ on $\overline{N_1 X(0)}$ maps uniquely into a point $\underset{\sim}{x}(u)$ on $\overline{B_1 A_{1\infty}}$ via the flow φ_1^t, where $X(0)$ is the limiting point which maps (under φ_1^t) into B_1. Note that any point d_1 between $X(0)$ and 0 in Fig. 18(a) must map (under φ_1^t) into a point d_2, where

$$d_2 = e^{2\pi\sigma_1} \cdot d_1 \tag{7.5}$$

because the expanding logarithmic spiral from d_1 can not touch $\overline{B_1 A_{1\infty}}$.

The *upper exit gate* $\overset{\frown}{B_1 C_1} = \pi_2(\overline{B_1 A_1})$ and *the lower exit gate* $\overset{\frown}{C_1 A'_{1\infty}} = \pi_2(\overline{A_1 A_{1\infty}})$ are shown in Fig. 18(a). Note that each point $\underset{\sim}{x}(u)$ on $\overline{B_1 A_{1\infty}}$ map under π_2 uniquely into a point

---

[†] We define $X(u)$ as the *distance* from 0 since we want the domain of π^* to be part of the positive real axis.

$\underset{\sim}{y}(u)$ with coordinates $(y_x(u), y_y(u), y_z(u))$. Now *assumption 2* is equivalent to the condition that the point D_1 in Fig. 18(a) is located below (relative to V_1plane) the lower exit gate $\overparen{C_1A'}_{1\infty}$. It follows from this condition that the flow φ_1^t from $\underset{\sim}{y}(u)$ must intersect the W_1 rectangle at $\underset{\sim}{Y}(u)$. This translates into Fig. 1 to mean that trajectories starting from the exit gates $\overparen{BC}$ and $\overparen{CA'}_\infty$ will always intersect the plane $W = \Psi_1^{-1}(W_1)$. Hence, the exit gates $\overparen{B_1C_1}$ and $\overparen{C_1A'}_{1\infty}$ in Fig. 18(a) must map into another double spiral on W_1 as shown in Fig. 18(a), where each point $\underset{\sim}{y}(u)$ maps into

$$\underset{\sim}{Y}' = (-|\underset{\sim}{y}(u)| \exp[\sigma_1(\pi - \arg \underset{\sim}{y}(u))], 0, y_z(u) \exp[\gamma_1(\pi - \arg \underset{\sim}{y}(u))]) \tag{7.6}$$

Now, if $|\widetilde{\gamma}_1|$ is relatively large, which is the case in the double scroll, then the double spiral on W_1 in reality is squeezed into a thin line sitting infinitesimally close to $\overline{N_{1\infty}O}$. Consequently, for all computation purposes, we can approximate $Y'(u)$ as the point $Y(u)$ on $\overline{N_{1\infty}O}$. Note that $Y(u)$ is a positive real number given by

$$Y(u) = |\underset{\sim}{y}(u)| \exp[\sigma_1(\pi - \arg \underset{\sim}{y}(u)], \quad 0 \le u \le \infty \tag{7.7}$$

Since $u = u^+(1,t)$ for $0 \le u \le 1$ is given explicitly by (4.14) and since $u = u^-(1,t)$ for $1 < u < \infty$ is given explicitly by (4.22), we can specify the graph of the Poincaré map π^* for $X(u) > X(0)$ by the following *explicit* parametric equations:

$$\left[X(u), Y(u)\right] = \begin{cases} \left[X(u^+(1,t)), Y(u^+(1,t))\right], & 0 \le t < \infty \quad \text{for } 0 \le u < 1 \\ \left[X(u^-(1,t)), Y(u^-(1,t))\right], & 0 < t < \infty \quad \text{for } 1 < u < \infty \end{cases} \tag{7.8}$$

Equation (7.8) defines the 1-D Poincaré map π^* for all $X(u)$ between $X(0)$ and $N_{1\infty}$. For points $X(u)$ between $X(0)$ and 0, where $u < 0$,[†] we simply make use of (7.5), namely,

$$Y(u) = e^{2\pi\sigma_1} \cdot X(u) \quad , \quad u < 0 \tag{7.9}$$

We will henceforth call (7.1), (7.8), and (7.9) the *1-D double scroll Poincaré map*.

A typical graph of π^* corresponding to the parameters $(\sigma_0, \gamma_0, \sigma_1, \gamma_1, k) = (-0.42, 0.50,$

[†]For convenience, we extend our local coordinate $u \ge 0$ to include *negative* u in order to parametrize the points between $X(0)$ and 0.

0.15, -1.5, 0.20) is shown in Fig. 18(b). Note that since σ_1 is a constant, the graph from $X = 0$ to $X' = X(0)$ is always a straight line with a slope equal to $e^{2\pi\sigma_1}$. Note also that to emphasize that the one-dimensional Poincaré map π^* as defined by (7.1), (7.8), and (7.9) is valid not only for system (1.1)-(1.3), but also for the entire double-scroll family of vector fields $\xi \in \mathcal{L}_0$, we use the normalized eigenvalue parameters instead of the usual $(\alpha, \beta, m_0, m_1)$ in Fig. 18(b).

Translating the V_1-portrait of V_0 in Fig. 18(a) back into Fig. 1, we can identify the above 1-D double scroll Poincaré map as

$$\tilde{\pi}^* : \overline{P^+N_\infty} \to \overline{P^+N_\infty} \tag{7.10}$$

The point B' on $\overline{P^+N}$ is identified with the point $X(0)$. For each point $\underset{\sim}{x} \in \overline{P^+B'}$, $\tilde{\pi}^*$ is a *linear* map from $\overline{P^+B'}$ onto $\overline{P^+\tilde{\pi}^*(B')}$. For points $\underset{\sim}{x} \in \overline{B'N_\infty}$, $\tilde{\pi}^*$ is a continuous nonlinear map from $\overline{B'N_\infty}$ into $\overline{P^+N_\infty}$.

We close this paper by exhibiting several different graphs of the 1-D double scroll Poincaré map π^* which illustrates the various qualitative behaviors analyzed in *Section 6*.

7.1. 1-D Poincaré Map π^* for Birth of Double Scroll

The graph of π^* for the parameter $(\alpha, \beta, m_0, m_1) = (8.8, 14.3, -1/7, 2/7)$ is shown in Fig. 19(a). Note that the maximum value of Y on the interval $[0, X(1)]$ is equal to $X(1)$; i.e., the point $Y(u_0) = \max_{0 \le u \le 1} Y(u)$ coincides with the point $X(1)$. Hence $\pi^*(X(u_0)) = X(1)$ maps precisely through point A_1 where $u=1$. All other trajectories have $Y(u) < X(1)$ and hence can only enter D_0 through the upper gate $\overline{B_1A_1}$. Hence, by definition, the graph in Fig. 19(a) heralds the *birth* of the double scroll.

7.2. 1-D Poincaré map π^* for Death of the Double Scroll

The graph of π^* for the parameter $(\alpha, \beta, m_0, m_1) = (10.73, 14.3, -1/7, 2/7)$ is shown in Fig. 19(b). Note that X_H is an *unstable fixed point* of π^* and the maximum value $\max Y(u)$ on the interval $[0, X(1)]$ is equal to X_H. Since $X_H > X(1)$, X_H corresponds to $u>1$ this situation corresponds to the case where the unstable (saddle-type) *periodic orbit* through X_H collides with the double scroll. It follows that the graph in Fig. 19(b) heralds the *death* of the double scroll.

7.3. 1-D Poincaré map π^* for a Hole-Filling Orbit

The graph of π^* for the parameter $(\alpha, \beta, m_0, m_1) = (9.85, 14.3, -1/7, 2/7)$ is shown in Fig. 19(c). Note that on the interval $[X(1), \infty]$, the *minimum value* of $Y(u)$ is zero, namely, $\min_{1 \le u < \infty} Y(u) = 0$. Since $\max_{0 \le u \le 1} Y(u) > X(1)$, the attractor $\tilde{\Lambda}$ is a double scroll. Now min

$Y(u) = 0$ implies that the spiral through $Y'(u)$ associated with this point is *tangent* to the z-axis. This situation corresponds to the case where $\overparen{CA'_{\infty}}$ in Fig. 1 passes through D. Hence, the graph in Fig. 19(c) is associated with a *hole-filling orbit*.

7.4. 1-D Poincaré Map π^* for a Homoclinic Orbit

The graph of π^* for the parameter $(\alpha, \beta, m_0, m_1) = (4.1, 4.7, -1/7, 2/7)$ is shown in Fig. 19(d). Note that $X(1)$ is a fixed point and hence $Y(1) = \pi^*(X(1)) = X(1)$. Since $u=1$ at point A_1, this implies that the trajectory originating from $X(1)$ would enter D_0 through A_1 on the stable eigenspace through 0 and^{hence}converges to 0. This trajectory continues along the unstable eigenvector through 0 until it hits U_1 at C, which is identified with C_1 in Fig. 18(a). Since $Y(1) = X(1)$, the trajectory continuing from C_1 must intersect W_1 at a point $Y'(1)$ whose projection $Y(1)$ is precisely equal to $X(1)$. Hence this trajectory is a *homoclinic orbit* of the origin and the graph in Fig. 19(d) therefore predicts the existence of the homoclinic orbit proved earlier in *Section 5*.

7.5. Periodic points of the 1D Poincaré map π^*

In this section, we will describe the correspondence between the periodic points of the 1D Poincaré map π^* and the periodic orbits in the double scroll system. The 1D Poincaré map π^* gives an excellent approximation under the condition that $|\gamma_1|$ is relatively large compared to the other eigenvalues, and that Λ is infinitesimally thin. This condition implies that each periodic orbit of the double scroll system has at least one stable direction (i.e. the magnitude of at least one characteristic exponent is less than one). In particular, a stable periodic point of π^* corresponds to a stable periodic orbit and an unstable periodic point of π^* corresponds to a saddle-type periodic orbit of the double scroll. Since $Y_{max} \overset{\Delta}{=} \max_{0 \le u \le 1} Y(u)$ corresponds to the outermost orbit of $\widetilde{\Lambda}$, if the period-n points $\{X = (\pi^*)^n(X), \pi^*(X), \ldots, (\pi^*)^{n-1}(X)\}$ satisfy

$$(\pi^*)^i(X) \le Y_{max} \quad, \quad 0 \le i \le n-1 \tag{7.11}$$

the periodic orbit of the double scroll system corresponding to X is located in the attractor $\widetilde{\Lambda}$. Define

$$a \overset{\Delta}{=} X(1). \tag{7.12}$$

As shown later, the type of periodic orbit of the double scroll system is determined by the position of the point a relative to the periodic points of π^*.

(1) **Fixed point** $X_1 = \pi^*(X_1)$

Case (i): $0 < X_1 < a$

Figure 20(a) shows a fixed point X_1 of $\pi^\bullet$ with $X_1 = X(u)$ for some $0 < u < 1$. The corresponding period-1 orbit in the double scroll system is depicted in Figure 20(b). The trajectory originating from X_1 would enter D_0 through a point on the upper entrance gate $\overline{AB}$, return to D_1 and hit X_1. By symmetry, we have a pair of periodic orbits as shown in Figure 20(b). The essential features of this situation are summarized in the "abstract sketch" shown in Figure 20(c), where $N^- = -N$, $a' = -X(1)$ and $X'_1 = -X_1$.

Case (ii): $a < X_1 < \infty$.

Figure 21(a) shows a fixed point X_1 with $X_1 = X(u)$ for some $u > 1$. The trajectory originating from X_1 would enter D_0 through a point on the lower entrance gate $\overline{AA}_\infty$, continue its downward motion until it hits $X'_1 = -X_1$. Therefore we have a period-1 orbit as shown in the abstract sketch in Figure 21(b).

(2) Period-2 point $\{X_2 = \pi^\bullet(X_1), X_1 = \pi^\bullet(X_2)\}$

Case (i): $0 < X_1 < X_2 < a$

Two period-2 points X_1 and X_2 satisfying (i) are shown in Figure 22(a). The trajectory originating from X_1 would enter D_0 through the upper entrance gate, return to D_1 and hit X_2. The trajectory continuing from X_2 would enter D_0 again through the upper entrance gate, and eventually return to X_1. Therefore we have a pair of period-2 orbits as depicted in Figure 22(b).

Case (ii): $a < X_1 < X_2$.

Two period-2 points satisfying (ii) are shown in Figure 23(a). The trajectory originating from X_1 would enter D_0 through the lower entrance gate, continue its downward motion through D_0 and hit $X'_2 = -X_2$. Note that X_1 and X'_1 (resp. X_2 and X'_2) of the double scroll system are "identified" as one point X_1 (resp. X_2) in the graph of $\pi^\bullet$. The trajectory continuing from X'_2 would enter and continue its upward motion through D_0 before returning to X_1. Therefore we have a pair of period-1 orbits as depicted in Figure 23(b), even though $\pi^\bullet$ in Figure 23(a) seems to suggest that we have a period-2 orbit. It follows from this analysis that the period-doubling of a fixed point X of $\pi^\bullet$ with $a < X < \infty$ (as in Fig. 21(a)) in Figure 23(a) corresponds to the splitting of the single "odd-symmetric" period-1 orbit into two period-1 orbits in Figure 23(b). Note that each of the orbits in Figure 23(b) is not odd symmetric, but the two orbits are odd-symmetric image of each other in view of the symmetry of the vector field. The orbit in Figure 21(b) exists by itself because it already exhibits odd symmetry.

Case (iii): $X_1 < a < X_2$.

Two period-2 points satisfying (iii) are shown in Figure 24(a). The trajectory originating from X_1 would enter D_0 through the upper entrance gate, return to D_1 and hit X_2. The

trajectory continuing from X_2 would then enter D_0 through the lower entrance gate, pass D_0 and hit $X'_1 = -X_1$. The portion of the trajectory from X'_1 to X_1 must be "symmetric" to the portion of the trajectory from X_1 to X'_1 with respect to the origin. Therefore this situation corresponds a period-3 orbit in the double scroll system as depicted in Figure 24(b).

(3) Period-n point $\{X = (\pi^\bullet)^n(X), \pi^\bullet(X), \ldots, (\pi^\bullet)^{n-1}(X)\}.$

Let the above period-n point be ordered as follows:

$$0 < X_1 < X_2 < \ldots < X_n < \infty \tag{7.13}$$

where we assume $X = X_1$ without loss of generality. Then the type of period-n orbit of $\pi^\bullet$ is uniquely characterized by a permutation of the indices $\{2, 3, \ldots, n\}$ following the index 1. For example, the permutation (1, 4, 2, 3, 5) corresponds to the following periodic points:

$$0 < X_1 < X_2 < X_3 < X_4 < X_5 < \infty \tag{7.14}$$

The type of periodic orbit of the double scroll system is therefore determined by the position of the symbol a among the symbols $\{0, X_1, X_2, \ldots, X_n, \infty\}$ along the half-line $\overline{P^+N}$, where P^+ may be 0 and N may be ∞. Hence, the *total number* N_T of distinct types of periodic orbits of the double scroll system is equal to

$$N_T = (n-1)! \times (n+1) = (n+1)!/n. \tag{7.15}$$

For example, in the case of $n=3$, we have 8 different types of periodic orbits in the double scroll system. Figures 25(b) and 26(b) show two periodic orbits corresponding to the following two "dynamic routes":

$$(i) \qquad 0 < X_1 < X_2 < a < X_3 < \infty, \tag{7.16}$$
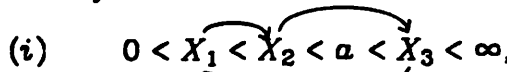
$$(ii) \qquad 0 < X_1 < a < X_2 < X_3 < \infty. \tag{7.17}$$

APPENDIX

Appendix 4. $\pi_1(\overline{F_1B_1})$ is tangent to $\overline{B_1E_1}$ at F_1

Proof. By Theorem 4.3, the spiral $\overset{\frown}{F_1W_1D_1} = \pi_1(\overline{F_1B_1})$ is defined explicitly by

$$\underset{\sim}{x}(t) = e^{-\sigma_1 t}\begin{bmatrix} \cos t & \sin t \\ -\sin t & \cos t \end{bmatrix}(v(t)\underset{\sim}{B}_1 + (1-v(t))\underset{\sim}{F}_1) \tag{A4.1}$$

where $v(t) \overset{\Delta}{=} v(0,t), 0 \le t < \infty$ $(u = 0$, see Fig. 6)

$$\underset{\sim}{B}_1 = (1, \sigma_1)^T, \tag{A4.2}$$

and

$$\underset{\sim}{F}_1 = (\gamma_1(\gamma_1 - 2\sigma_1)/Q_1, \gamma_1[1 - \sigma_1(\sigma_1 - \gamma_1)]/Q_1)^T. \tag{A4.3}$$

Since

$$\underset{\sim}{x}'(t) \overset{\Delta}{=} \frac{d}{dt}\underset{\sim}{x}(t) = e^{-\sigma_1 t}\left\{ -\sigma_1\begin{bmatrix} \cos t & \sin t \\ -\sin t & \cos t \end{bmatrix} + \begin{bmatrix} -\sin t & \cos t \\ -\cos t & -\sin t \end{bmatrix}\right\}(v(t)\underset{\sim}{B}_1 + (1-v(t))\underset{\sim}{F}_1)$$
$$+ e^{-\sigma_1 t}\begin{bmatrix} \cos t & \sin t \\ -\sin t & \cos t \end{bmatrix}v'(t)(\underset{\sim}{B}_1 - \underset{\sim}{F}_1) \ . \tag{A4.4}$$

Substituting $t = 0$ and $v(0) = 0$ in (A4.4), and making use of (A4.2)-(A4.3), we obtain

$$\underset{\sim}{x}'(0) = (\gamma_1 + v'(0))(\underset{\sim}{B}_1 - \underset{\sim}{F}_1). \tag{A4.5}$$

Since $\gamma_1 + v'(0)$ is a scalar, $\underset{\sim}{x}'(0)$ is a vector in the direction of $\underset{\sim}{B}_1 - \underset{\sim}{F}_1$, i.e., along the line segment $\overline{B_1E_1}$. Since $\underset{\sim}{x}(0) = F_1$, it follows that $\underset{\sim}{x}(t)$ is tangent to $\overline{B_1E_1}$ at F_1 when $t = 0$.

Appendix 5: Properties of Trapping Region

(1) In Fig. 6, if $\underset{\sim}{x}$ tends to F_1 from the inside of the "curvilinear wedge" region bounded by $\overset{\frown}{W_1F_1}$ and $\overline{F_1e_1}$, $\pi_1^{-1}(\underset{\sim}{x})$ tends to F_1, and so $\lim \pi_1^{-1}(\underset{\sim}{x}) = F_1 \ne f_1 = \pi_1^{-1}(F_1)$. However, if $\underset{\sim}{x}$ tends to F_1 from the outside of this "curvilinear wedge" region, $\pi_1^{-1}(\underset{\sim}{x})$ tends to f_1, and so $\lim \pi_1^{-1}(\underset{\sim}{x}) = f_1 = \pi_1^{-1}(F_1)$. Since the double-snake area $S_1 \overset{\Delta}{=} S_a \cup S_b$ in Fig. 12 lies outside of this "curvilinear wedge" region near F_1, it follows that

$$\pi_1^{-1}|_{S_1}: S_1 \to \Delta A_{1u} B_1 E_{1u} \tag{A5.1}$$

is a *homeomorphism* from the compact domain S_1 into $\Delta A_{1u} B_1 E_{1u}$. Since $\pi_2|\Delta A_{1u} B_1 E_{1u}$: $\Delta A_{1u} B_1 E_{1u} \to S_1$ is continuous, we have

$$\pi \mid \mathcal{J}: \quad \mathcal{J} = \Delta A_{1u} \, B_1 \, E_{1u} \to \mathcal{J} \tag{A5.2}$$

is continuous. Since the image of a compact set under a continuous map is compact, $\pi(\mathcal{J})$ is a compact subset of $\mathcal{J}$. This proved (6.8) and (6.9).

(2) Equation (6.9) implies $\pi(\Lambda) \subset \Lambda$. Hence, to prove (6.11), we only need to prove $\pi(\Lambda) \supset \Lambda$. Take $\underset{\sim}{x} \in \Lambda \overset{\Delta}{=} \cap_{n \geq 0} \pi^n(\mathcal{J})$. Since $\underset{\sim}{x} \in \pi^{n+1}(\mathcal{J})$, and since $\pi^n(\mathcal{J})$ is compact, the set

$$Y_n = \pi^{-1}(\underset{\sim}{x}) \cap \pi^n(\mathcal{J}) \tag{A5.3}$$

is non-empty and compact. Since

$$Y_{n+1} = \pi^{-1}(\underset{\sim}{x}) \cap \pi^{n+1}(\mathcal{J}) \subset Y_n = \pi^{-1}(\underset{\sim}{x}) \cap \pi^n(\mathcal{J}), \tag{A5.4}$$

we have $Y = \cap_{n \geq 0} Y_n \subset \cap_{n \geq 0} \pi^n(\mathcal{J})$ is non-empty and $\pi(Y) = \underset{\sim}{x}$. Therefore,

$$\underset{\sim}{x} = \pi(Y) \in \pi(\cap_{n \geq 0} \pi^n(\mathcal{J})) = \pi(\Lambda) \tag{A5.5}$$

that is, $\Lambda \subset \pi(\Lambda)$.

(3) In Fig. 12, we can observe that π_1^{-1} maps $S_1 \setminus \{B_1\}$ into the interior of $\Delta A_{1u} \, B_1 \, E_{1u}$. However, the point B_1 maps into the point a_2 on $\overline{B_1 A_{1u}}$ in Fig. 6. From this we have

$$\pi(\mathcal{J}) \subset \{a_2\} \cup \text{interior } \mathcal{J} \tag{A5.6}$$

Since $a_2 \neq B_1$, we have

$$\pi(a_2) = \pi_1^{-1} \pi_2(a_2) \in \text{interior } \mathcal{J}. \tag{A5.7}$$

Therefore, it follows that

$$\pi^2(\mathcal{J}) \subset \pi(a_2) \cup \pi(\text{interior } \mathcal{J}) \tag{A5.8}$$

$$\subset \text{interior } \mathcal{J} \tag{A5.9}$$

because $\pi(\text{interior } \mathcal{J}) \subset \text{interior } \mathcal{J}$. It follows from $\pi(\mathcal{J}) \subset \mathcal{J}$ that

$$\pi^n(\mathcal{J}) \subset \text{interior } \mathcal{J}. \tag{A5.10}$$

To prove existence of an open neighborhood $N(\widetilde{\Lambda})$ which satisfies (6.14), take a small open ball $B(C_1)$ at C_1 such that

$$\pi_1^{-1}(B(C_1)) \subset \text{interior } \mathcal{J}. \tag{A5.11}$$

Then the set

$$N_1 \triangleq B(C_1) \cup \text{interior} \quad S_1 \cup \text{interior} \ \mathcal{J} \tag{A5.12}$$

is an open neighborhood of Λ_1 in the V_1-plane which satisfies

$$\Lambda_1 = \cap_{n \geq 0} \pi^n (N_1).$$

Choose a small neighborhood $N(\widetilde{\Lambda})$ of $\widetilde{\Lambda}$ in the double scroll system such that any trajectory originating in $N(\widetilde{\Lambda})$ intersects $U_1 \cup U_{-1}$ only at points belonging to the set $\Psi_1^{-1}(N_1) \cup (-\Psi_1^{-1}(N_1))$, where N_1 is defined in (A5.12). Then $N(\widetilde{\Lambda})$ satisfies (6.14).

In the more general situation, the double-snake area S_1 may intersect the spiral $\widehat{F_1 W_1 D_1} = \pi_1(\widehat{F_1 B_1})$. Figure 27(a) shows the V_1-portrait of V_0 with such a double-snake area S_1, where $(\alpha, \beta, m_0, m_1) = (4, 4.85, -1/7, 2/7)$ and $u = 2$. Note that the spiral $\widehat{F_1 W_1 D_1}$ intersects the spiral $\widehat{A_{1u} C_1} = \pi_2 (\widehat{A_1 A_{1u}})$ at two points a and b, and the spiral $\widehat{E''_{1u} C_1} = \pi_2(\widehat{E_1 E_{1u}})$ at two points d and c. Since $\widehat{F_1 W_1 D_1}$ is the set of discontinuous points of π_1^{-1} (see (6) in Example 4.3), it follows that the set $\pi_1^{-1}(S_1) = \pi(\Delta A_{1u} B_1 E_{1u})$ must be as depicted in Figure 27(b),[†] where $C_1' = \pi_1^{-1}(C_1)$, $\pi(A_{1u}) = \pi_1^{-1}(A''_{1u})$, $\pi(E_{1u}) = \pi_1^{-1}(E''_{1u})$, $\pi(F_1) = \pi_1^{-1}(F_1) = f_1$ and $\pi(B_1) = \pi_1^{-1}(B_1) = a_2$ (see Fig. 6), where C_1, A''_{1u}, E''_{1u} are indicated in Fig. 12(a). In this case, we expect that $\mathcal{J} = \Delta A_{1u} B_1 E_{1u}$ to be a *trapping region* and that $\Lambda = \cap_{n \geq 0} \pi^n (\mathcal{J})$ is a π-invariant compact subset of $\mathcal{J}$. The proof of this statement, however, is complicated because we must consider the discontinuity of the map π_1^{-1}.

Appendix 6. $\overline{E_{1u_0} A_{1u_0}}$ approximates $W^s(H_1^-)$

Suppose that the magnitude of the real eigenvalue $\widetilde{\gamma}_1$ at $P^+(\gamma_1 < 0)$ is very large compared to the real part of the other eigenvalue. This is equivalent to considering the limit as $\widetilde{\gamma}_1 \to -\infty$. Hence, upon substituting $\gamma_1 = \widetilde{\gamma}_1/\widetilde{\omega}_1$ and $\sigma_1 = \widetilde{\sigma}_1/\widetilde{\omega}_1$ into the coordinates for F_1 and E_1, and then taking the limit as $\widetilde{\gamma}_1 \to -\infty$, we obtain

$$F_1 = (\gamma_1(\gamma_1-2\sigma_1)/[(\gamma_1-\sigma_1)^2+1], \ \gamma_1[1-\sigma_1(\sigma_1-\gamma_1)]/[(\gamma_1-\sigma_1)^2+1])$$

$$= (\widetilde{\gamma}_1(\widetilde{\gamma}_1-2\widetilde{\sigma}_1)/[(\widetilde{\gamma}_1-\widetilde{\sigma}_1)^2+\widetilde{\omega}_1^2], \ \widetilde{\gamma}_1[\widetilde{\omega}_1-\sigma_1(\widetilde{\sigma}_1-\widetilde{\gamma}_1)]/[(\widetilde{\gamma}_1-\widetilde{\sigma}_1)^2+\widetilde{\omega}_1^2])$$

$$\to (1,\sigma_1) = B_1 \ , \quad \text{as } \widetilde{\gamma}_1 \to -\infty \tag{A6.1}$$

and

$$E_1 = (\gamma_1(\gamma_1-\sigma_1-p_1)/[(\gamma_1-\sigma_1)^2+1], \ \gamma_1[1-p_1(\sigma_1-\gamma_1)]/[(\gamma_1-\sigma_1)^2+1])$$

$$= (\widetilde{\gamma}_1(\widetilde{\gamma}_1-\widetilde{\sigma}_1-p_1\widetilde{\omega}_1)/[(\widetilde{\gamma}_1-\widetilde{\sigma}_1)^2+\widetilde{\omega}_1^2], \ \widetilde{\gamma}_1[\widetilde{\omega}_1-p_1(\widetilde{\sigma}_1-\widetilde{\gamma}_1)]/[(\widetilde{\gamma}_1-\widetilde{\sigma}_1)^2+\widetilde{\omega}_1^2])$$

[†] The symbol □ ( ) in Fig. 27(b) denotes a curvilinear region with boundary points listed inside the parentheses.

$$\to (1, p_1) = A_1 \quad , \quad \text{as } \tilde{\gamma}_1 \to -\infty. \tag{A6.2}$$

It follows from (A6.1) and (A6.2) that

$$E_{1u_0} = u_0 E_1 + (1-u_0)F_1 \to u_0 A_1 + (1-u_0)B_1 = A_{1u_0} \tag{A6.3}$$

Under this condition the arc $\overparen{E_{1u_0}H_1^+ A'_{1u_0}}$ shrinks to one point $E_{1u_0} = H_1^- = A_{1u_0}$ under π_1^{-1}, and therefore also under π. Therefore the arc $\overparen{E_{1u_0}A'_{1u_0}}$ may be considered as the stable manifold $W^s(H_1^+)$ as $\tilde{\gamma}_1 \to -\infty$, i.e. $\overparen{E_{1u_0}A'_{1u_0}} \approx W^s(H_1^+)$. This implies that

$$\overline{E_{1u_0}A_{1u_0}} = \pi_1^{-1}(\overparen{E_{1u_0}A'_{1u_0}}) \approx \pi_1^{-1}(W^s(H_1^+)) = W^s(H_1^-) \tag{A6.4}$$

REFERENCES

[1] T. Matsumoto, "A chaotic attractor from Chua's circuit," *IEEE Trans. on Circuits and Systems*, vol. CAS-31, pp. 1055-1058, Dec. 1984.

[2] G.-Q. Zhong and F. Ayrom, "Experimental confirmation of chaos from Chua's circuit," *Int. J. of Circuit Theory and Applications*, vol. 13, pp. 93-98, Jan. 1985.

[3] T. Matsumoto, L. O. Chua, and M. Komuro, "The double scroll," *IEEE Trans. on Circuits and Systems*, vol. CAS-32, no. 8, pp. 797-818, August 1985.

[4] T. Matsumoto, L. O. Chua, and K. Tokumasu, "Double Scroll via a two-transistor circuit," in preparation.

[5] G.-Q. Zhong and F. Ayrom, "Periodicity and chaos in Chua's circuit," *IEEE Trans. on Circuits and Systems*, vol. CAS-32, no. 5, pp. 501-503, May 1985.

[6] T. Matsumoto, L. O. Chua, and M. Komuro, "The double scroll bifurcations," *Int. J. of Circuit Theory and Applications*, in press.

[7] J. P. Eckmann, "Roads to turbulence in dissipative dynamical systems," *Review of Modern Physics*, vol. 53, no. 4, Part 1, pp. 643-654, Oct. 1981.

[8] P.Cvitanovic, / *Universality in chaos*, Adam Hilger Ltd., Bristol 1984.

[9] J. Guckenheimer and P. Holmes, *Nonlinear oscillations, dynamical systems, and biurcations of* vector fields, Springer Verlag, New York, 1983.

[10] Y. S. Tang, A. I. Mees, and L. O. Chua, "Synchronization and chaos," *IEEE Trans. on Circuits and Systems*, vol. CAS-30, p. 620-626, Sept. 1983.

[11] A. Rodriguez-Vasquez, J. L. Huertas, and L. O. Chua, "Chaos in a switched-capacitor circuit," *IEEE Trans. on Circuits and Systems*, vol. CAS-32, pp. 1083-1085, Oct. 1985.

[12] F. M. A. Salam and S. S. Sastry, "Dynamics of the forced Josephson junction circuit: The regions of chaos," *IEEE Trans. on Circuits and Systems*, vol. CAS-32, pp. 784-796, August 1985.

[13] L. O. Chua and R. Ying, "Canonical piecewise-linear analysis," *IEEE Trans. on Circuits and Systems*, vol. CAS-30, pp. 125-140, March 1983.

[14] Th. Bröcker *Differential germs and catastrophes*, Cambridge University Press, Cambridge, England, 1975.

[15] A. I. Mees and P. B. Chapman, "Homoclinic and heteroclinic orbits in the double scroll attractor, *IEEE Trans. on Circuits and Systems*, submitted.

[16] M. W. Hirsh and S. Smale, *Differential Equations, Dynamical Systems, and Linear Algebra*, Academic Press, New York, 1974.

[17] L. O. Chua, C. A. Desoer, and E. S. Kuh, *Linear and Nonlinear Circuits*, McGraw-Hill, New York, NY 1969.

[18] R. W. Brockett, "On conditions leading to chaos in feedback systems," Proc. 1982 CDC, Dec. 1982.

[19] A. Arneodo, P. Coulett and C. Tresser, "Possible new strange attractors with spiral structure," *Communications in Mathematical Physics*, vol. 79, pp. 573-579,1981.

[20] C. Kahlert and L. O. Chua, "Transfer maps and return maps for piecewise-linear three-region dyanamical systems," University of California, Berkeley, Electronics Research Laboratory Memorandum No. UCB/ERL M85/101, November 29, 1985.

[21] Otto E. Rössler, "Continuous chaos—Four prototype equations," Annals of N.Y. Academy of Science, Vol. 31, 1979, pp. 376-392.

[22] M. Hurley, "Attractors: persistence and density of their basins," *Trans. Amer. Math. Society*, vol. 269, pp. 247-271.

[23] R. F. Williams, "Expanding attractors," *IHES Publication*, Math., vol 43, pp. 169-203, 1974.

[24] L. O. Chua and P. M. Lin, *Computer-Aided Analysis of Electronic Circuits: Algorithms and Computational Techniques*, Prentice Hall, Englewood, NJ, 1975.

[25] C. T. Sparrow, "Chaos in a three-dimensional single loop feedback system with a piecewise-linear feedback function," *J. Math. Analy. Appl.* vol. 83, pp. 275-291, 1981.

[26] P. Glendinning and C. Sparrow, "Local and global behavior near homoclinic orbits," *J. Stat. Phys.*, vol. 35, pp. 645-697, 1984.

[27] M. Yuri, "The existence of an invariant stable foliation and the problem of reducing to a one-dimensional map," *Tokyo J. Math.*, vol. 6, pp. 247-266, 1983.

Figure Captions

Fig. 1. Eigenspaces of the equilibria and related sets.

Fig. 2. Geometrical structure and typical trajectories of the original piecewise-linear system and their images in the D_0–unit and D_1–unit of the transformed system (real Jordan form). (a) Original system and typical trajectories. (b) D_0–,D_1–units and half-return maps.

Fig. 3. Geometrical interpretations of the local $u-v$ coordinate system for representing the half-return map π_0^+. (a) Details of the D_0-unit: thick arrows denote the direction of the vector field at various points along $L_{2_0} = \Psi_0(L_2)$ where all vectors lie on the V_0-plane. (b) Graph of a possible inverse return-time function $u = u^+(v,t)$. Here, $I^+(v)$ denotes the set of first-return times which is not connected whenever $u^+(v,t)$ is not a monotone function.

Fig. 4. π_0 associated with a monotone inverse return-time functions. (a) V_0-plane. $(\sigma_0, \gamma_0, \sigma_1, \gamma_1, k) = (-0.3, 1.5, 0.2, -2.0, 0.75)$. (b) Graph of the inverse return-time functions $u = u^-(1,t)$ and $u = u^+(1,t)$. (c) Magnification of (b) over the region $0.90 < u < 1.10$.

Fig. 5. π_0 associated with a non-monotone inverse return-time functions. (a) V_0-plane. $(\sigma_0, \gamma_0, \sigma_1, \gamma_1, k) = (-0.2, 0.75, 0.2, -1.0, 0.75)$ The positions of points a, b', $\underset{\sim}{x}_0(u_1,1)$ and $\underset{\sim}{x}_0(u_{2,}1)$ are not exact but are exaggerated to give more space. (b) Graph of the inverse return-time functions $u = u^-(1,t)$ and $u = u^+(1,t)$. (c) Magnification of (b) over the region $0.90 < u < 1.10$.

Fig. 6. V_1-plane. $(\sigma_0, \gamma_0, \sigma_1, \gamma_1, k) = (-0.4, 0.3, 0.2, -1.0, 0.3)$. $\widehat{F_1 W_1 D_1} \triangleq \pi_1(\overline{F_1 B_1})$, $\widehat{e_1 F_1 W_2 D_1} \triangleq \pi_1(\overline{e_1 a_1})$, $\widehat{e_2 B_1} \triangleq \pi_1(\overline{e_2 a_2})$, $\widehat{E_1 A_1} \triangleq \pi_1(\overline{E_1 A_1})$ and $f_1 \triangleq \pi_1^{-1}(F_1)$. The position of f_1 is exaggerated in this figure for clarity. The actual position of f_1 is "infinitesimally" close to a_1.

Fig. 7. Graphs of the inverse return-time functions $v = v(u,t)$. The parameter values are the same as those of Fig. 6. (a) $v = v(0,t)$. (b) Magnification of (a) over the region $0.995 < v < 1.005$. (c) $v = v(u_1, t)$ where $u_1 = 0.570$. (d) Magnification of (c) over the region $0.995 < v < 1.005$. (e) $v = v(u_2, t)$ where $u_2 = 0.786$. (f) Magnification of (e) over the region $0.995 < v < 1.005$. (g) $v = v(1,t)$. (h) Magnification of (g) over the region $0.995 < v < 1.005$.

Fig. 8. V_1-portrait of V_0 for $(\sigma_0, \gamma_0, \sigma_1, \gamma_1, k) = (-0.4, 0.5, 0.05, -2.0, 0.25)$.

Fig. 9.   Homoclinic orbits. (a) V_1-portrait of V_0. (b) Two odd-symmetric homoclinic orbits through the origin.

Fig. 10.   The two circles bounding S_a and S_b on the V_1-plane and related arcs.

Fig. 11. V_1-portrait of V_0 and the two bounding circles S_a and S_b (which appear as ellipses due to unequal horizontal and vertical scales). The parameters $(\alpha, \beta, \dot{m}_0, \dot{m}_1)$ are: (a) (10.5, 7, -1/7, 2/7); (b) (8.6, 7, -1/7, 2/7); (c) (6.5, 7, -1/7, 2/7).

Fig. 12. V_1-portrait of V_0 with trapping region $\mathtt{J} \triangleq \Delta A_{1u} B_1 E_{1u}$.

Fig. 13.   Geometrical structure at the birth of the double scroll. (a) Macroscopic picture of the original system. (b) Enlargement of the V_1-portrait of V_0. $\widehat{B_1C_1} \triangleq \pi_2(\overline{B_1A_1})$ is tangent to $\widehat{E_1A'_1} \triangleq \pi_1(\overline{A_1E_1})$ at Q_1. $S_\alpha \triangleq \pi_1^{-1}(S_a)$ is an "infinitesimally" thin set (infinitely many layers compressed into a sheet) whose actual location is very close to $\overline{A_1B_1}$. (c) V_1-portrait of V_0 for $(\alpha, \beta, m_0, m_1) = $ (8.8, 14.3, -1/7, 2/7). $\widehat{B_1C_1} \triangleq \pi_2(\overline{B_1A_1})$ is tangent to $\widehat{E_1A'_1} \triangleq \pi_1(\overline{A_1E_1})$ at Q_1.

Fig. 14.   Geometrical structure at the death of the double scroll. (a) Macroscopic picture of the original system. (b) Enlargement of the V_1-portrait of V_0. H_1^+ and H_1^- denote the position of the saddle-type periodic orbit. $\widehat{B_1C_1} \triangleq \pi_2(\overline{B_1A_1})$ is tangent to $\widehat{E_{1u_0}A'_{1u_0}} \triangleq \pi_1(\overline{E_{1u_0}A_{1u_0}})$ at Q_1. $\widetilde{S}_a \cup \widetilde{S}_b$ is an "infinitesimally" thin set (infinitely many layers compressed into a sheet) whose actual location is very close to $\overline{A_{1u_0}B_1}$. (c) V_1-portrait of V_0 for $(\alpha,\beta,m_0,m_1) = $ (10.73, 14.3, -1/7, 2/7).

Fig. 15.   A hole-filling double scroll appears when $(\alpha, \beta, m_0, m_1) = $ (9.85, 14.3, -1/7, 2/7). (a) V_1-portrait of V_0. (b) The double scroll with hole-filling orbits.

Fig. 16.   The V_1-portrait of V_0 which give rise to two odd-symmetric homoclinic orbits through the origin when $(\alpha,\beta,m_0,m_1) = $ (4.1, 4.7, -1/7, 2/7).

Fig. 17.   The bifurcation diagram on the $\alpha-\beta$ plane (drawn with $(m_0,m_1) = $ (-1/7, 2/7)).

Fig. 18.   Geometrical interpretation of the definition of the 1-D Poincaré map π^*. (a) W_1 plane in the D_1-unit. (b) Graph of π^* for $(\sigma_0,\gamma_0,\sigma_1,\gamma_1,k) = $ (-0.42, 0.5, 0.15, -1.5, 0.2).

Fig. 19.   1-D Poincaré maps corresponding to (a) the birth of the double scroll when $(\alpha,\beta,m_0,m_1) = $ (8.8, 14.3, -1/7, 2/7); (b) the death of the double scroll when $(\alpha,\beta,m_0,m_1) = $ (10.73, 14.3, -1/7, 2/7); (c) a hole-filling double scroll when $(\alpha,\beta,m_0,m_1) = $ (9.85, 14.3, -1/7, 2/7); (d) the existence of two odd-symmetric homoclinic orbits when $(\alpha,\beta,m_0,m_1) = $ (4.1, 4.7, -1/7, 2/7).

Fig. 20. Fixed point X_1 of π^* with $0<X_1<a$. (a) Graph of 1-D Poincaré map π^*. (b) Corresponding periodic orbits in the original double-scroll system. (c) Abstraction of the main features of (b).

Fig. 21. One Period-1 fixed point X_1 of π^* with $a<X_1<\infty$. (a) Graph of 1-D Poincaré map π^*. - (b) Abstraction of the corresponding periodic orbits in the original double-scroll system.

Fig. 22. Two Period-2 points X_1 and X_2 with $0<X_1<X_2<a$. (a) Graph of 1-D Poincaré map π^*. (b) Abstraction of the corresponding periodic orbits in the original double-scroll system.

Fig. 23. Two Period-2 points X_1 and X_2 with $a<X_1<X_2<\infty$. (a) Graph of 1-D Poincaré map π^*. (b) Abstraction of corresponding periodic orbits in the original double-scroll system.

Fig. 24. Two Period-2 points X_1 and X_2 with $X_1<a<X_2$. (a) Graph of 1-D Poincaré map π^*. (b) Abstraction of the corresponding periodic orbit in the original double-scroll system.

Fig. 25. Three Period-3 points X_1, X_2, and X_3 with $0<X_1<X_2<a<S_3$. (a) Graph of 1-D Poincaré map π^*. (b) Abstraction of the corresponding periodic orbit in the original double-scroll system.

Fig. 26. Three Period-3 points X_1, X_2 and X_3 with $0<X_1<a<X_2<X_3$. (a) Graph of 1-D Poincaré map π^*. (b) Abstraction of the corresponding periodic orbits in the original double-scroll system.

Fig. 27. A general trapping region corresponding to $(\alpha,\beta,m_0,m_1) = (4, 4.85, -1/7, 2/7)$ and $u=2$. (a) V_1-portrait of V_0. The snake $A_{1u}''C_1E_{1u}''$ intersects the spiral $\overgroup{F_1W_1D_1} \triangleq \pi_1(\overline{F_1B_1})$, which coincides with the set of discontinuous points of π_1^{-1}. (b) Illustration of $\pi(\Delta A_{1u} B_1 E_{1u})$. The snake-like area $\pi(\Delta A_{1u} B_1 E_{1u})$ is actually an "infinitesimal" thin set located very near $\overline{B_1A_{1u}}$.
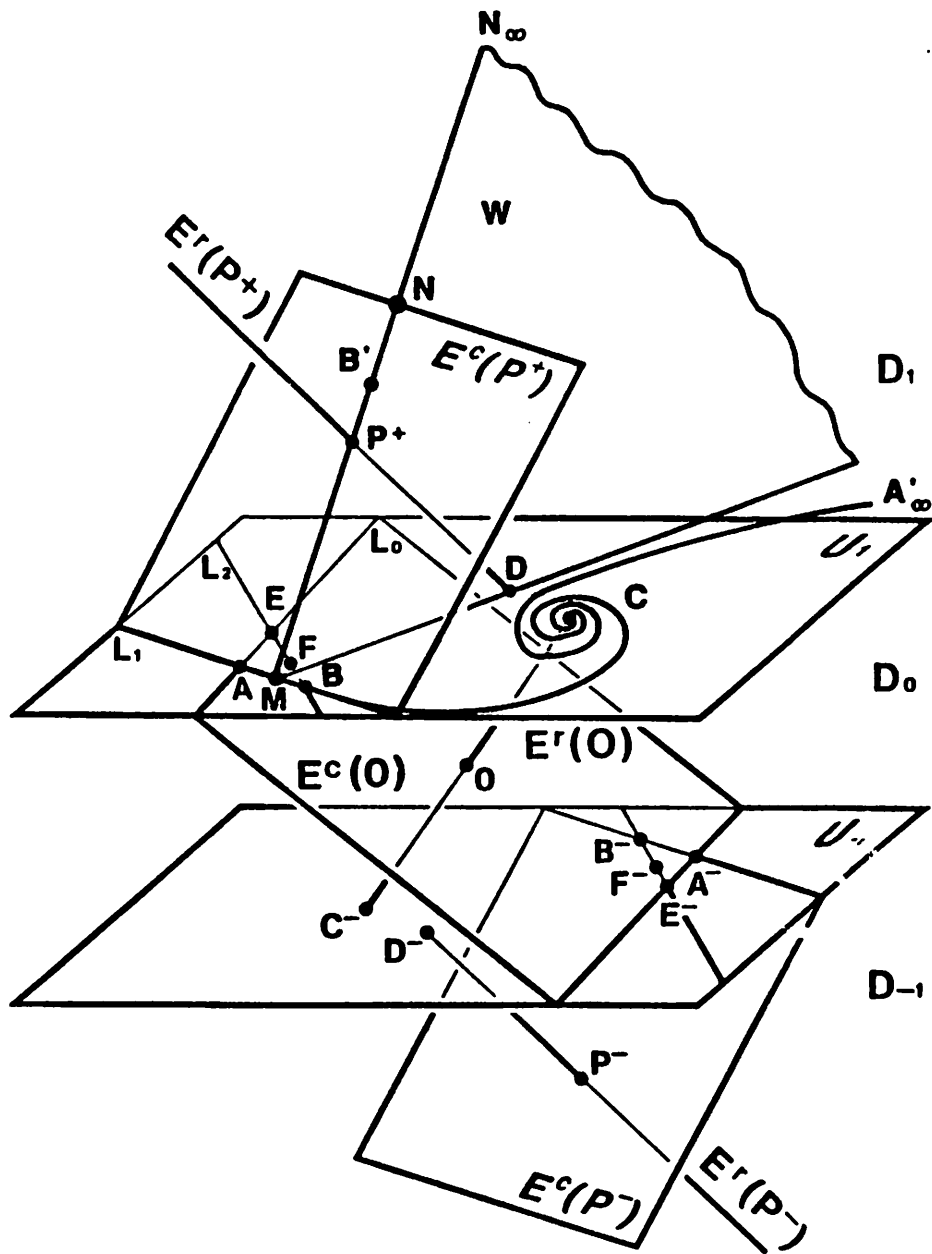
$L_0 = E^c(O) \cap U_1$

$A = L_0 \cap L_1$

$L_1 = E^c(P^+) \cap U_1$

$B = L_1 \cap L_2$

$L_2 = \{\underline{x} \in U_1 : \xi(\underline{x}) /\!/ U_1\}$

$C = E^r(O) \cap U_1$

$D = E^r(P^+) \cap U_1$

$E = L_0 \cap L_2$

$F = \{\underline{x} \in L_2 : \xi(\underline{x}) /\!/ L_2\}$

Fig. 1

stable eigenvector
$E^r(P)$

unstable eigenspace
$E^c(P)$

Γ_1

P^+

Ψ_1

E_∞

A_∞

L_2

E

F

A B

D

C

Ψ_0

U_1

D_1

0

stable eigenspace
$E^c(0)$

D_0

B^- A^-

C^-

F^- E^-

U_{-1}

unstable eigenvector
$E^r(0)$

P^-

D_{-1}

Γ_2

(a)

z

D_1**-unit**

$\Psi_1(E^r(P))$

V_1

y

$V_1 = \Psi_1(U_1)$

D_1

$C_1 F_1$

$x = 1$

$x = -1$

π_1

E_1 B_1

x

A_1

$L_{2_1} = \Psi_1(L_2)$

$\Psi_1(E^c(P))$

Φ

V_0

z

B_0

$\Psi_0(E^r(0))$

C_0

F_0

$x = 1$

$V_0 = \Psi_0(U_1)$

π_0^+

y

$x = -1$

A_0

x

E_0

$\Psi_0(E^c(0))$

π_0^-

$L_{2_0} = \Psi_0(L_2)$

D_0**-unit**

V_0^-

$V_0^- = \Psi_0(U_{-1})$

(b)
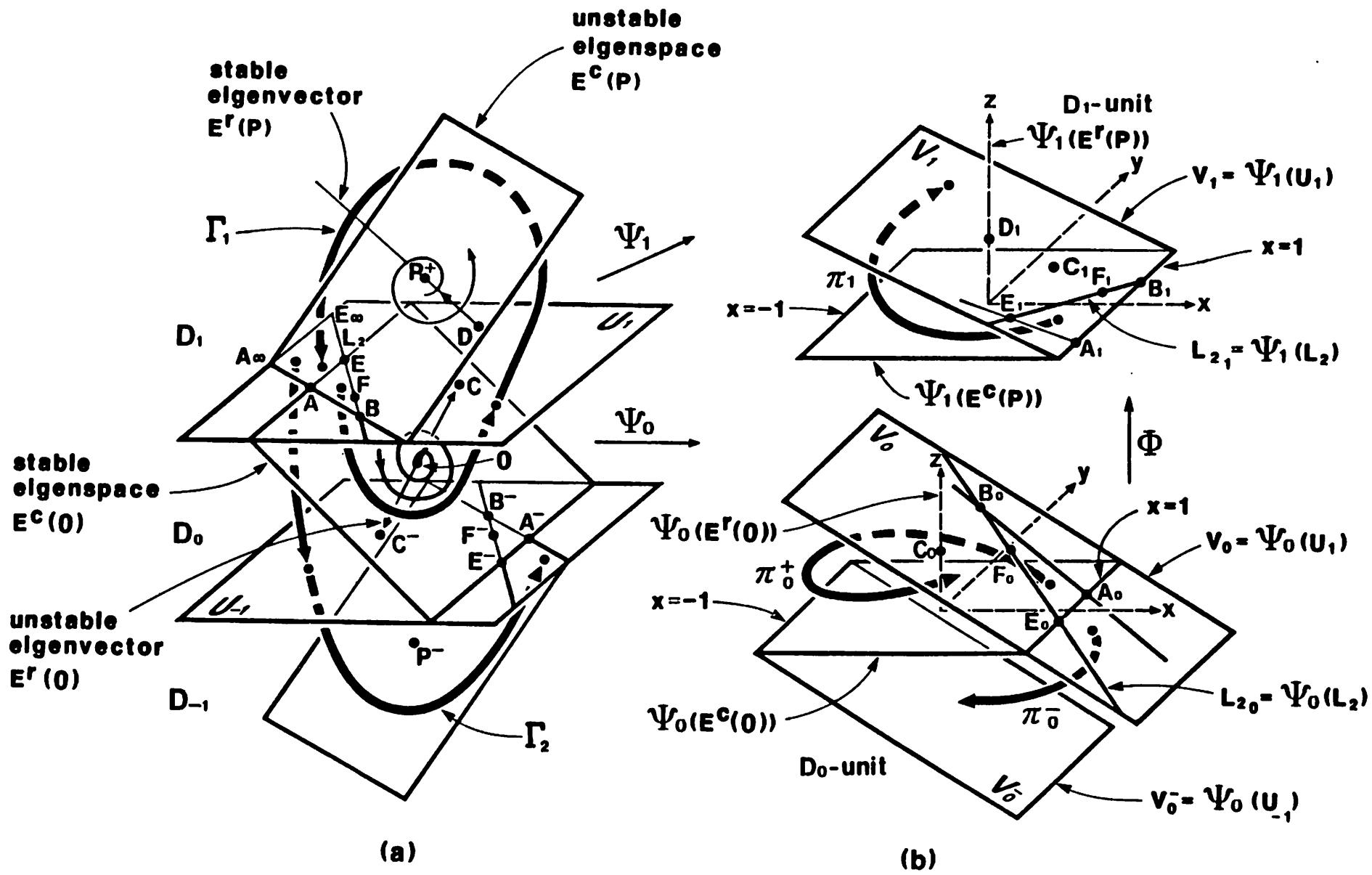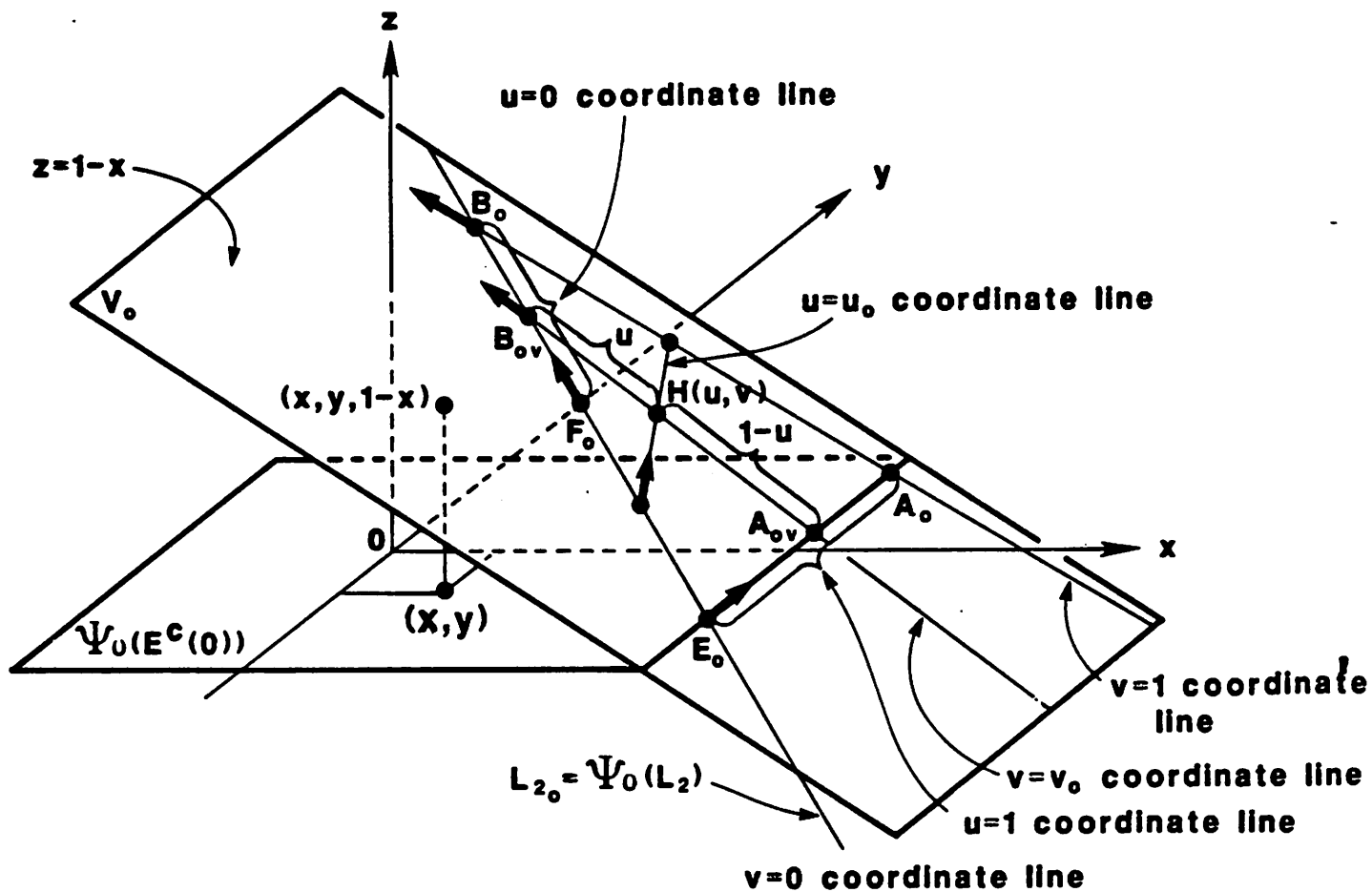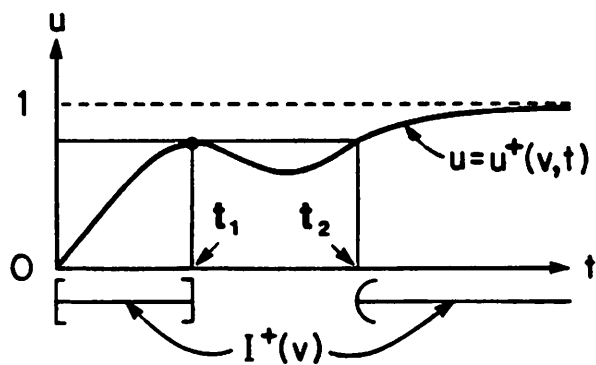
Fig. 2

Fig. 3
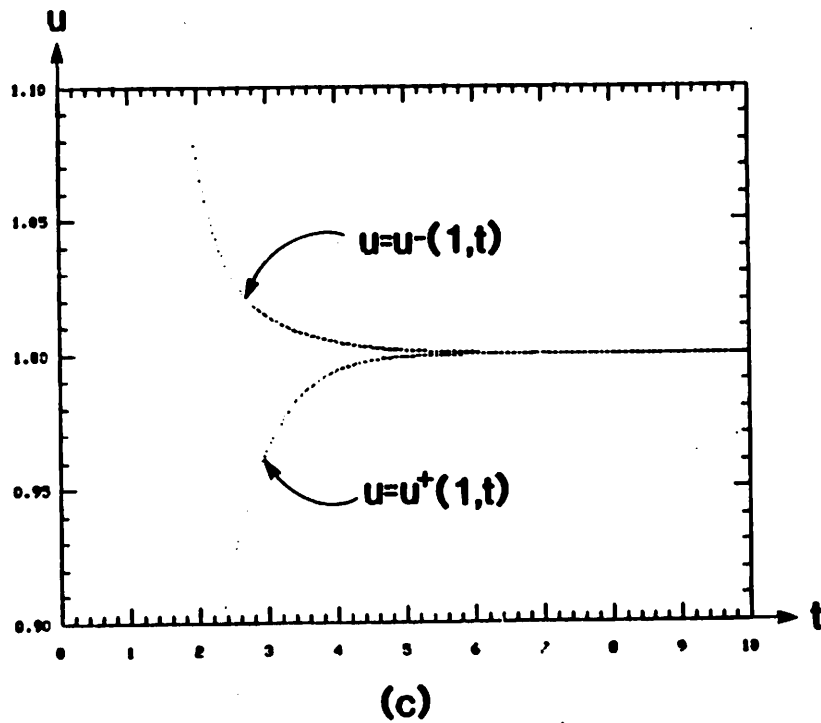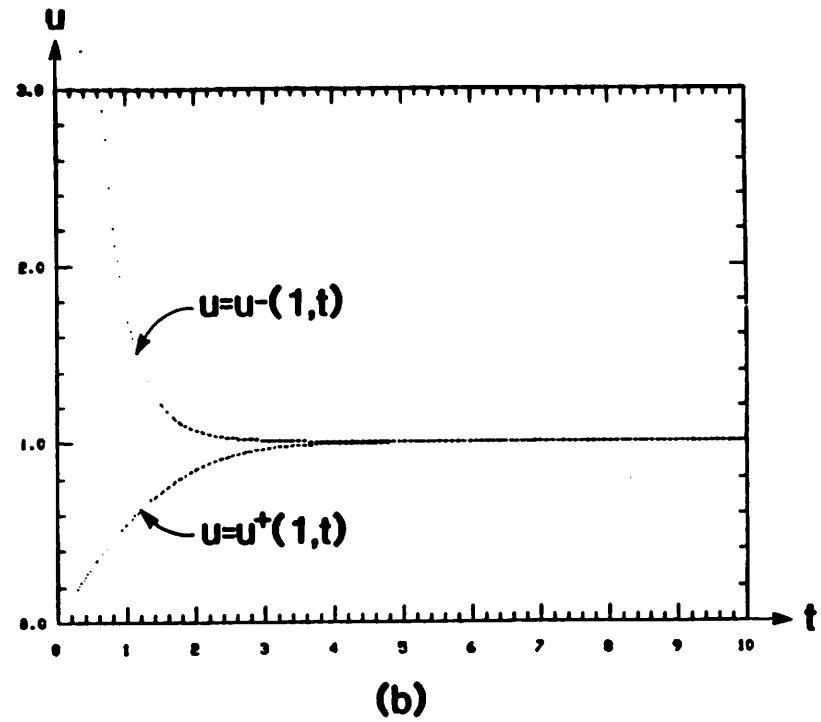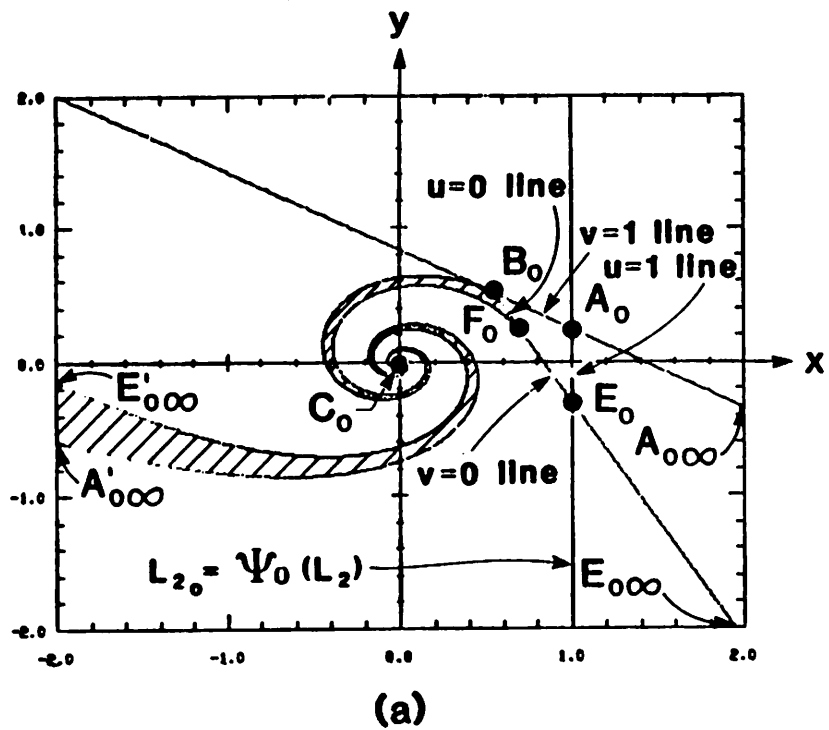
Fig. 4
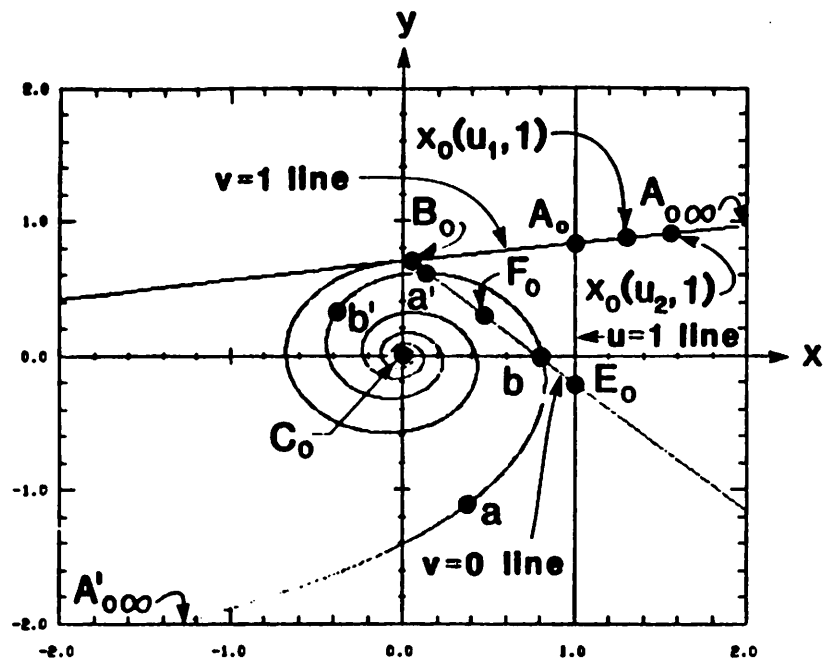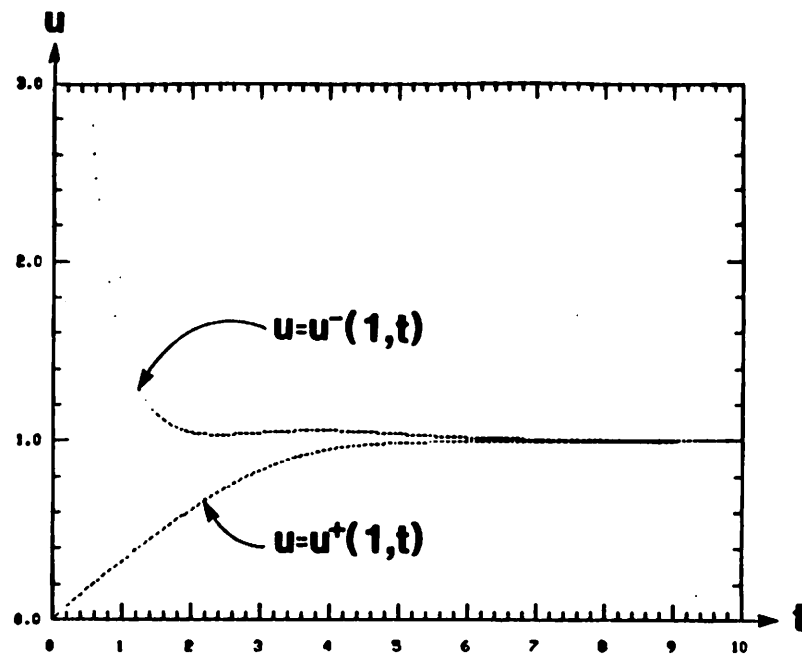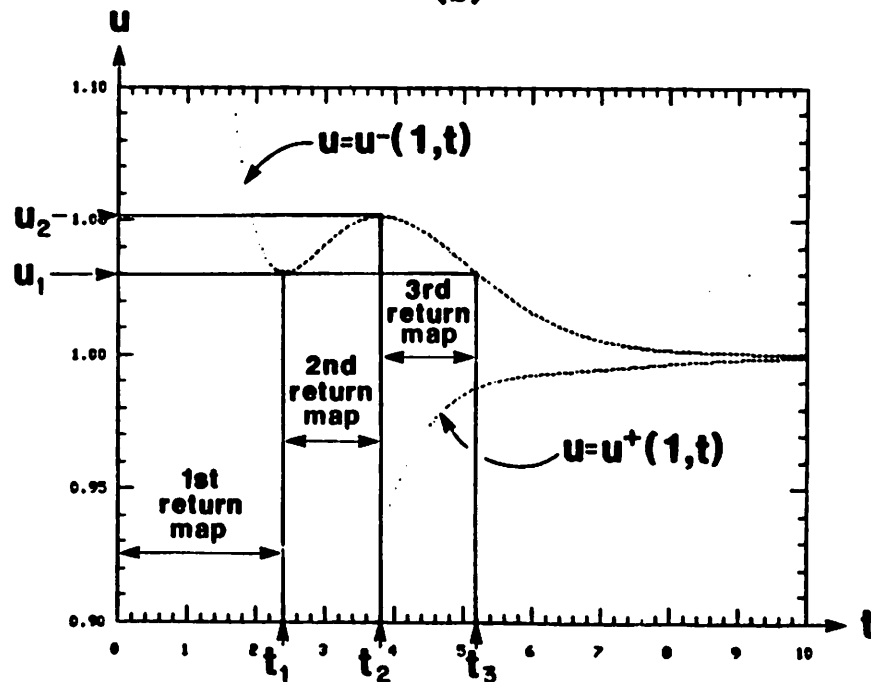
Fig. 5
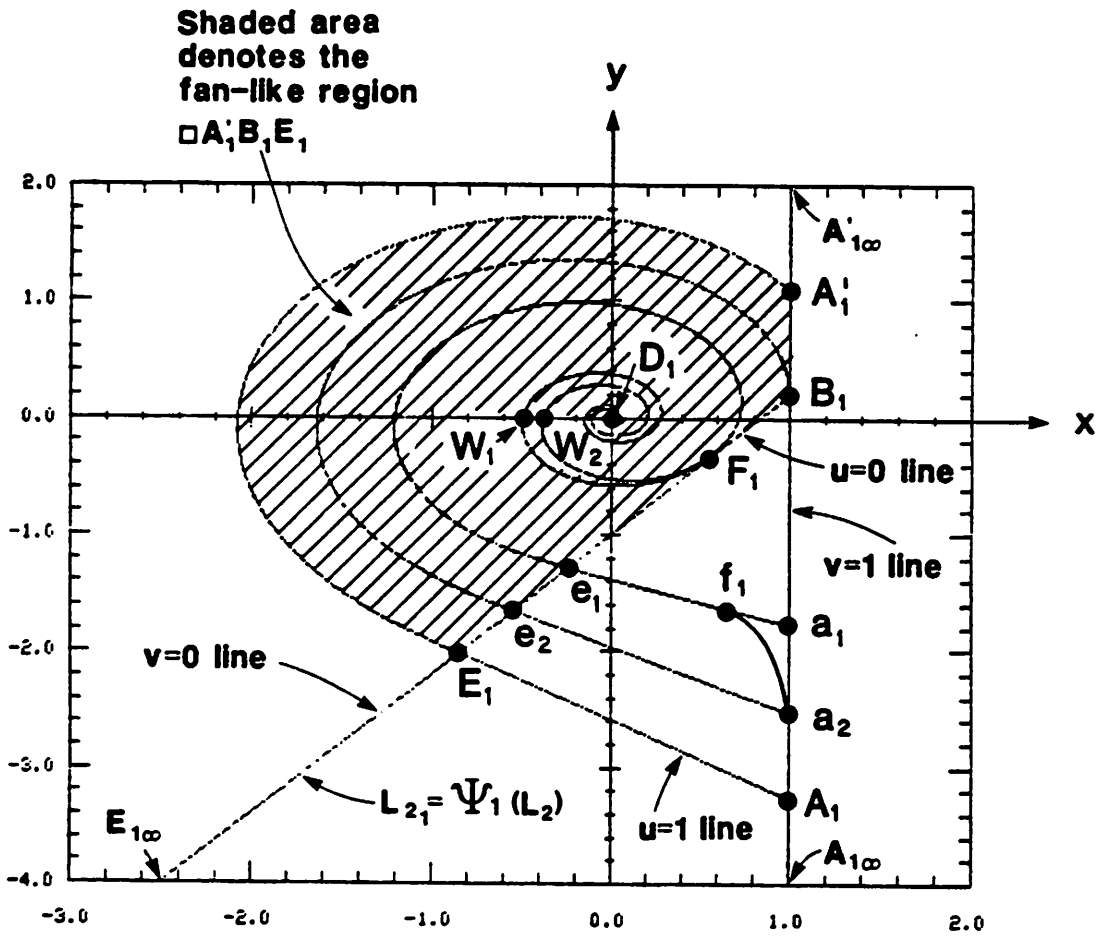
Fig. 6
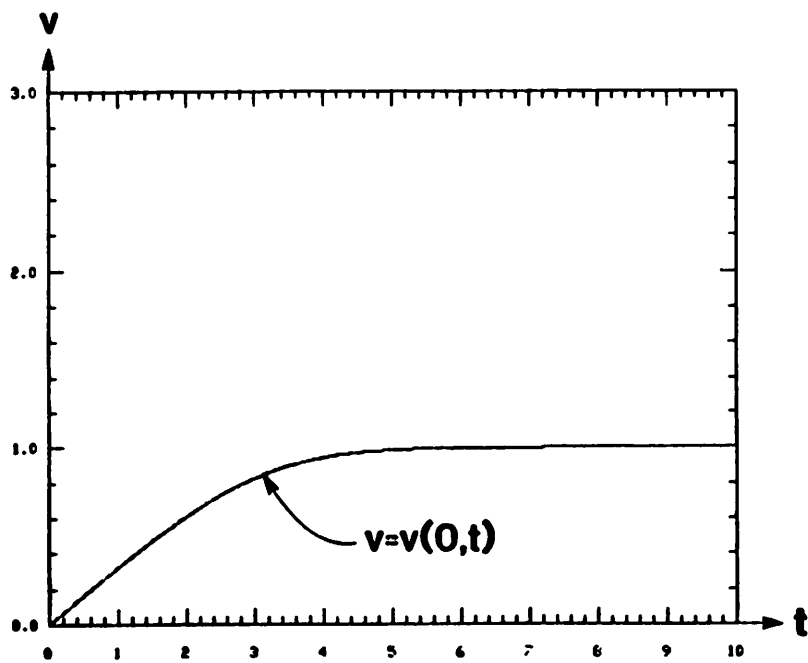
(a)
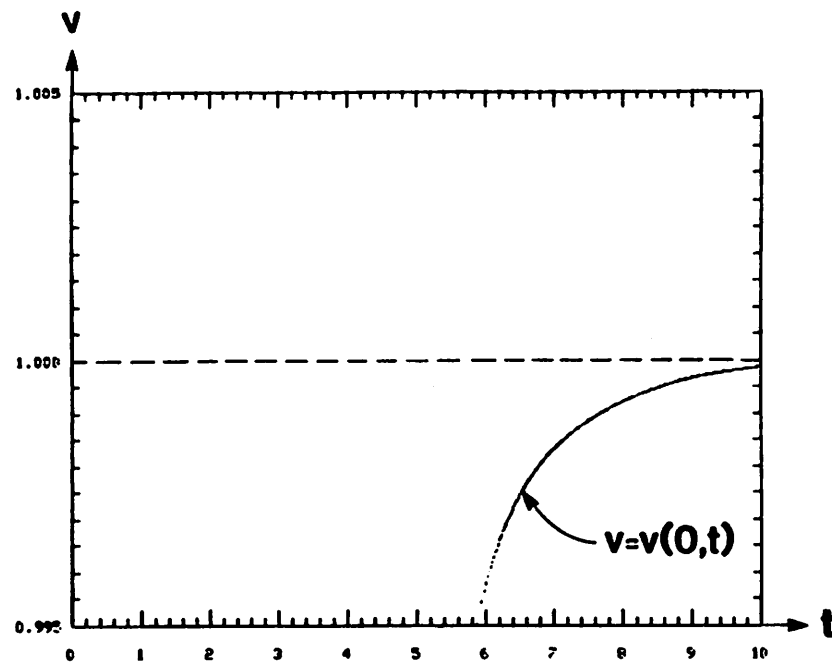
(b)
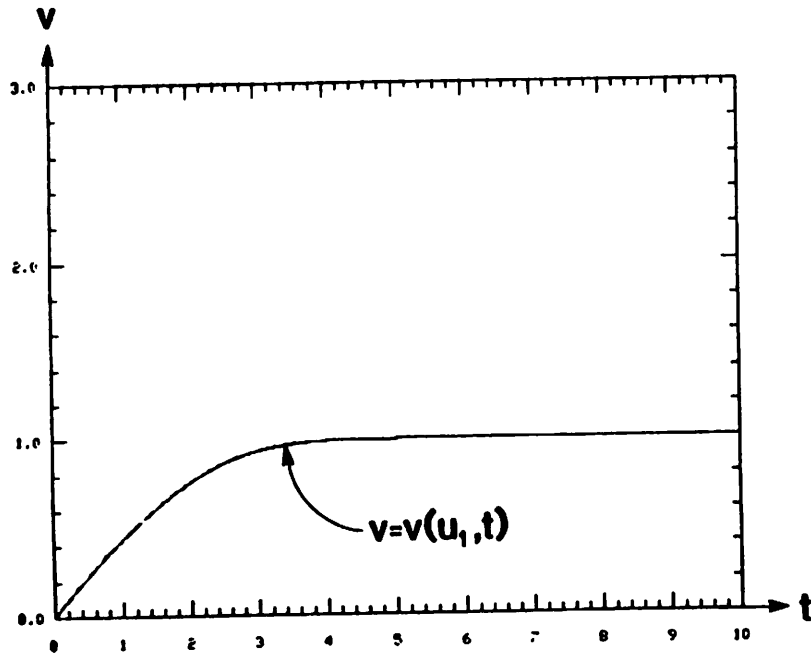
Fig. 7

(c)
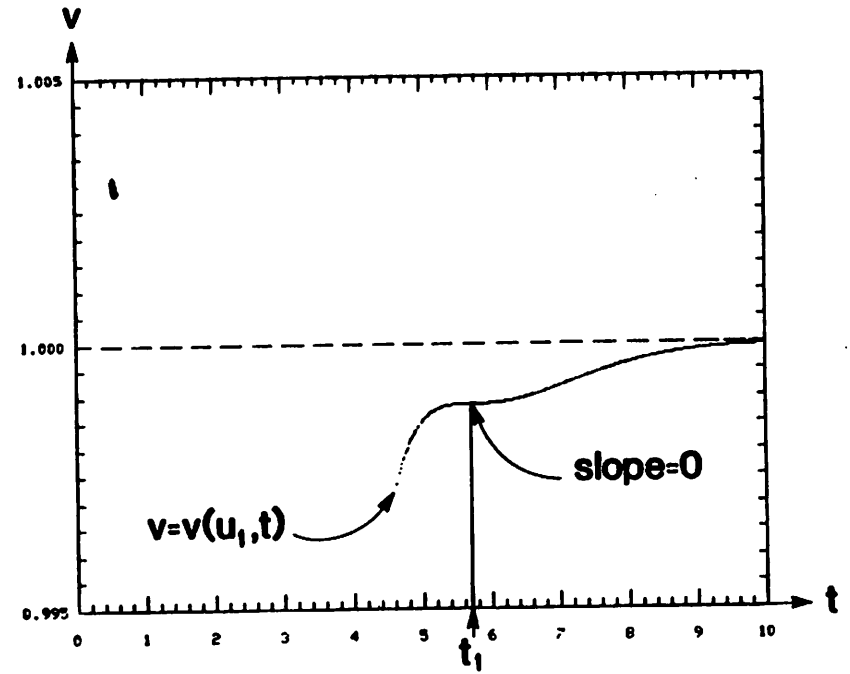
(d)
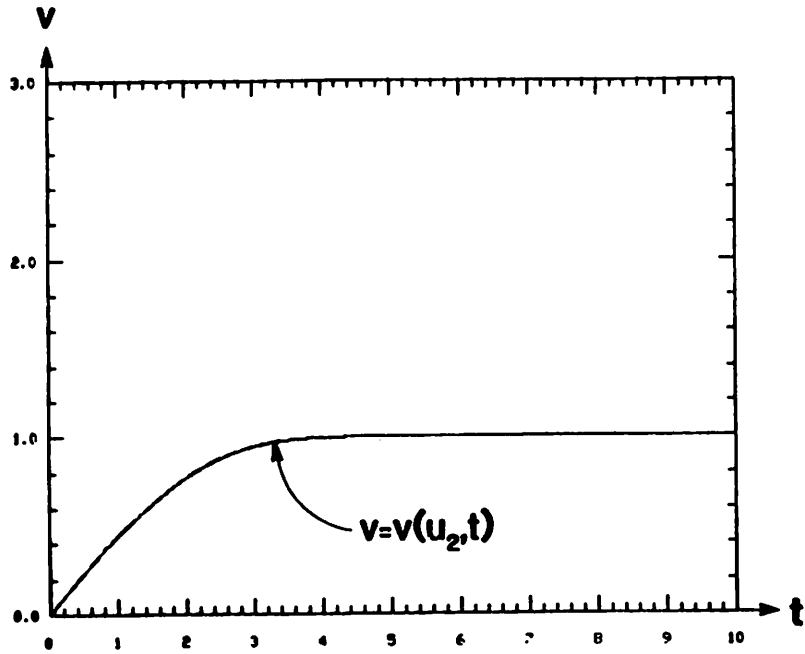
Fig. 7

(e)
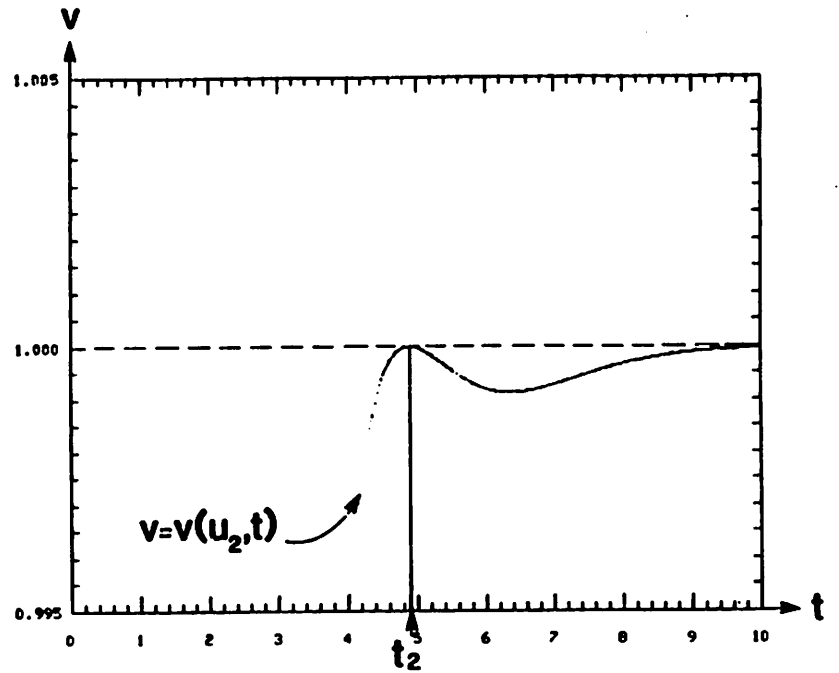
(f)

Fig. 7
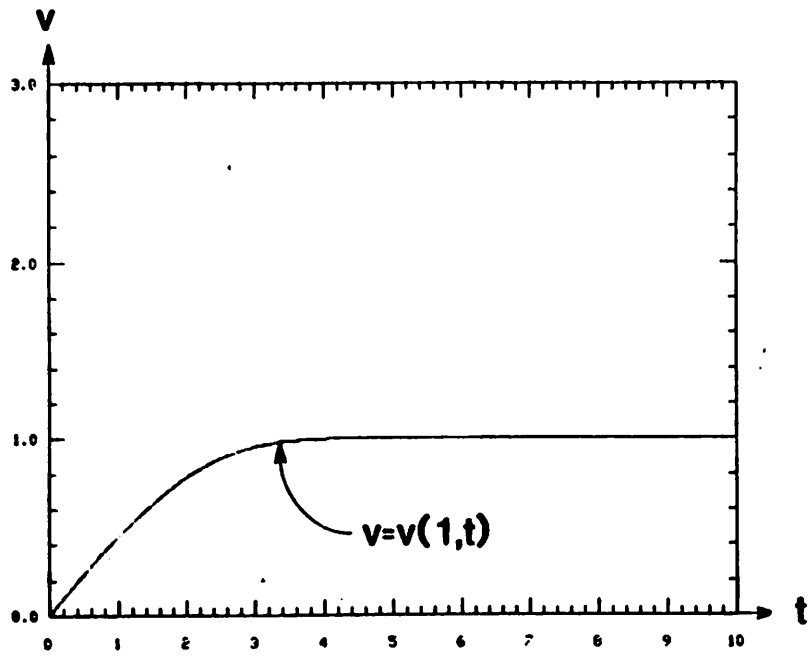
(g)
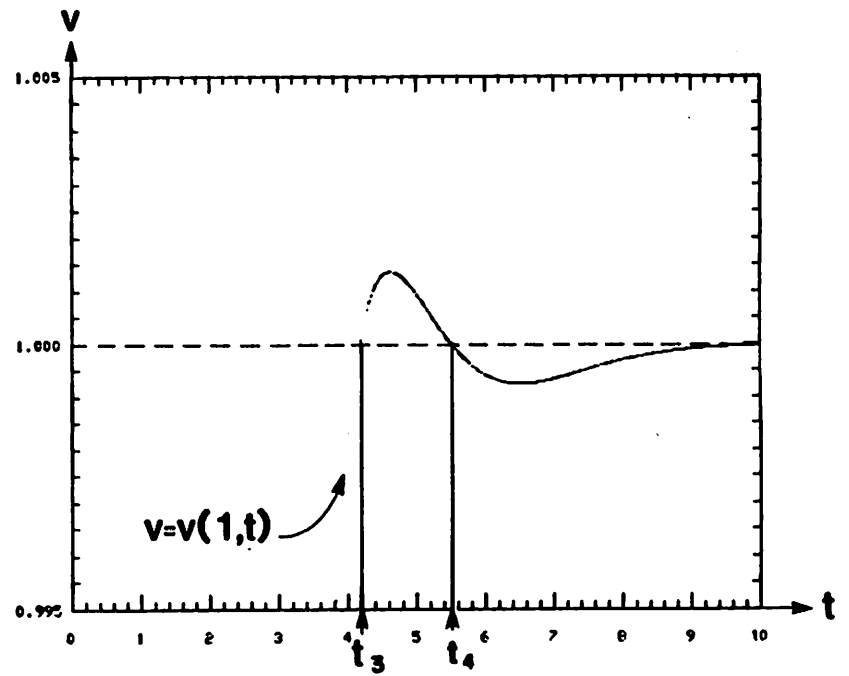
(h)

Fig. 7
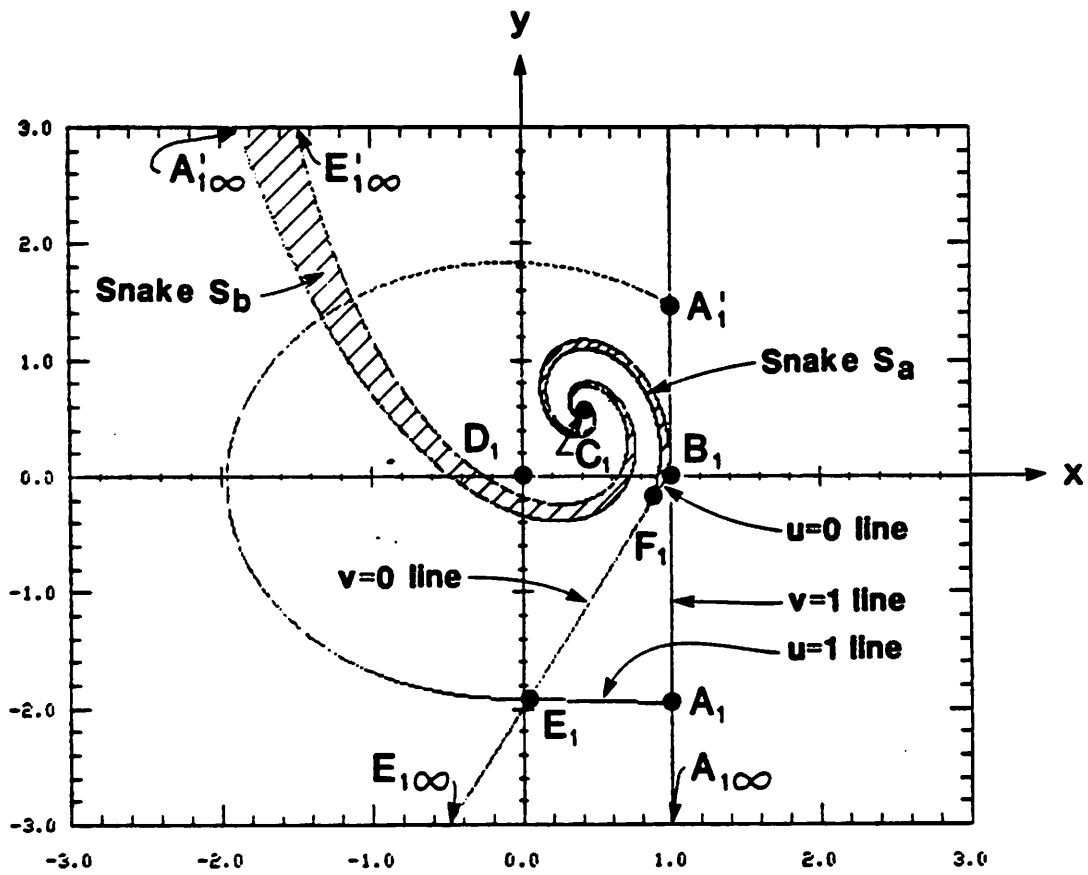
Fig. 8
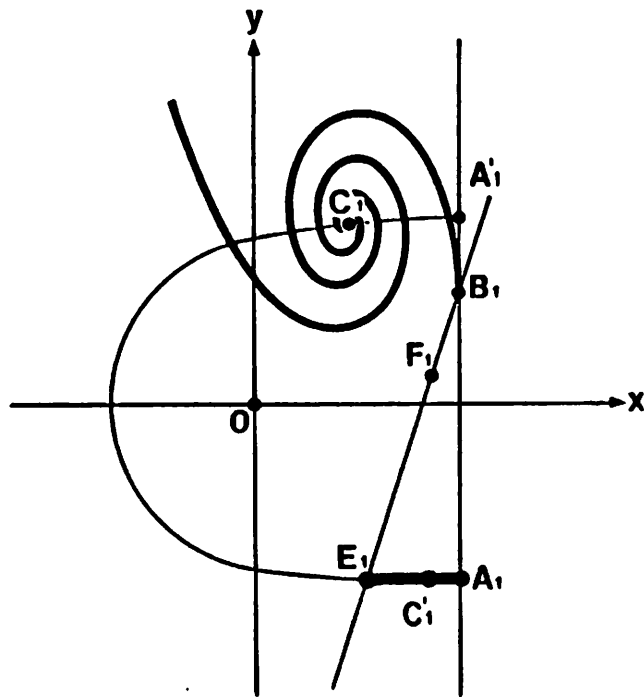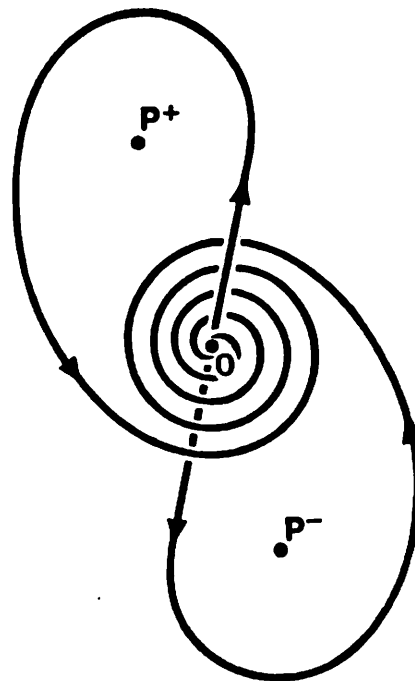
(a)   (b)

Fig. 9
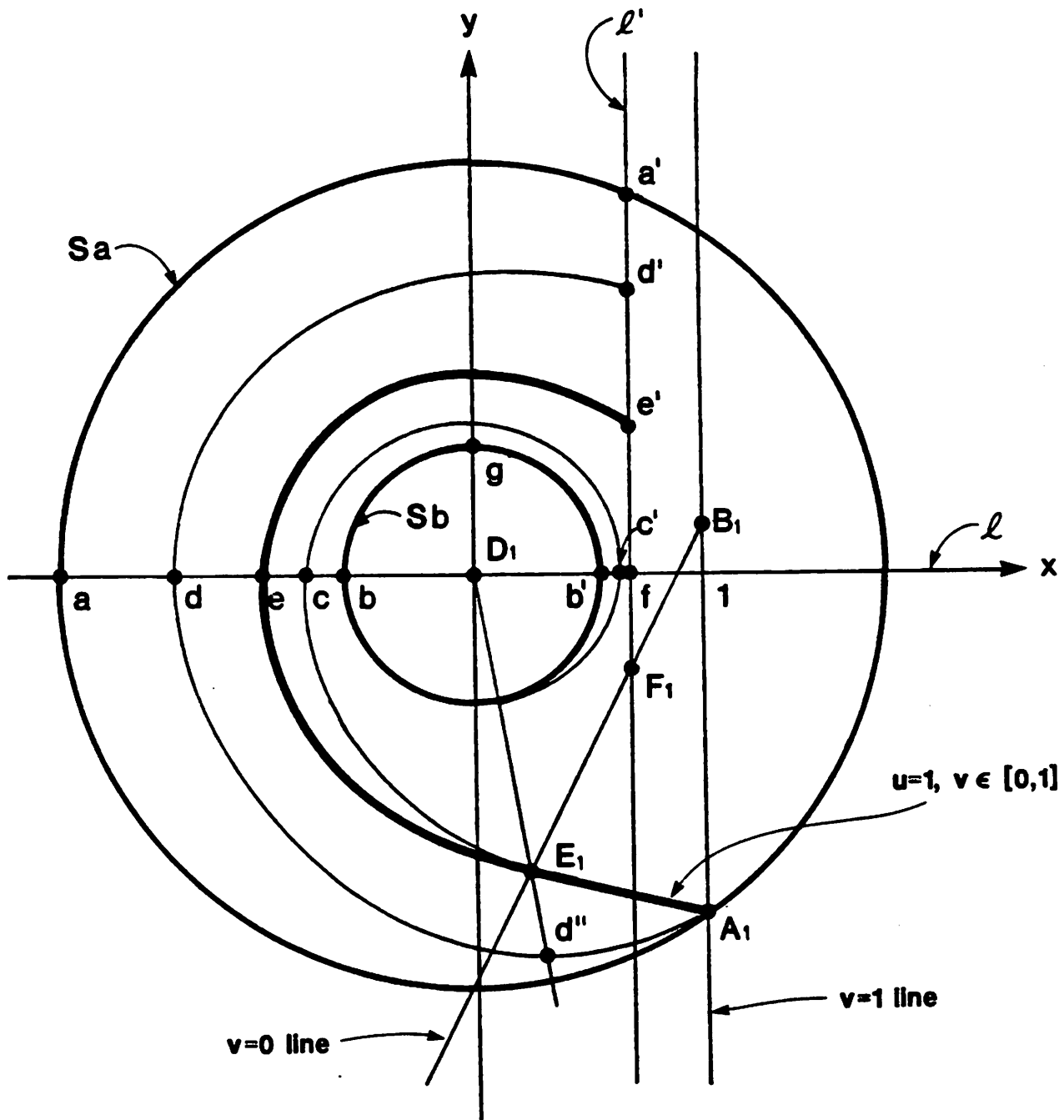
Fig. 10
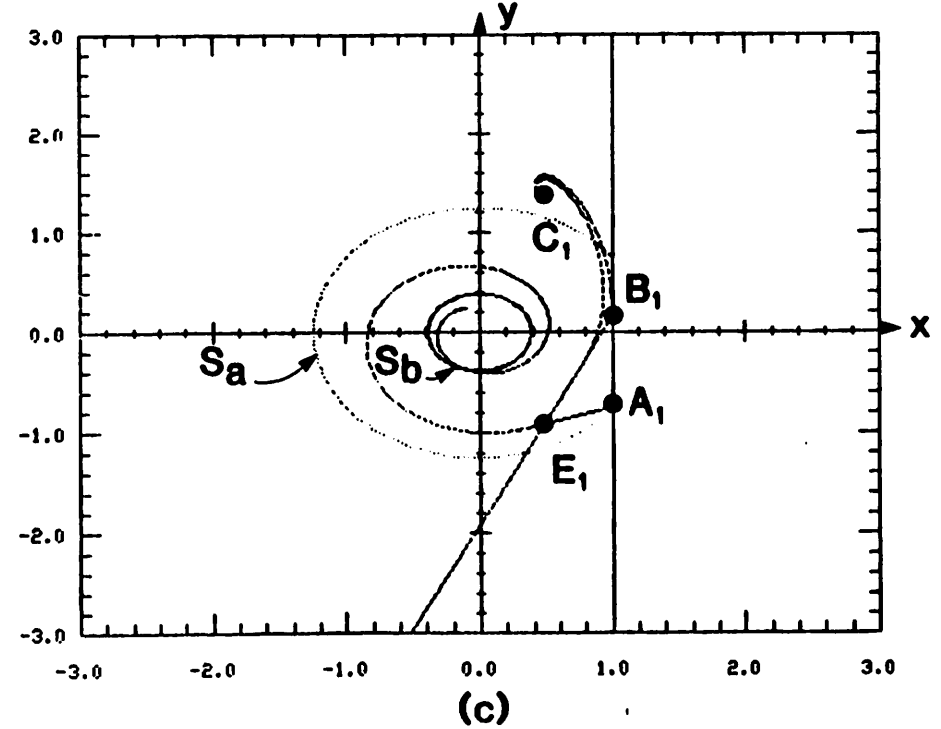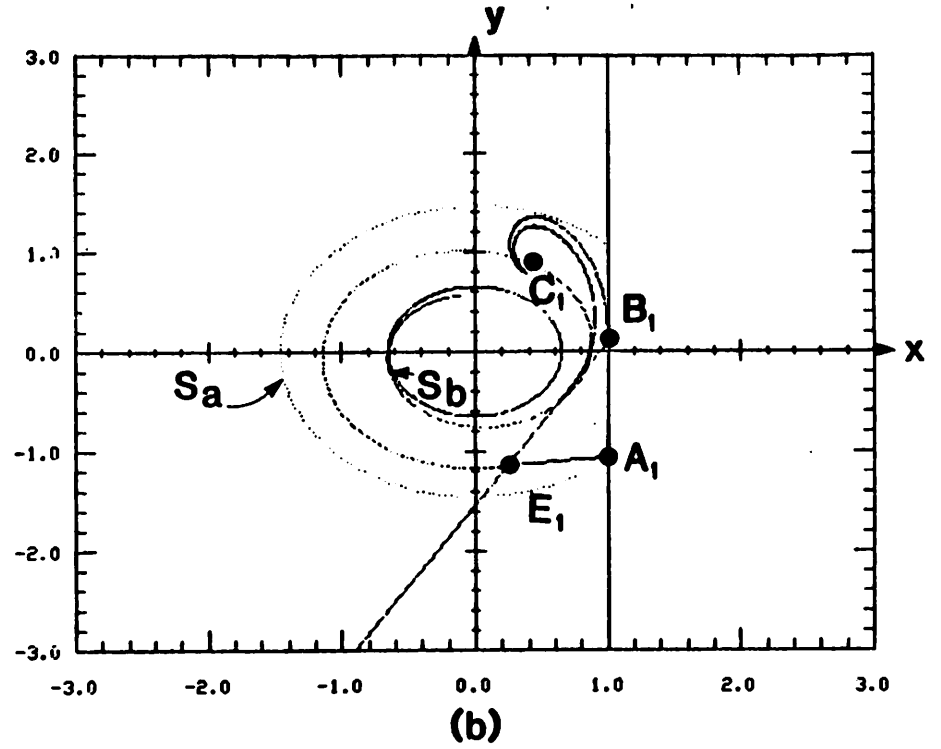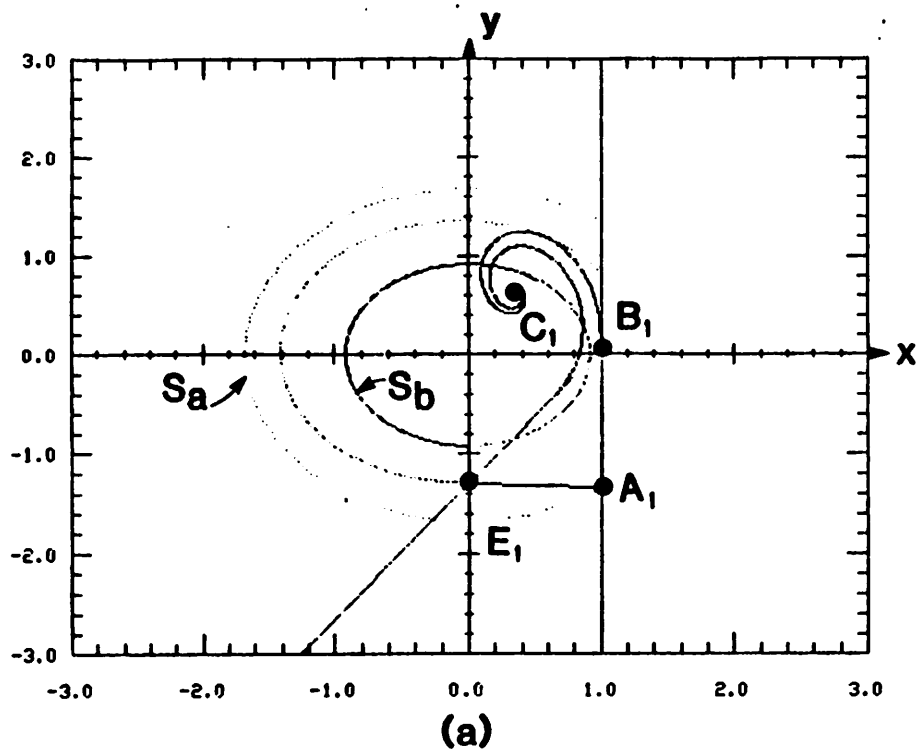
Fig. 11
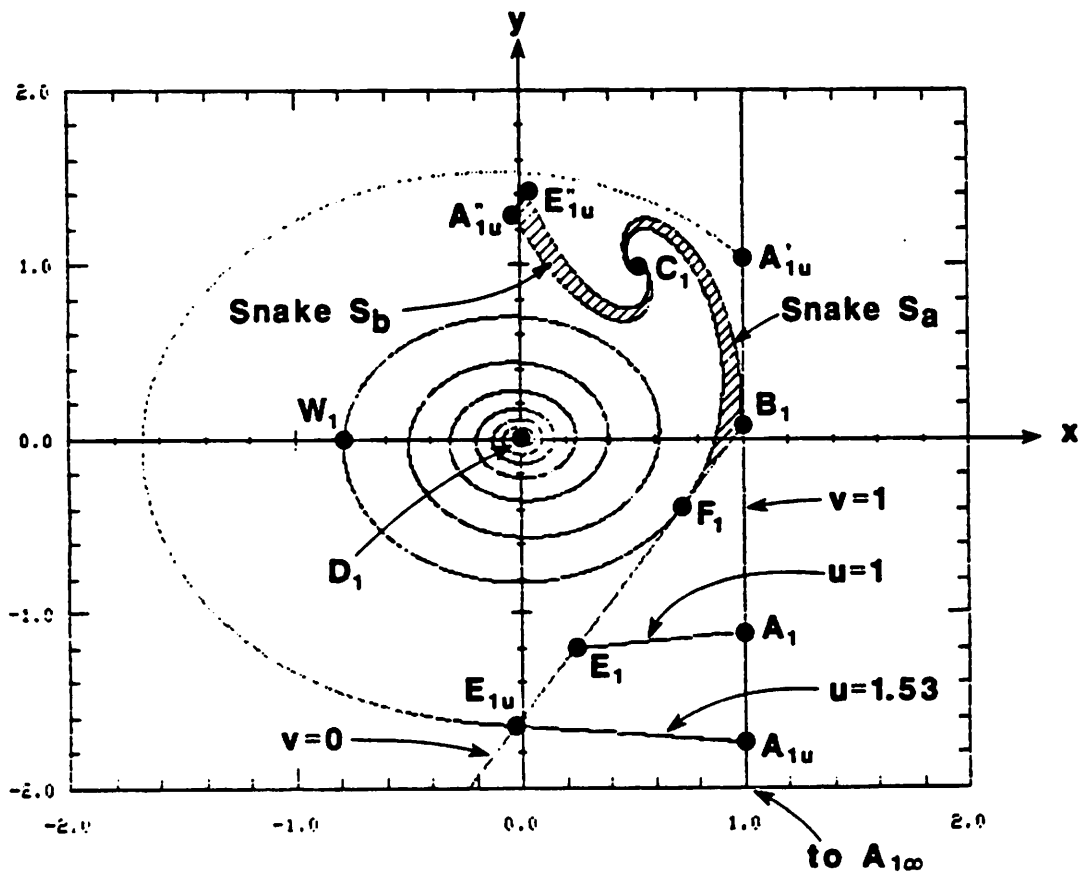
Fig. 12

(a)

(b)

Fig. 13

(c)

Fig. 13

Fig.14

Fig. 14

Fig. 15

Fig. 16

Fig. 17

(a)

(b)
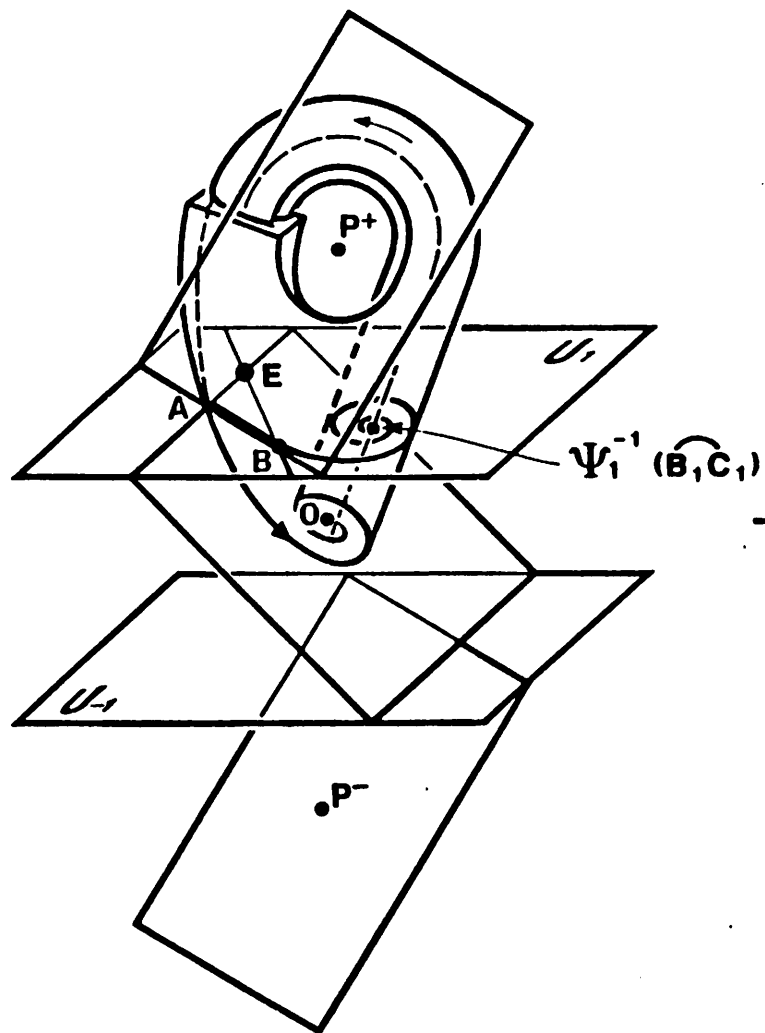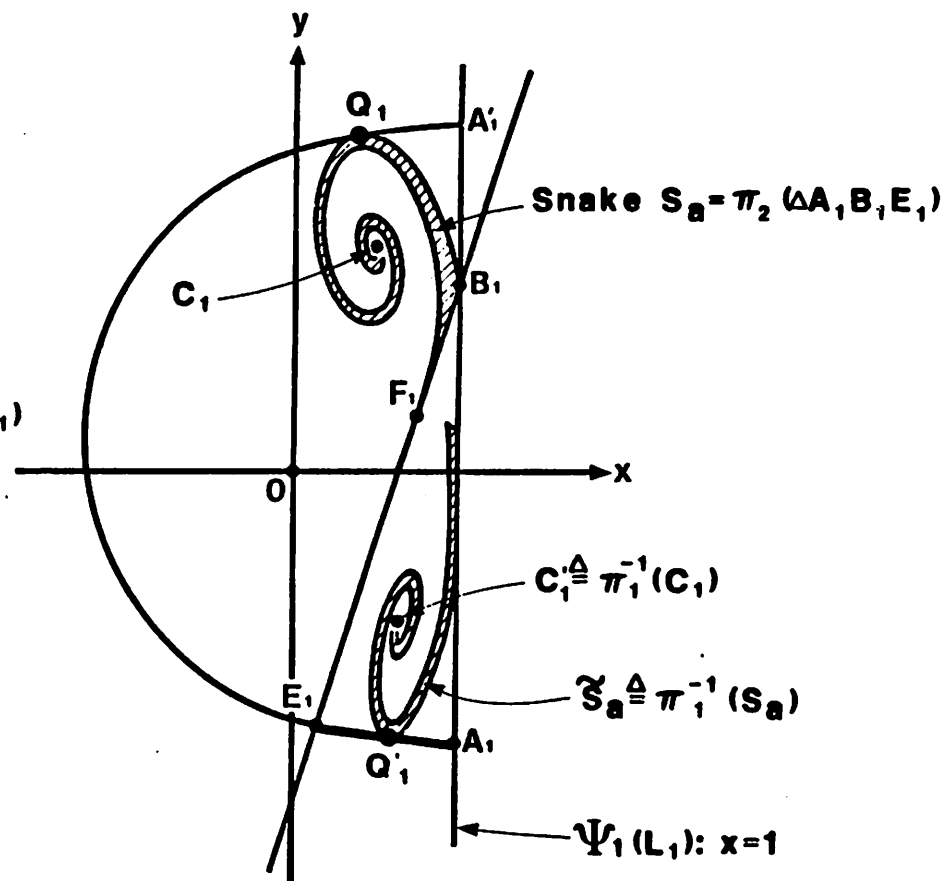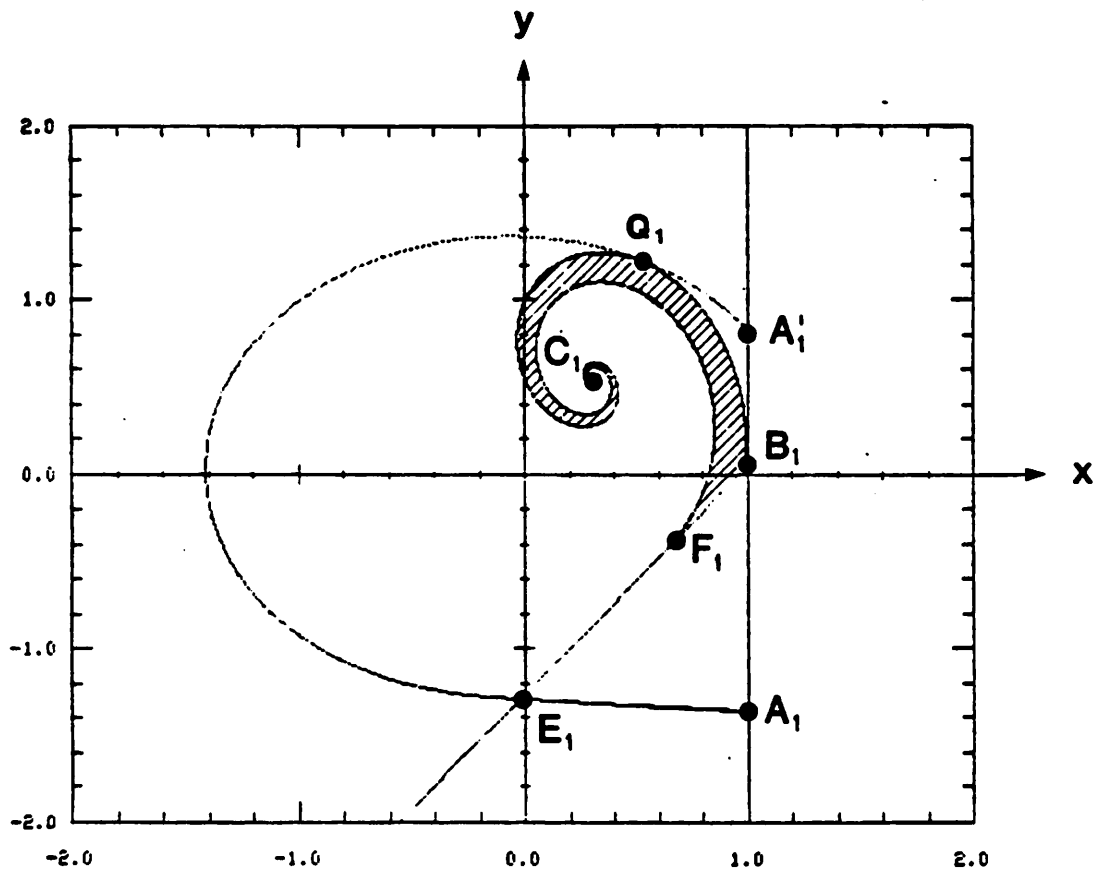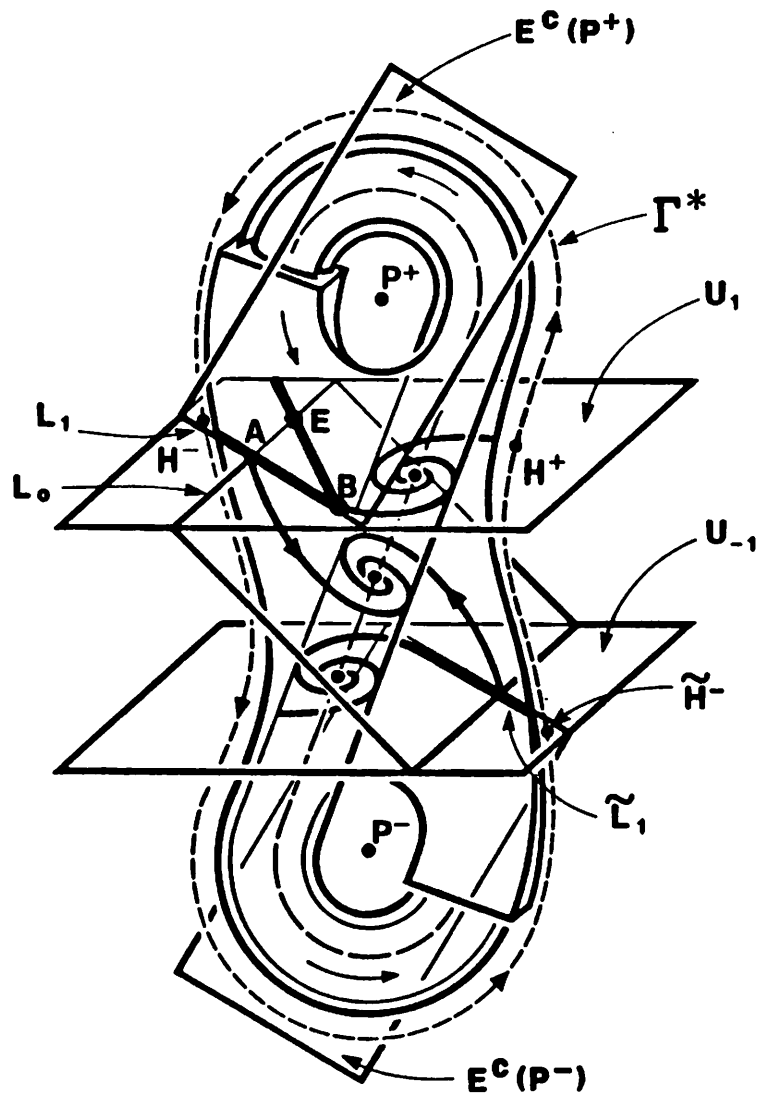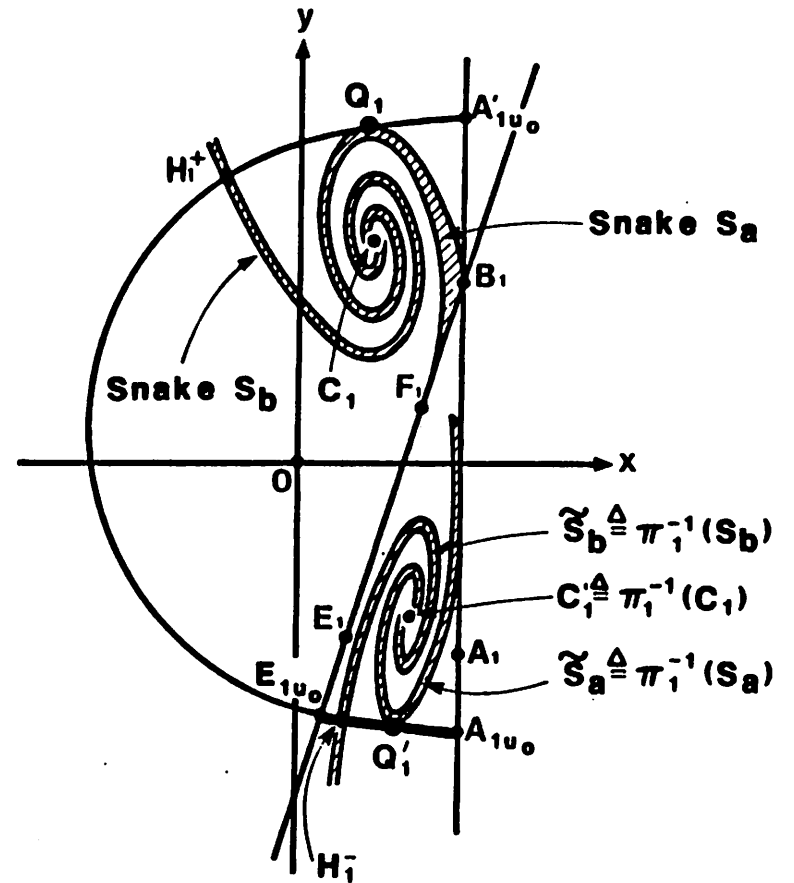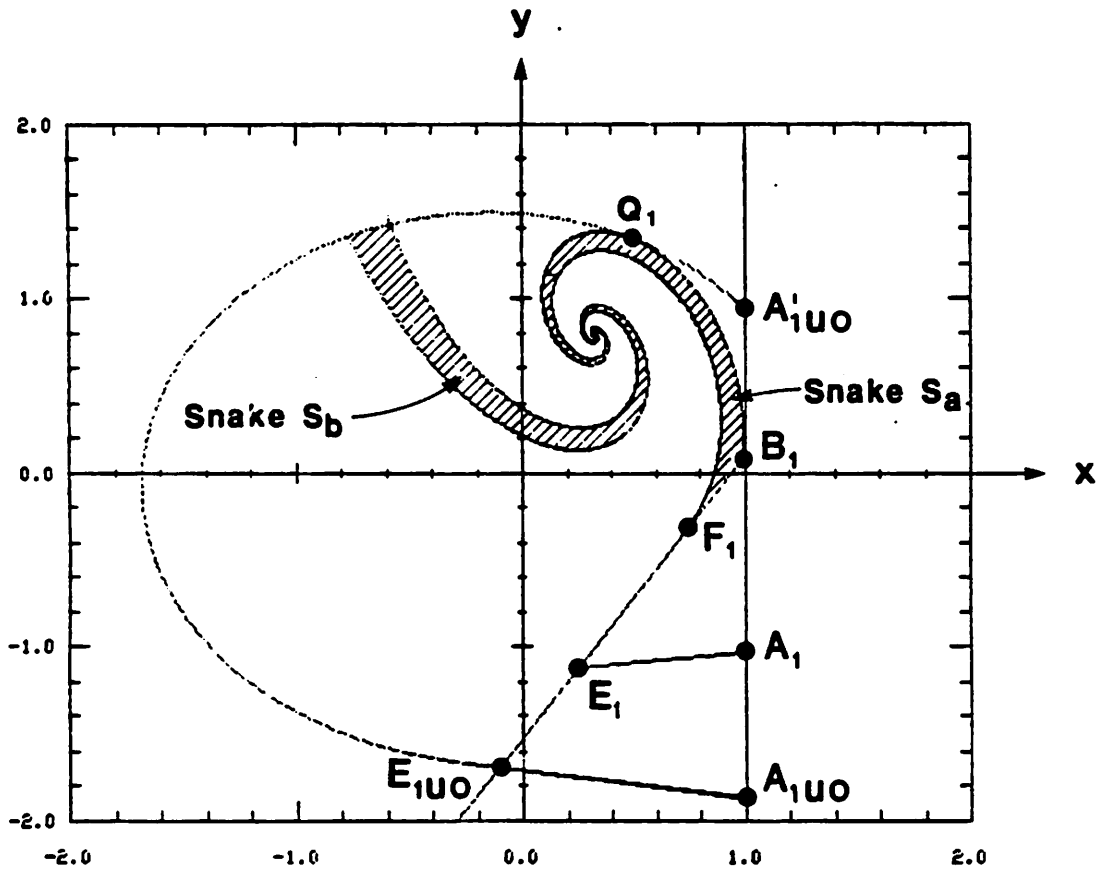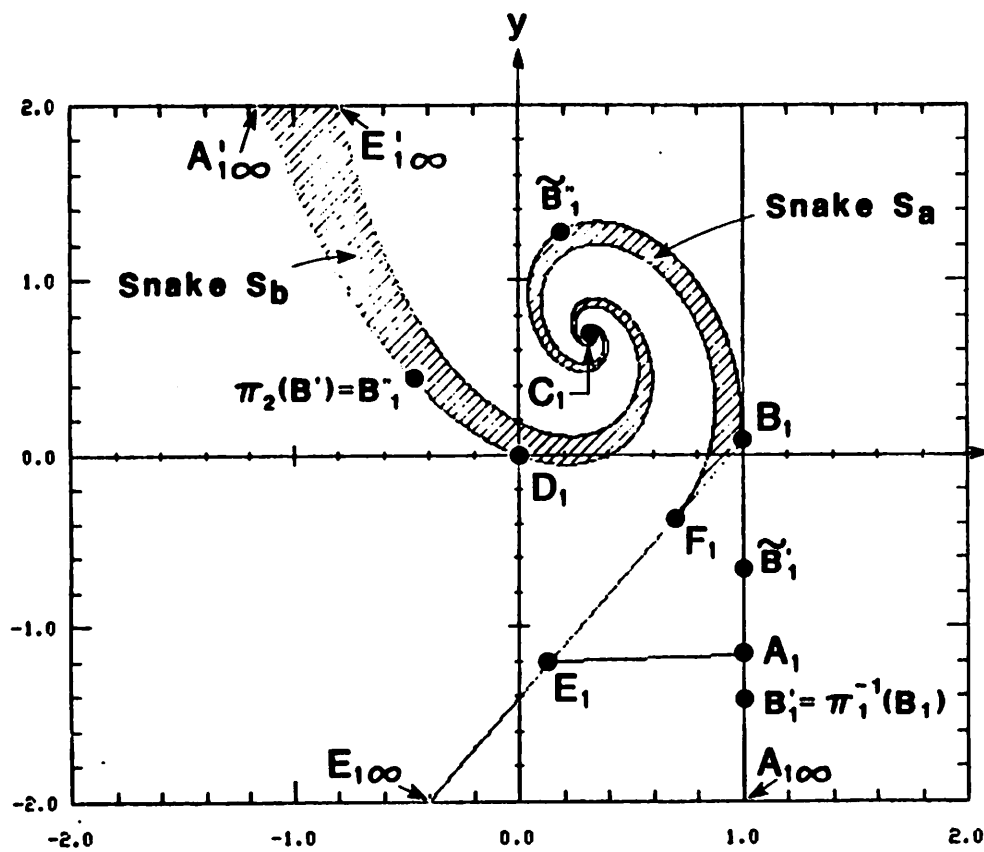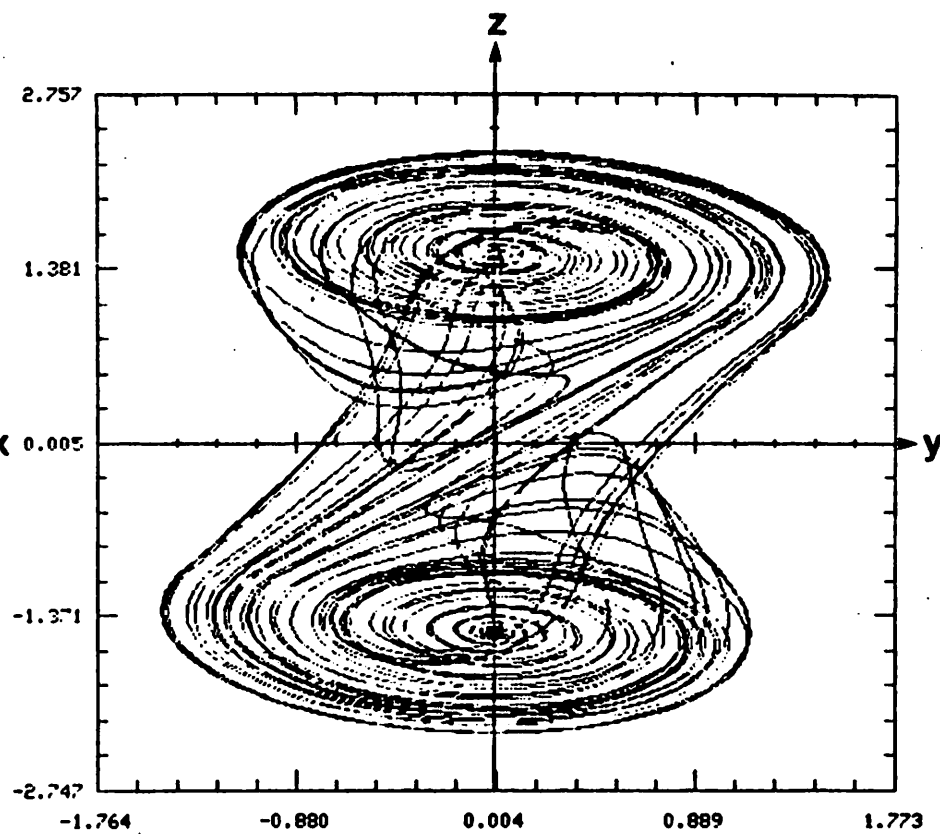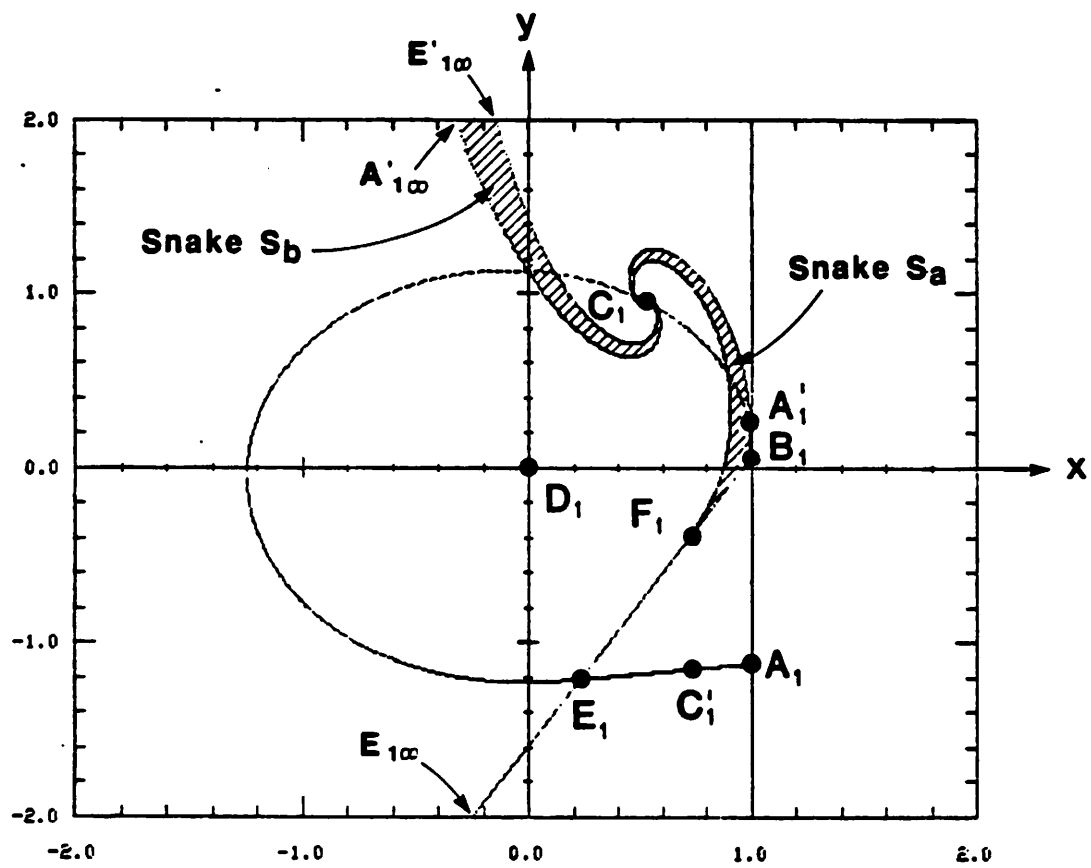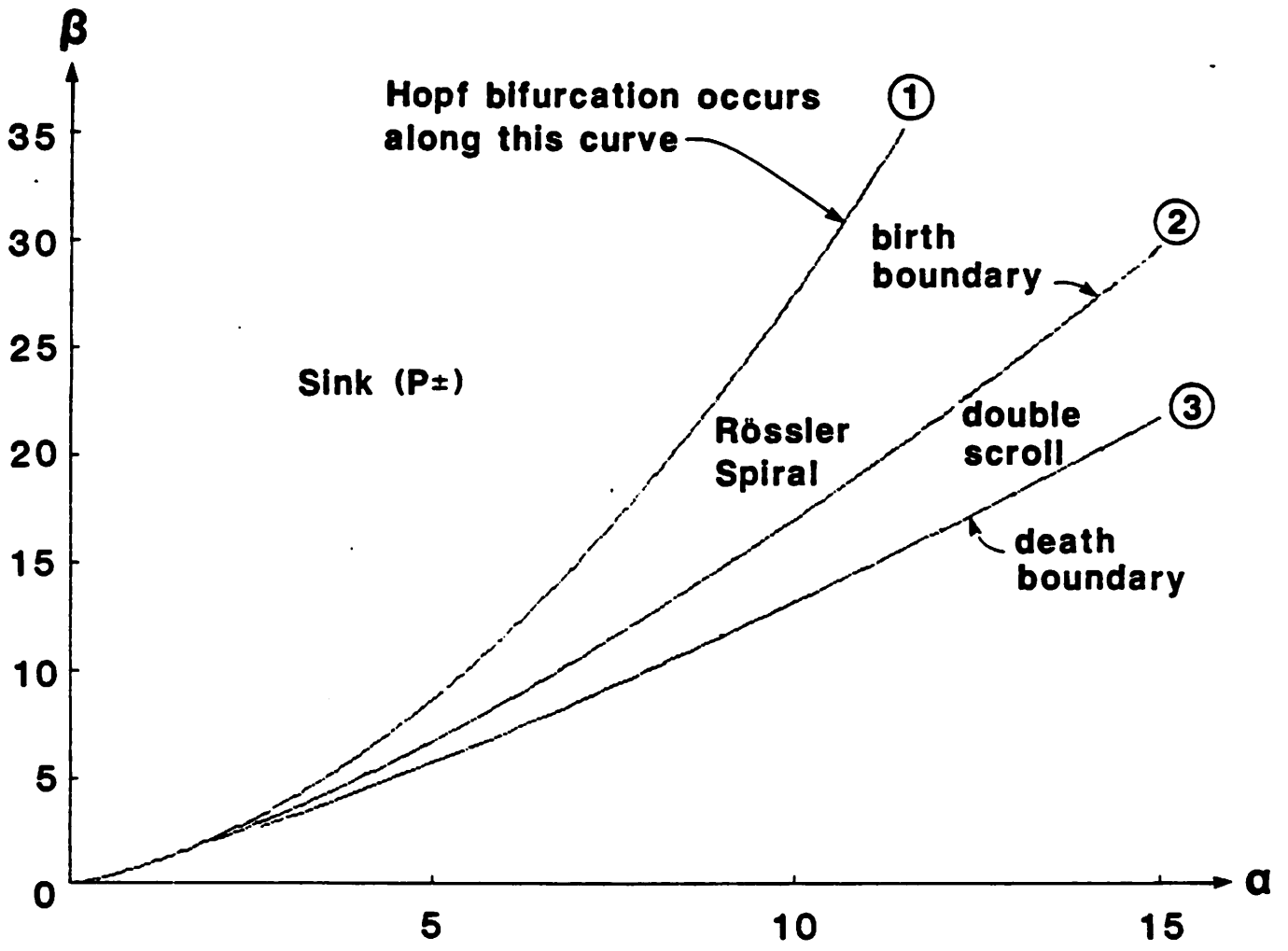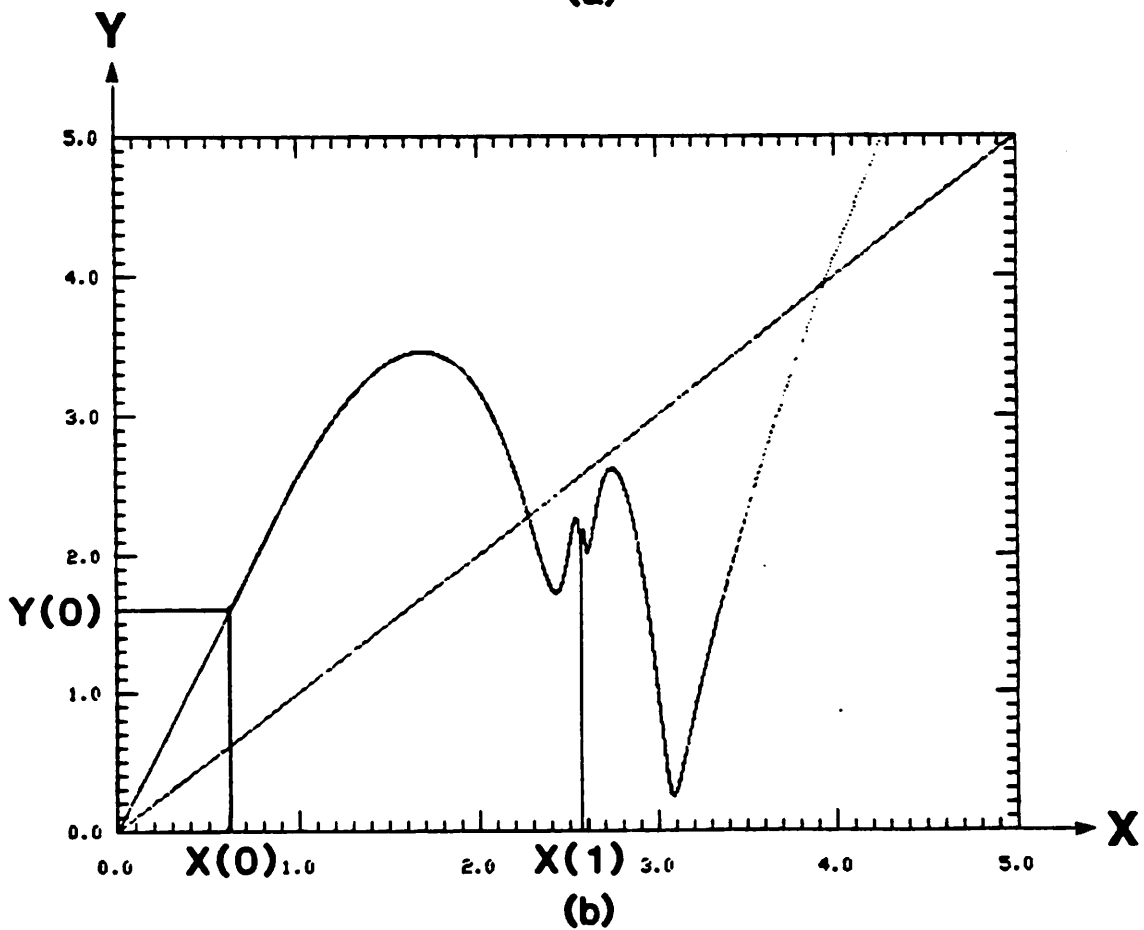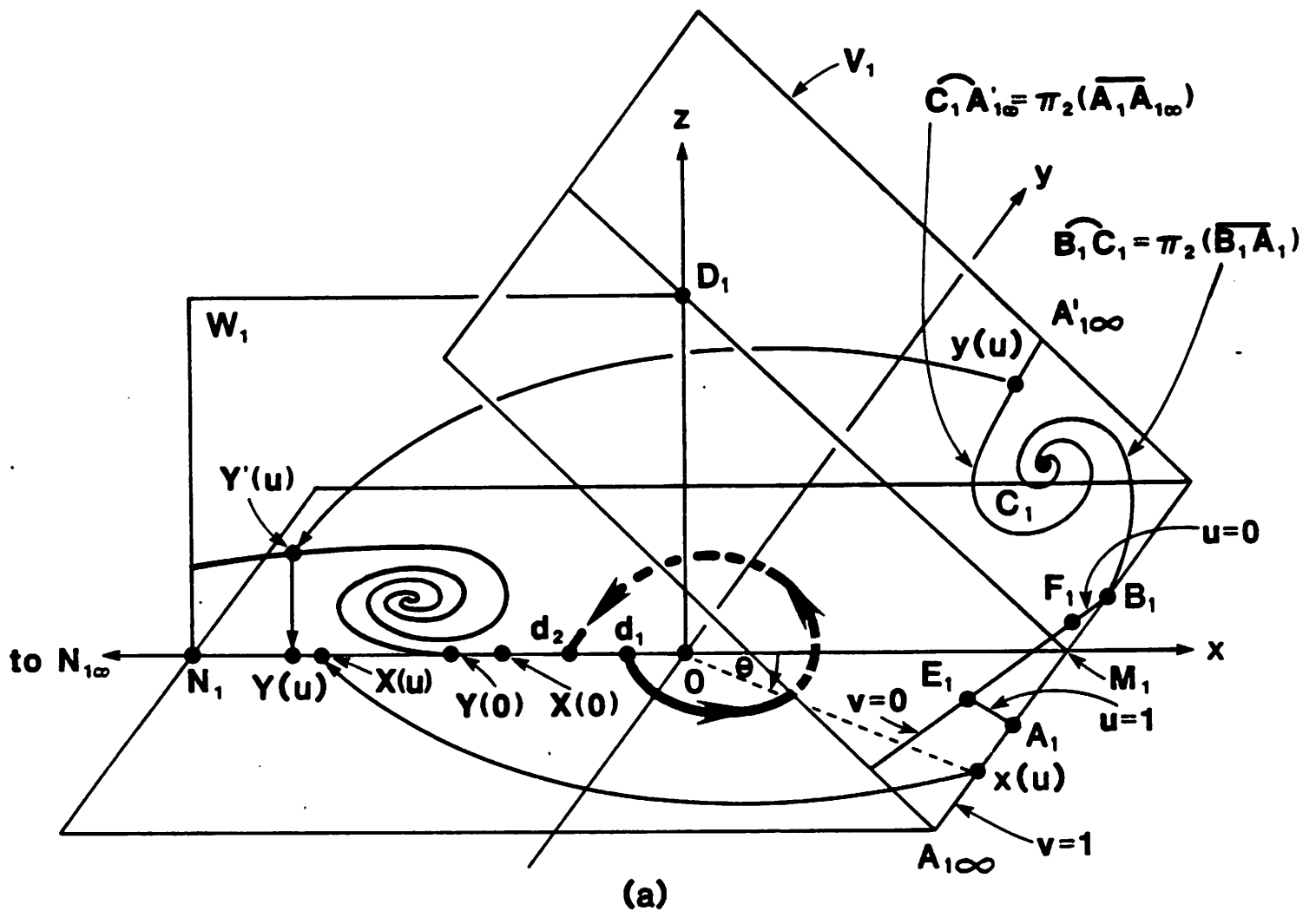
Fig. 18
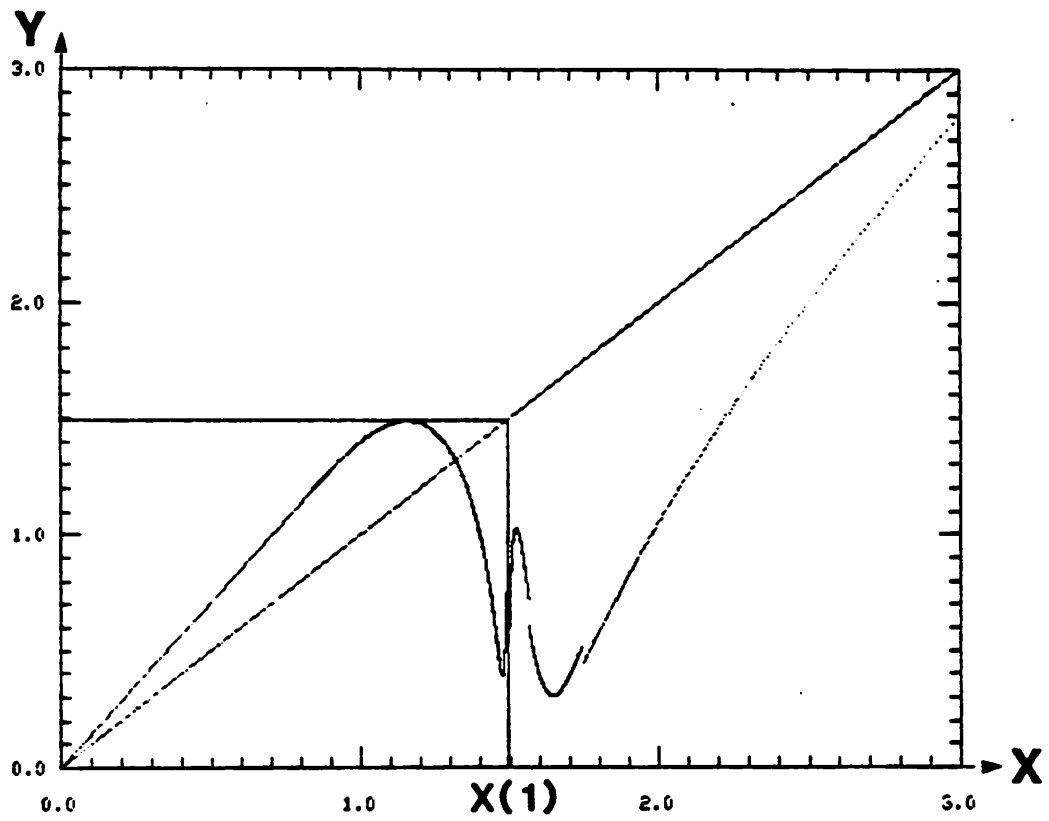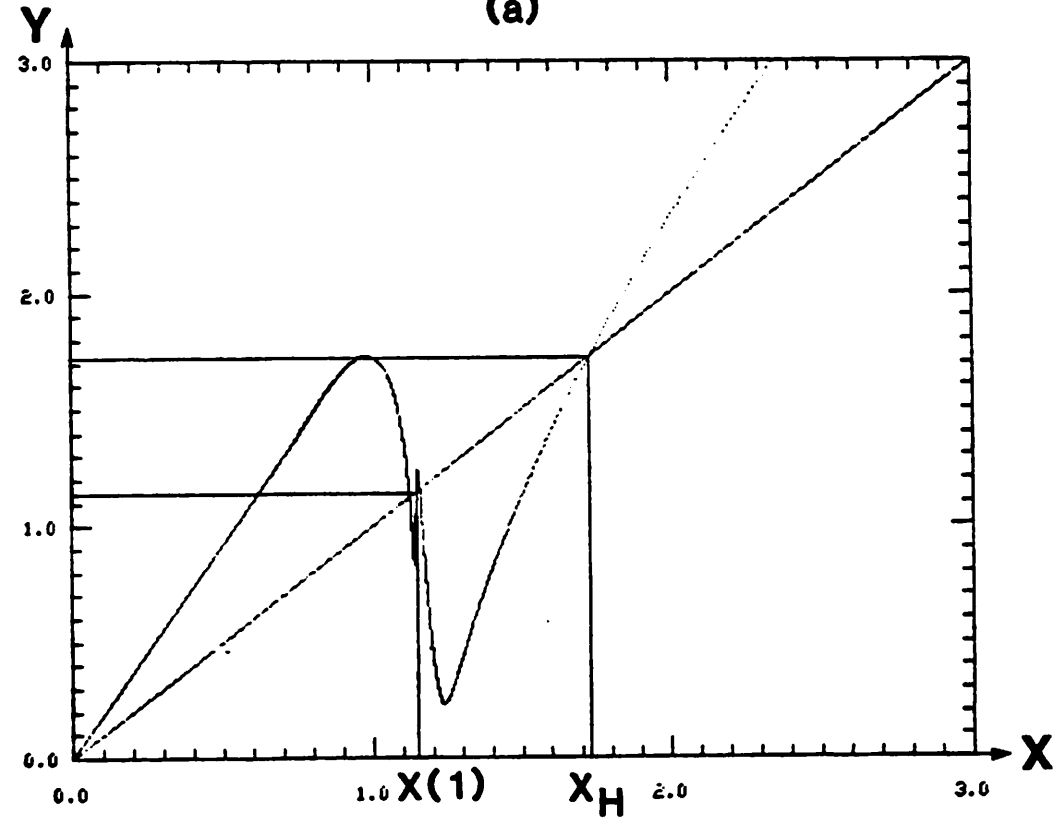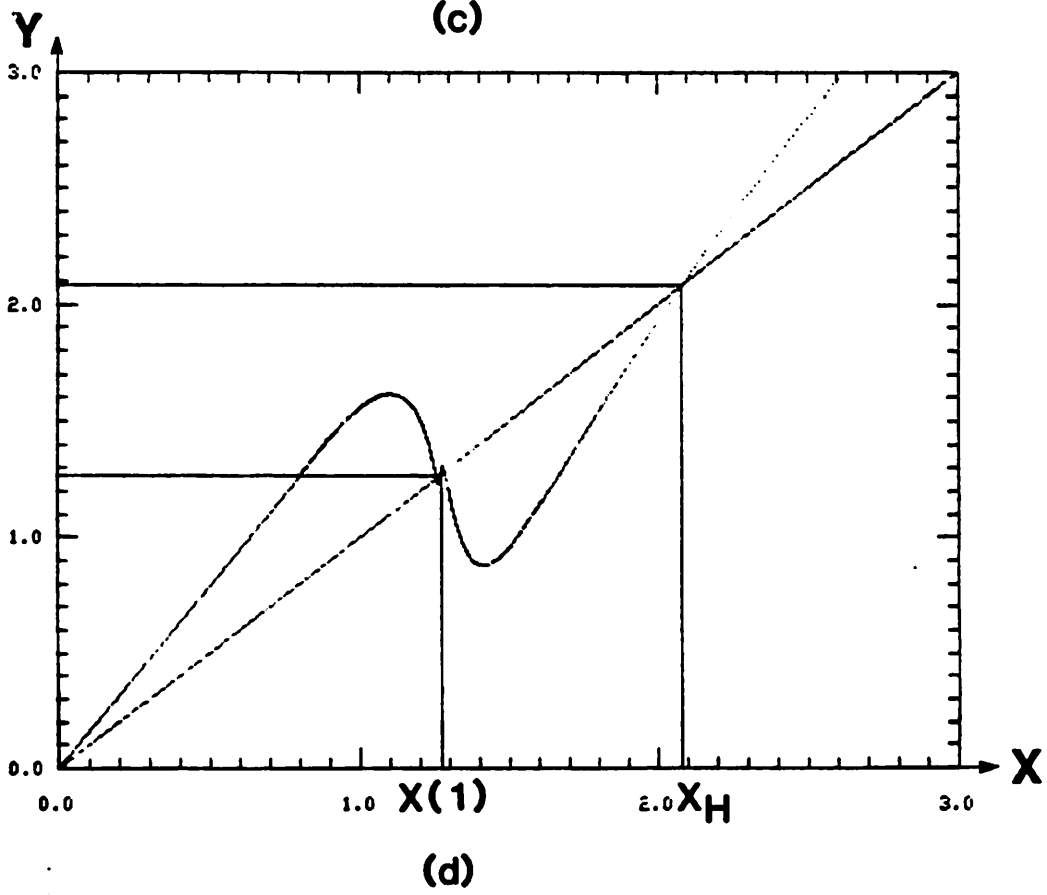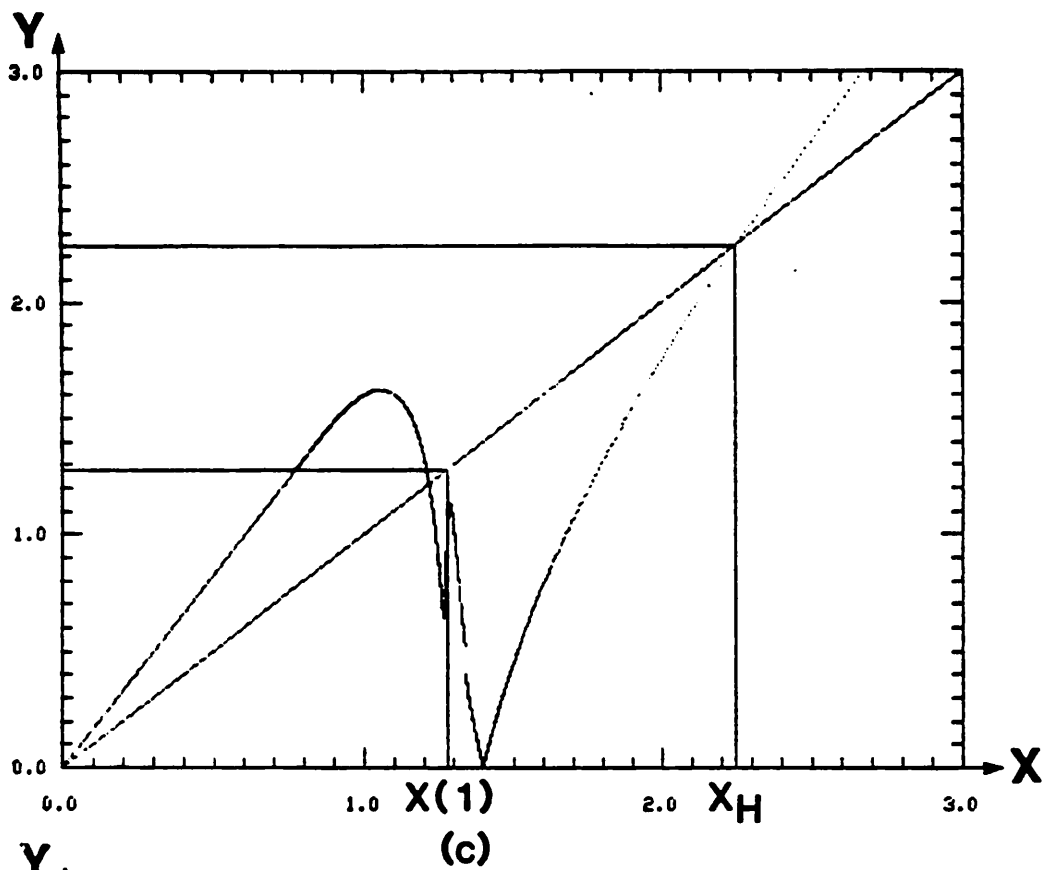
Fig. 19

Fig. 19
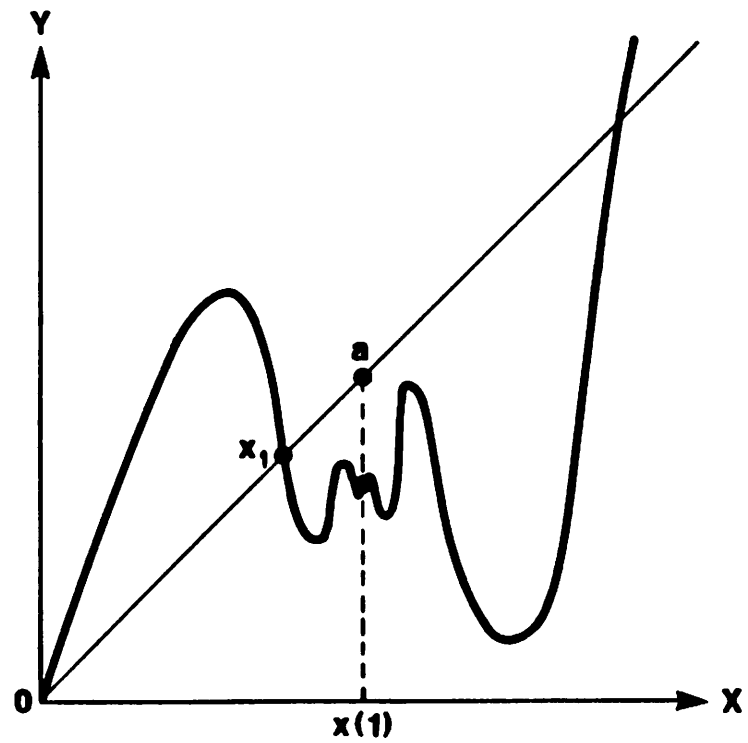
(a)

Fig. 20
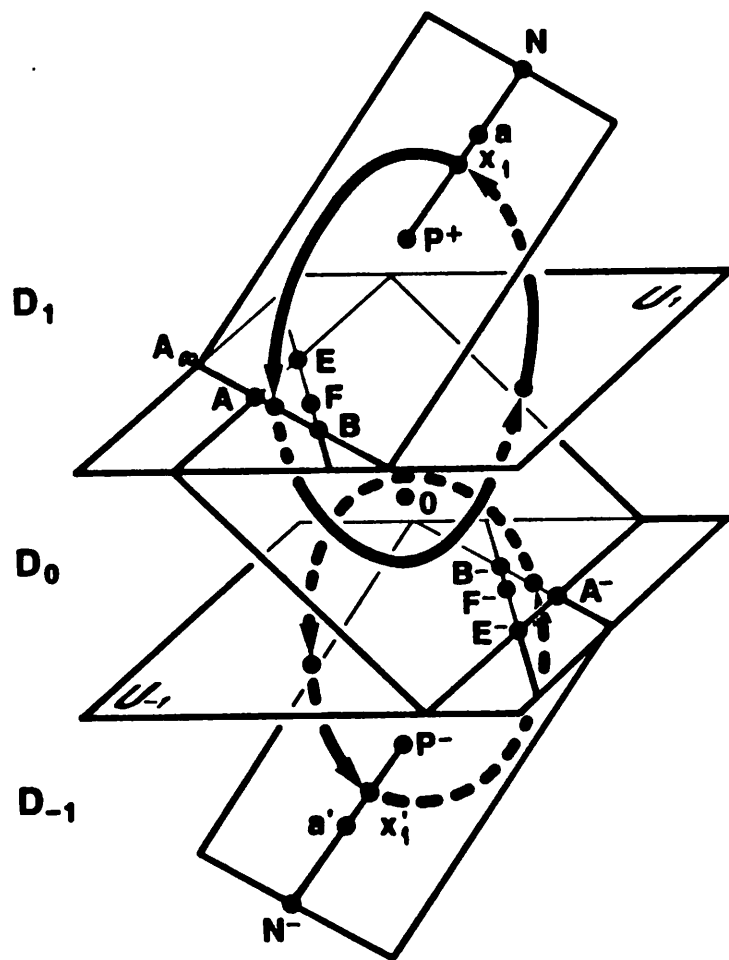
(b)
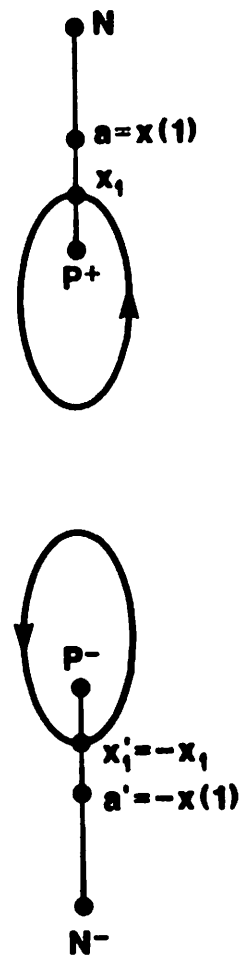
(c)

Fig. 20
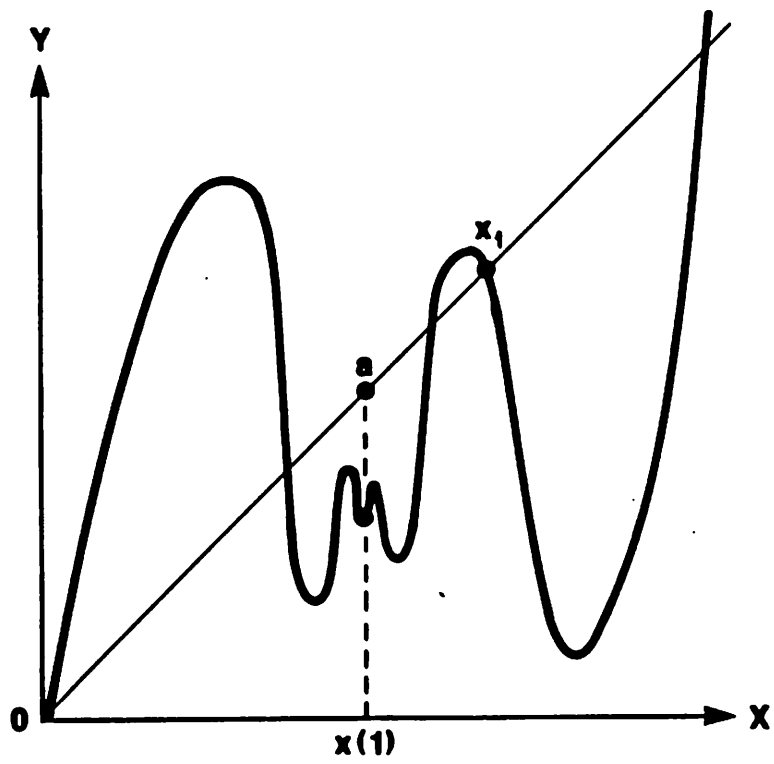
(a)
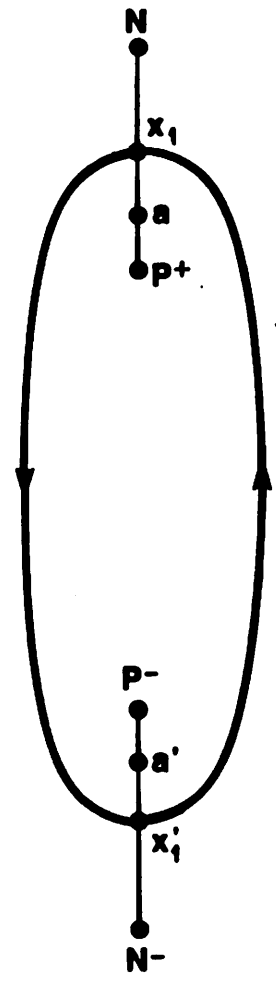
(b)

Fig. 21
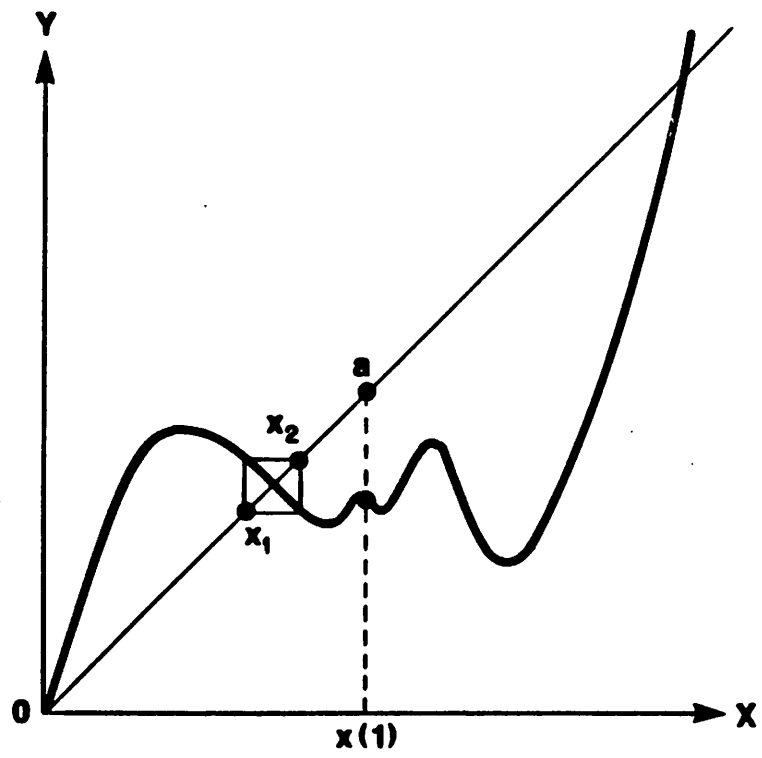
(a)
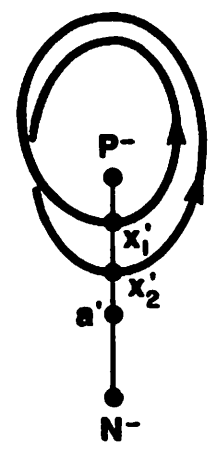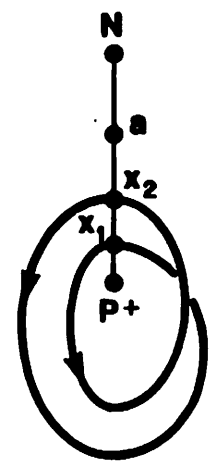
(b)

Fig. 22
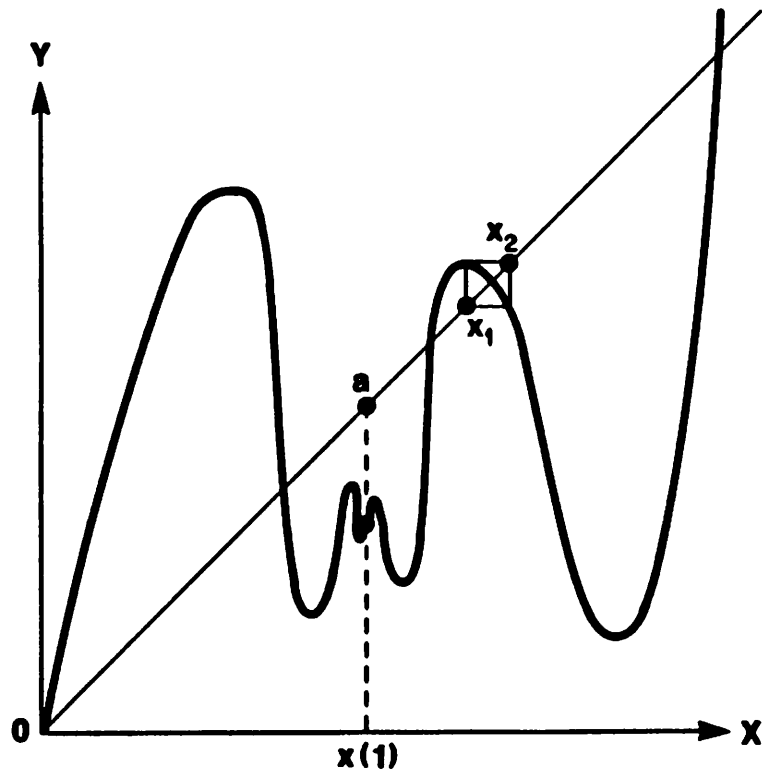
(a)
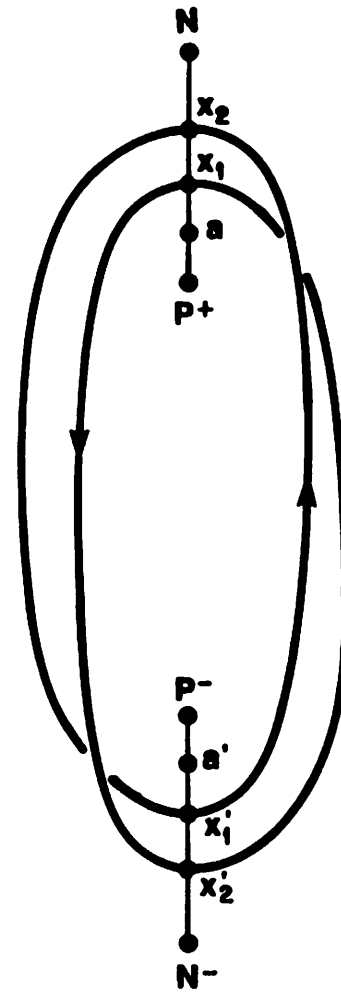
(b)

Fig. 23
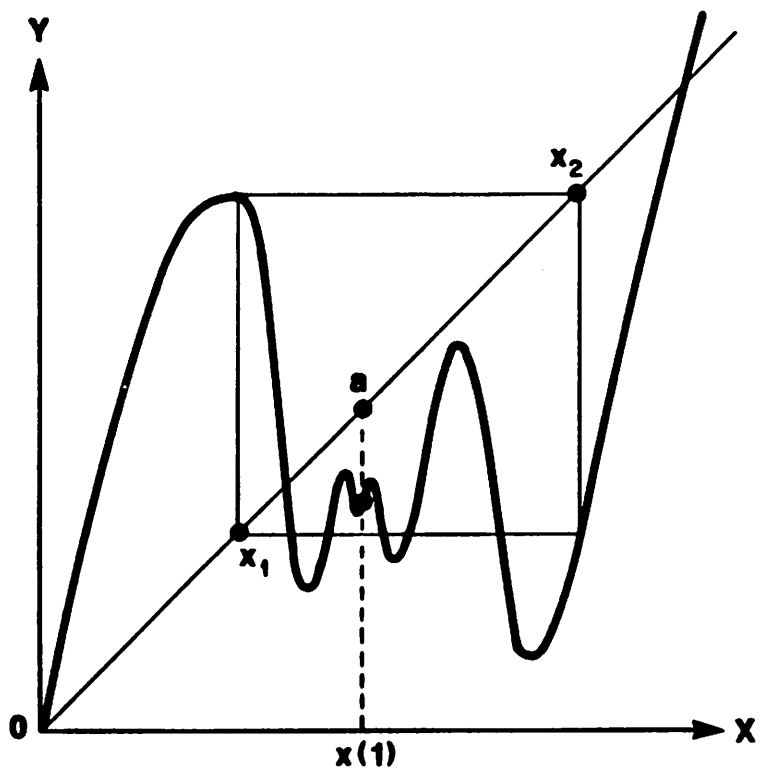
(a)
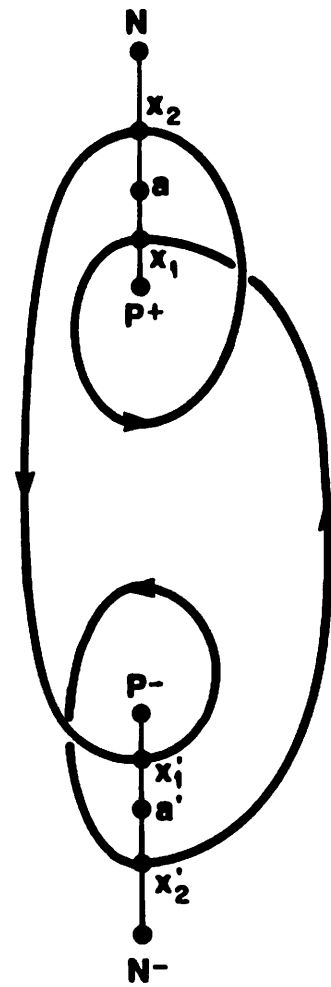
(b)

Fig. 24
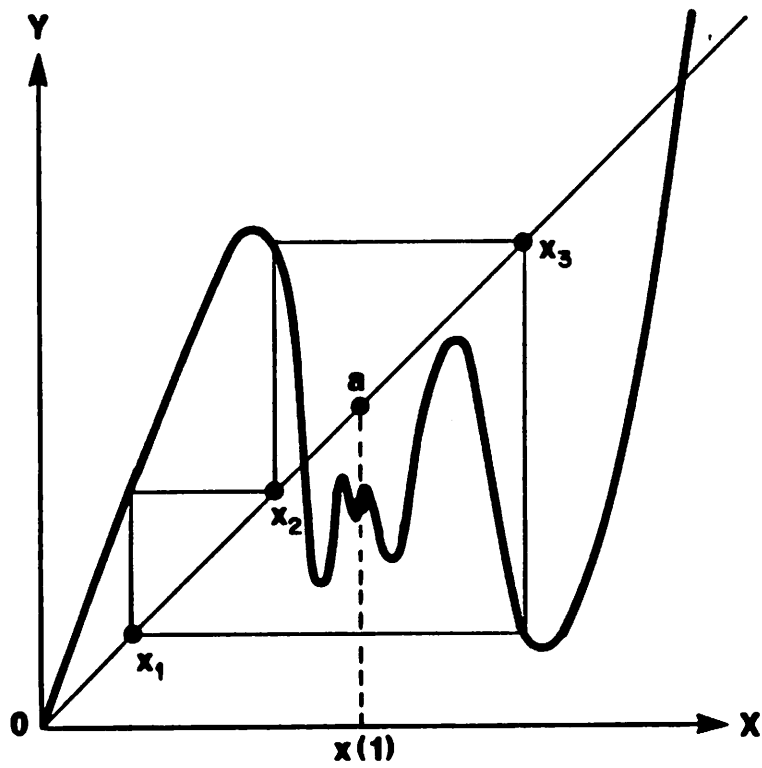
(a)

(b)

Fig. 25

(a)

(b)

Fig. 26

(a)

(b)

Fig. 27